# Dynamics of large-amplitude internal waves in stratified flows over topography

by

Dilip Prasad

B. Tech., Mechanical Engineering (1990)
Indian Institute of Technology

S. M., Mechanical Engineering (1993)
Massachusetts Institute of Technology

Submitted to the Department of Mechanical Engineering
in partial fulfillment of the requirements for the degree of

DOCTOR OF PHILOSOPHY

at the

Massachusetts Institute of Technology

February 1997



Signature of Author _____
Department of Mechanical Engineering
September 11, 1996

Certified by _____
Triantaphyllos R. Akylas
Professor of Mechanical Engineering
Thesis Supervisor

Accepted by _____
Ain A. Sonin
Professor of Mechanical Engineering
Chairman, Graduate Committee

# Dynamics of large-amplitude internal waves in stratified flows over topography

by

Dilip Prasad

Submitted to the Department of Mechanical Engineering
on September 11, 1996 in partial fulfillment
of the requirements for the degree of
Doctor of Philosophy

## ABSTRACT

The present research is comprised of theoretical investigations of three problems in the mechanics of internal waves of large amplitude, using analysis and numerical methods.

In the first problem, the flow of a Boussinesq density-stratified fluid of large depth past the algebraic mountain ('Witch of Agnesi') is studied in the hydrostatic limit using the asymptotic theory of Kantzios & Akylas (1993). The upstream conditions are those of constant velocity and Brunt–Väisälä frequency. On the further assumptions that the flow is steady and there is no permanent alteration of the upstream flow conditions (no upstream influence), Long's model (Long 1953) predicts a critical amplitude of the mountain ($\epsilon = 0.85$) above which local density inversions occur, leading to convective overturning. Linear stability analysis demonstrates that Long's steady flow is in fact unstable to infinitesimal modulations at topography amplitudes below this critical value, $0.65 \lesssim \epsilon < 0.85$. This instability grows at the expense of the mean flow and may be attributed to a discrete spectrum of modes that become trapped over the mountain in the streamwise direction. The transient problem is also solved numerically, mimicking impulsive startup conditions. In the absence of instability, Long's steady flow is reached. For topography amplitudes in the unstable range $0.65 \lesssim \epsilon < 0.85$, however, the flow fluctuates about Long's steady state over a long timescale; there is no significant upstream influence and no evidence of transient wave breaking is found for $\epsilon \leq 0.75$.

In the second problem, the phenomenon of shelf generation by nonlinear waves in two-dimensional stratified flows is investigated. The case of a uniformly stratified, Boussinesq fluid of finite depth is of primary interest; it is shown that the use of asymptotically matched (streamwise) regions becomes necessary. The 'inner region' is described by the fully nonlinear theory of Grimshaw & Yi (1991), while the 'outer region' consists of linear, downstream-propagating fronts, the cumulative effect of which is to give the appearance of a shelf that carries mass but no energy. A similar shelf is found to exist in the corresponding infinite-depth problem. The case of weakly nonlinear waves in an arbitrarily stratified fluid is also examined, where it is found that a shelf of fourth order in wave amplitude is generated. Moreover, the shelf extends both upstream and downstream in general and could thus lead to an upstream influence of a type that has not been previously considered. The mechanism of shelf generation in all cases is shown to be a self-interaction of the nonlinear wave, where transience is an essential ingredient.

In the third problem, a theory is developed for the resonant generation by submerged topography of weakly three-dimensional internal waves in a fluid with a linearly varying density distribution. The flow is shown to be governed by an integro-differential equation, which is capable of describing finite-amplitude waves and is valid until incipient density inversions take place. In addition to the nonlinearity caused by the presence of a topographic forcing, it is found that three-dimensional effects are also manifested as nonlinear terms in this evolution equation. The theory is observed to break down in the far-field, owing to the formation of an infinite downstream shelf, which results in a flux of both mass and energy from the resonant wave. As in the two-dimensional problem, matched asymptotic expansions are used to resolve the difficulties caused by the shelf. Numerical solutions of the nonlinear evolution equation for waves in a channel are presented; the parameter space consists of a resonance detuning and a relative blockage, which measures three-dimensional effects. Wave breaking is found to occur over a finite range of detuning for a given relative blockage. The scaling of the breaking time is also investigated.

Thesis Supervisor: Triantaphyllos R. Akylas
Title: Professor of Mechanical Engineering

# ACKNOWLEDGEMENTS

I am indebted to Professor Akylas for his patience and encouragement over the past three years. It has truly been a pleasure and indeed, a privilege to have had him as an advisor and teacher. His clarity of thought and exposition and his emphasis on thoroughness serve as an inspiring example of the way research ought to be done. I would also like to thank Professor Lienhard and Professor Patera for consenting to serve on my committee. Financial support from the Air Force Office of Scientific Research (Grant F49620-92-J-0086) and the National Science Foundation (Grant DMS-9404673) is gratefully acknowledged.

I am deeply obliged to my office-mates, Arthur T.-S. Yang, Alfred Pettinger and David Calvo who have, over the years, provided intellectual stimulation through numerous discussions of both a technical and non-technical nature. A special thanks to Debra Blanchard for creating a student-friendly working environment and for her assistance with typesetting. I am also grateful for the support of my twin brother, Anil, whose shared interest in the field of fluid mechanics has made for a friendship and rapport that far transcends a sibling relationship. This thesis is dedicated to my father, who taught me the value of living up to exacting standards and for encouraging a little boy to dream big.

CONTENTS

# LIST OF FIGURES

# CHAPTER 1

# GENERAL INTRODUCTION

The study of wave phenomena in fluids, in addition to presenting several fascinating fundamental challenges, is also important in understanding the mechanics of geophysical flows. The present investigation is concerned with internal waves. Although these waves are less familiar than their surface counterparts, they are in fact far more ubiquitous. Like surface waves, they owe their existence to gravity and occur in density-stratified fluids such as the ocean and atmosphere. While variations in temperature are partly responsible for the stratification of these natural fluid bodies, changes in the salinity (in the case of the oceans) and pressure (in the case of the atmosphere) substantially contribute to the stratification as well. Geophysical internal waves are known to possess enormous scales: wavelengths of the order of 10 km and amplitudes of 20 m are not uncommon in the oceans while atmospheric waves with wavelengths of several hundred kilometers have been observed. It is therefore not surprising that they play a crucial role in determining local weather patterns and climate dynamics. For example, the overturning of internal waves in the lee of mountain ranges is believed to be responsible for windstorms such as the föhn and the chinook. Similarly, the breaking of oceanic internal waves enhances momentum and scalar transport, which substantially alters temperature and circulation patterns. The goal of a fundamental investigation such as the present one is to understand and parametrize the phenomena that are characteristic of these flows with the ultimate objective of incorporating them into global circulation models which are used for weather prediction.

An important parameter that characterizes a continuous density distribution is the Brunt-Väisälä frequency, $N$, defined by

$$N^2(y) = -\frac{g}{\rho}\frac{d\rho}{dy}, \tag{1.1}$$

where $\rho$ is the density, $y$ is the vertical coordinate and $g$ is the acceleration due to gravity. It is evident from (1.1) that $N$ is real only as long as $\rho$ is a decreasing funcion of $y$, *i.e.*, the stratification is statically stable. Furthermore, $N$ has the physical interpretation of being the frequency of the oscillation that results from an infinitesimal displacement of a fluid particle from its equilibrium position.

Owing to the large length scales of geophysical flows, the Reynolds number is typically very high so that viscous effects are confined to relatively thin boundary layers; moreover, the extended time periods of these waves implies that dissipation within the bulk of the fluid is negligible. Thus, in the absence of separation, an inviscid model suffices to capture the essential physics of geophysical internal waves. We further assume that the background flow satisfies the criterion for dynamic, linear stability of inviscid, stratified shear flows, $Ri > \frac{1}{4}$ (Drazin & Reid 1981, p. 328). Here $Ri$ denotes the local Richardson number, defined in terms of the mean shear $U'(y)$ by

$$Ri = -\frac{g}{\rho}\frac{\rho'(y)}{U'^2(y)}.$$

As we have seen, stratification is usually the consequence of variations in a scalar such as temperature or salinity and this can result in diffusion. However, in most natural flows, the Prandtl (or Schmidt) number is so large that diffusive effects are negligible. In addition, the Mach number is very small so that the fluid may be treated as being essentially incompressible. This permits a decoupling of the momentum and energy equations, which

greatly simplifies the analysis.

Finally, we note that the effect of a rotating planet is potentially significant in geophysical flows. It is assumed in the flows considered here that the $Ro \ll 1$, where the $Ro$ is the Rossby number, defined in terms of the angular speed $\Omega$ and a characterisitc length, $L$ by the relation

$$Ro = \frac{U}{\Omega L}.$$

Thus the effect of rotation can be neglected. The present descriptions may be extended to finite Rossby numbers although this would entail a considerable increase in analytical complexity.

The present investigation is concerned with waves of large amplitude. One way in which large-amplitude internal waves are generated is by a resonant flow past submerged topography. This term is used to signify a condition where the long waves are nearly stationary relative to the forcing and their group velocity simultaneously vanishes so that energy accumulates close to the forcing. Although this mechanism is our primary focus, the applicability of the theoretical development here to freely-propagating, nonlinear internal waves must also be borne in mind. The uniqueness of the present approach lies in its ability to describe finite-amplitude waves within the context of analytical theory.

This thesis is comprised of three related problems, described in Chapters 2, 3 and 4, each of which is essentially self-contained. These chapters are based on the studies of Prasad, Ramirez & Akylas (1996), Prasad & Akylas (1996*a*) and Prasad & Akylas (1996*b*) respectively. The principal results of each problem are summarized at the end of each chapter. The flow of a stratified fluid of infinite depth past finite-amplitude topography is addressed in Chapter 2, with regard to the stability of a classical steady state. In particular, the mod-

ulational stability of the steady state is examined using a recently developed asymptotic theory and it is shown that the flow can, in certain instances, be unstable. The second part of the research, presented in Chapter 3 focuses on the curious phenomenon of shelf formation in two-dimensional stratified flows of finite depth. This phenomenon is shown to be a result of self-interaction of nonlinear, long waves and appears to be generic to all waveguide systems. In Chapter 4, we investigate fully nonlinear, weakly three-dimensional waves. A new theory is developed for these waves and is applied to the resonant generation of internal waves in a channel filled with a uniformly stratified, Boussinesq fluid. This system is found to possess a shelf as well, which leads to considerable difficulty. Numerical solutions of the nonlinear, transient problem are presented.

# CHAPTER 2

# STABILITY OF FLOW OF LARGE DEPTH OVER FINITE-AMPLITUDE TOPOGRAPHY

## 2.1 Introduction

The present chapter is concerned with the flow of density-stratified fluid over an obstacle of finite amplitude. This problem was first studied systematically by Long (1953), who devised an analytical model that accounts, under specific flow conditions, for finite-amplitude effects. Long's model hinges on the fact that the equations governing inviscid, steady, two-dimensional flow reduce to a linear form for certain background velocity and density profiles under the hypothesis that the topography does not alter these profiles far upstream—the so-called assumption of no 'upstream influence'. In particular, for a weakly stratified (Boussinesq) fluid, Long's model applies when the upstream velocity and Brunt–Väisälä frequency are independent of height. According to this model, given the topography shape and for fixed values of the other flow parameters, there is a critical amplitude of the obstacle above which the predicted steady flow features locally reversed density gradients ('breaking' streamlines) that would result in static instability (see, for example, Miles 1969).

In more recent work, Kantzios & Akylas (1993, hereinafter referred to as KA) proposed an asymptotic theory that describes the long-time dynamics of vertically unbounded stratified flow over extended finite-amplitude topography; this flow configuration is most relevant to atmospheric applications (Baines 1987) and is also the subject of the present study. The approach of KA generalizes Long's model by allowing for slightly unsteady disturbances with the proviso that wave breaking is not present. Within this framework, it is

then possible to examine the realizability of Long's steady states for subcritical topography amplitudes (below that required to cause overturning).

The problem of stratified flow of large depth over topography has also been studied extensively through direct numerical simulations. These studies solve the full Euler equations of motion in a finite computational domain, imposing the radiation condition at the upper boundary via a 'sponge layer', and are not limited to flow conditions that preclude wave breaking.

Specifically, Clark & Peltier (1977), Pierrehumbert & Wyman (1985) and Laprise & Peltier (1989*a*,*b*), among others, concentrate on two-dimensional Boussinesq flow with constant velocity and Brunt–Väisälä frequency far upstream past the algebraic mountain ('Witch of Agnesi'). They all appear to agree that the steady state furnished by Long's model is reached as long as the amplitude of the topography is subcritical. In another numerical study of the same problem, however, Pierrehumbert & Bacmeister (1987) find that instability may occur at a slightly subcritical (about 5%) topography amplitude owing to convective overturning induced by transient effects. Moreover, the simulations of Laprise & Peltier (1989*a*,*b*) reveal that the dominant instability mechanism even for slightly supercritical topography is of a shear-flow type, owing to the steepening of streamlines of the background flow over the topography.

Pierrehumbert & Bacmeister (1987) also discussed the assumption of no upstream influence in the context of related experimental observations by Baines & Hoinka (1985). The experiments were conducted in a novel apparatus to simulate an infinite medium, and revealed upstream motions at significantly subcritical amplitudes, suggesting that Long's model ceases to be valid at relatively low obstacle steepness. In their numerical simulations,

however, Pierrehumbert & Bacmeister (1987) did not observe any permanent alterations in the upstream flow field, and cautioned that slowly varying transient disturbances could be mistaken for true upsteam influence.

In this chapter, we shall discuss the dynamics of nonlinear stratified flow over topography on the basis of the asymptotic theory of KA. We concentrate on the simplest case of uniformly stratified hydrostatic flow of large depth over the algebraic mountain which, as already mentioned, has also been explored in previous numerical work. There is, in fact, numerical evidence that this flow quickly evolves into a quasi-steady Long state as long as the topography amplitude is not highly supercritical (Pierrehumbert & Bacmeister 1987); the flow dynamics is then controlled by slowly varying disturbances, making the asymptotic theory most relevant.

The ensuing analysis centres on two main issues: the stability of Long's steady state for subcritical topography amplitudes and the long-time behaviour of the flow in case this state is unstable. Based on the evolution equations derived in KA, a linear stability analysis of Long's state to infinitesimal modulations is carried out first. Instability sets in at a topography amplitude well below (by about 25%) the critical value for overturning, owing to a shear-flow mechanism brought about by the steepening of streamlines of the steady flow over the topography. The transient flow development in the unstable régime is then studied by integrating the evolution equations numerically, starting from rest. The effect of instability turns out to be rather subdued: the flow oscillates slowly about the corresponding Long steady state and no transient breaking is found for subcritical topography amplitudes within 10% of the critical value. These findings are discussed in connection with previous related work at the end of the chapter.

## 2.2 Preliminaries

Consider the flow of an inviscid, incompressible, vertically unbounded stratified fluid past a two-dimensional obstacle having peak height $h$ and horizontal dimension $L$. Far upstream of the topography, the fluid is assumed to have uniform stratification (constant Brunt–Väisälä frequency $N_0$) and constant velocity $U_0$, as shown in figure 2-1. The acceleration due to gravity is denoted by $g$. These flow quantities may be combined to yield three non-dimensional parameters:

$$\mu = \frac{U_0}{N_0 L}, \qquad \beta = \frac{N_0 U_0}{g}, \qquad \epsilon = \frac{N_0 h}{U_0}.$$

Here $\mu$ measures dispersive effects, $\beta$ is the Boussinesq parameter which is a measure of stratification, and $\epsilon$ controls nonlinear effects.

Scaling the horizontal (streamwise) coordinate $x$ with $L$, the vertical coordinate $y$ with $U_0/N_0$ and time $t$ with $L/U_0$, the governing equations of incompressibility, mass conservation and momentum balance may be cast in non-dimensional form as

$$\boldsymbol{\nabla} \cdot \boldsymbol{u} = 0, \tag{2.1}$$

$$\rho_t + \boldsymbol{u} \cdot \boldsymbol{\nabla}\rho = 0, \tag{2.2}$$

$$\beta\rho(\boldsymbol{u}_t + \boldsymbol{u} \cdot \boldsymbol{\nabla}\boldsymbol{u}) = -\left(p_x,\ \mu^{-2}(\rho + p_y)\right), \tag{2.3}$$

where $\boldsymbol{u} = (u, v)$ is the velocity field, and $p$ and $\rho$ are the pressure and density respectively. The boundary condition of zero normal velocity on the topography $y = \epsilon f(x,t)$ is

$$v = \epsilon(u f_x + f_t) \qquad (y = \epsilon f). \tag{2.4}$$

The asymptotic theory of KA describes the dynamics of finite-amplitude, long-wave disturbances in a Boussinesq fluid. In terms of the non-dimensional parameters introduced

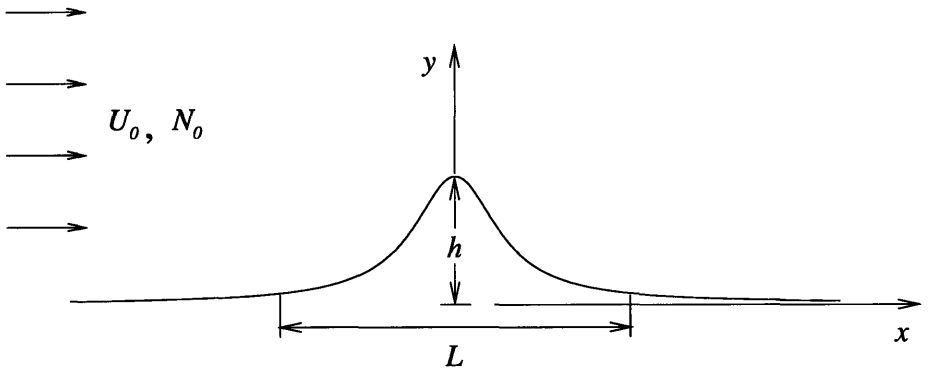


FIGURE 2-1. Schematic of the flow geometry for large-depth flow.

above, this régime corresponds to $\mu \ll 1$, $\beta \to 0$, $\epsilon = O(1)$. Here we shall only outline the salient features of the theory; details may be found in the original paper.

The theory is motivated by the observation that, in the hydrostatic limit ($\mu \to 0$), Long's steady state consists of a long-wave mode with vertical wavenumber equal to unity. The corresponding group velocity vanishes in the reference frame of the obstacle; energy is therefore trapped near the topography and the transient response is expected to develop slowly. This resonance suggests that the long-time response takes the form of a slowly varying Long state, in line with the results of numerical simulations noted earlier (Pierrehumbert & Bacmeister 1987).

Accordingly, the streamfunction $\psi(x, y, T)$ is posed as

$$\psi \sim \psi^{(0)} = y + (A\,\mathrm{e}^{\mathrm{i}y} + \text{c.c.}). \tag{2.5}$$

Here $A(x, Y, T) = a + \mathrm{i}b$ denotes the complex envelope of the resonant long-wave mode; it accounts for the evolution of the disturbance in terms of the 'slow' time $T = \mu^2 t$ and the 'stretched' vertical coordinate $Y = \mu^2 y$. As explained in KA, one may obtain evolution

equations for the real amplitudes $a$ and $b$ following a perturbation procedure, and thereby describe the long-time dynamics of the flow through (2.5).

Briefly, deriving these amplitude equations makes use of the fact that, if one neglects transient effects altogether, the density $\rho$ and the quantity

$$S = \rho\psi_{yy} + \rho_\psi \left(\frac{y}{\beta} + \tfrac{1}{2}\psi_y^2\right) \tag{2.6}$$

remain constant along streamlines. This suggests replacing the coordinate $y$ by $\psi$:

$$(x, y, T) \to (x, \psi, T)$$

on the condition that no flow reversal (wave breaking) is present in the flow field. The mass-conservation equation (2.2) then takes the form

$$\psi_y \rho_x|_\psi = -\mu^2 \rho_T, \tag{2.7}$$

and the momentum equations (2.3) can be manipulated to

$$\psi_y S_x|_\psi = \mu^2 \left\{\rho(\psi_x\psi_{xy} - \psi_y\psi_{xx})\right\}_x - \mu^2(\rho\psi_{yT})_y + \left\{\rho_x|_\psi \left(\frac{y}{\beta} + \tfrac{1}{2}\psi_y^2\right)\right\}_y, \tag{2.8}$$

where $|_\psi$ indicates that $\psi$ is held fixed.

Using the upstream conditions of uniform stratification and constant velocity and invoking the Boussinesq approximation $\beta \to 0$, (2.7) and (2.8) may be integrated to yield

$$\rho = \rho_0(\psi) - \mu^2 \rho_{0\psi} \int_{-\infty}^{x} \left.\frac{\psi_T}{\psi_y}\right|_\psi \mathrm{d}x', \tag{2.9}$$

$$S = -\rho_0(\psi)\psi - \mu^2 \rho_0(\psi)\psi_{xx} - \mu^2 \int_{-\infty}^{x} \left.\frac{R}{\psi_y}\right|_\psi \mathrm{d}x' \tag{2.10}$$

with $$R = \rho_0(\psi)\left\{\psi_{yyT} - (y\psi_T/\psi_y)_y\right\},$$

$\rho_0(y)$ being the (known) density upstream.

Making use of (2.6) and (2.9), (2.10) may be rearranged as

$$\psi_{yy} + (\psi - y) = \mu^2(H - \psi_{xx}), \tag{2.11}$$

where

$$H = \frac{\partial}{\partial\psi}\int_{-\infty}^{x}\left\{y\frac{\psi_T}{\psi_y} - \psi_{yT}\right\}\Bigg|_{\psi} \mathrm{d}x' - y\frac{\partial}{\partial\psi}\int_{-\infty}^{x}\frac{\psi_T}{\psi_y}\Bigg|_{\psi}\mathrm{d}x'.$$

As expected, if transient effects (the term involving $H$ above) are neglected, (2.11) becomes linear and Long's steady-flow model is recovered.

To describe the flow evolution, we work with (2.11) and follow a multiple-scale perturbation procedure: the streamfunction $\psi$ is expanded as

$$\psi = \psi^{(0)} + \mu^2\psi^{(1)} + \cdots,$$

where $\psi^{(0)}$ is the slowly modulated Long's solution (2.5) proposed earlier on physical grounds. In terms of the envelope $A = a + ib$, the boundary condition (2.4) on the topography is also cast in the form (to leading order in $\mu$)

$$a\cos\epsilon f - b\sin\epsilon f = -\tfrac{1}{2}\epsilon f \qquad (Y = 0). \tag{2.12}$$

At the next order in $\mu$, the following equation is obtained

$$\psi^{(1)}_{yy} + \psi^{(1)} = H^{(0)} - \psi^{(0)}_{xx} - 2\psi^{(0)}_{yY}, \tag{2.13}$$

where the superscript $^{(0)}$ indicates that the quantity is to be evaluated using the known expression (2.5) for $\psi^{(0)}$. The desired evolution equations for the amplitudes $a(x, Y, T)$ and $b(x, Y, T)$ are then obtained by imposing secularity conditions on the right-hand side of (2.13):

$$\frac{1}{4\pi}\int_0^{2\pi} H^{(0)}\cos y\,\mathrm{d}y - \tfrac{1}{2}a_{xx} + b_Y = 0, \tag{2.14a}$$

$$\frac{1}{4\pi}\int_0^{2\pi} H^{(0)}\sin y\,\mathrm{d}y + \tfrac{1}{2}b_{xx} + a_Y = 0. \tag{2.14b}$$

As already indicated, we shall focus on purely hydrostatic flow, in which case the dispersive terms involving $a_{xx}, b_{xx}$ in (2.14) are dropped. Furthermore, based on the assumption made earlier that precludes wave breaking, the flow field described by (2.5) is such that $y$ is defined uniquely as a function of $\psi^{(0)}$, $y = y(\psi^{(0)};\, a, b)$, and one may replace the $y$-integrations with $\psi^{(0)}$-integrations in (2.14). After this change of integration variable is implemented and one differentiation with respect to $x$, (2.14) reduce to

$$K_{11}^c a_T + K_{12}^c b_T + b_{xY} + \int_{-\infty}^{x} \mathrm{d}x' \left(K_{11x} a_T' + K_{12x} b_T'\right) = 0, \tag{2.15a}$$

$$K_{21}^c a_T + K_{22}^c b_T - a_{xY} + \int_{-\infty}^{x} \mathrm{d}x' \left(K_{21x} a_T' + K_{22x} b_T'\right) = 0. \tag{2.15b}$$

Here the kernels $K_{11}, \ldots, K_{22}$ are defined by

$$K_{11}(x,x') = \frac{1}{8\pi}\int_0^{2\pi} \mathrm{d}\psi^{(0)} y_a \left(y_a' + (y'y_a')_{\psi^{(0)}} - y y_{a\psi^{(0)}}'\right), \tag{2.16a}$$

$$K_{12}(x,x') = \frac{1}{8\pi}\int_0^{2\pi} \mathrm{d}\psi^{(0)} y_a \left(y_b' + (y'y_b')_{\psi^{(0)}} - y y_{b\psi^{(0)}}'\right), \tag{2.16b}$$

$$K_{21}(x,x') = \frac{1}{8\pi}\int_0^{2\pi} \mathrm{d}\psi^{(0)} y_b \left(y_a' + (y'y_a')_{\psi^{(0)}} - y y_{a\psi^{(0)}}'\right), \tag{2.16c}$$

$$K_{22}(x,x') = \frac{1}{8\pi}\int_0^{2\pi} \mathrm{d}\psi^{(0)} y_b \left(y_b' + (y'y_b')_{\psi^{(0)}} - y y_{b\psi^{(0)}}'\right), \tag{2.16d}$$

with the notation that primed variables are functions of $x'$, and $K_{11}^c \equiv K_{11}(x,x), \ldots,$ $K_{22}^c \equiv K_{22}(x,x)$.

Equations (2.15) subject to the boundary condition (2.12) and appropriate initial conditions govern the evolution of $a$ and $b$ (and hence the dynamics of the flow through (2.5))

as long as no wave breaking is present; this is indeed the case if

$$a^2 + b^2 < \tfrac{1}{4} \tag{2.17}$$

throughout the flow field.

As discussed in KA, Long's steady flow (in the hydrostatic limit) corresponds to a particular steady-state solution of (2.15), $\overline{A} = \overline{a} + \mathrm{i}\overline{b}$, with no modulation in $Y$:

$$\overline{A}(x;\epsilon) = \overline{a} - \mathrm{i}\,\mathcal{H}\{\overline{a}\}, \tag{2.18}$$

where $$\mathcal{H}\{\overline{a}\} = \frac{1}{\pi}\int_{-\infty}^{\infty} \frac{\overline{a}(s)}{s-x}\mathrm{d}s$$

stands for the Hilbert transform of $\overline{a}$. Imposing the boundary condition (2.12) then determines $\overline{a}(x;\epsilon)$ through the integral equation

$$\overline{a}\cos\epsilon f + \mathcal{H}\{\overline{a}\}\sin\epsilon f = -\tfrac{1}{2}\epsilon f. \tag{2.19}$$

As the topography amplitude is increased, there generally is a critical value of $\epsilon$ above which $\overline{A}$ is such that condition (2.17) is violated, so Long's steady flow features density inversions and flow reversals. In this study, attention is confined to the algebraic mountain (also known as 'Witch of Agnesi'),

$$f(x) = \frac{1}{1+x^2},$$

for which this critical overturning amplitude is $\epsilon = 0.85$ (Miles & Huppert 1969).

## 2.3 Stability analysis

The goal now is to examine the stability of Long's steady flow in the hydrostatic limit on the basis of the asymptotic theory. To this end, we write

$$\psi^{(0)} = \overline{\psi} + \widetilde{\psi}, \qquad A = \overline{A}(x;\epsilon) + \widetilde{A}(x,Y,T), \tag{2.20}$$

where $\overline{A}$ corresponds to Long's hydrostatic steady state $\overline{\psi}(x,y)$, as obtained from (2.5), (2.18) and (2.19), and $\widetilde{A} = \widetilde{a} + \mathrm{i}\widetilde{b}$ to a small perturbation $\widetilde{\psi}(x,y,T)$. Substituting (2.20) into (2.15) and linearizing, the perturbation equations are

$$\overline{K}^c_{11}\widetilde{a}_T + \overline{K}^c_{12}\widetilde{b}_T + \widetilde{b}_{xY} + \int_{-\infty}^{x} \mathrm{d}x' \left(\overline{K}_{11x}\widetilde{a}'_T + \overline{K}_{12x}\widetilde{b}'_T\right) = 0, \tag{2.21a}$$

$$\overline{K}^c_{21}\widetilde{a}_T + \overline{K}^c_{22}\widetilde{b}_T - \widetilde{a}_{xY} + \int_{-\infty}^{x} \mathrm{d}x' \left(\overline{K}_{21x}\widetilde{a}'_T + \overline{K}_{22x}\widetilde{b}'_T\right) = 0, \tag{2.21b}$$

where the kernels are evaluated in terms of the known steady state (as indicated by the overbar). Moreover, the boundary condition (2.12) yields

$$\widetilde{a}\cos\epsilon f - \widetilde{b}\sin\epsilon f = 0 \qquad (Y = 0). \tag{2.22}$$

Some insight into the stability problem is gained by looking at the behaviour of perturbations at a long distance from the topography ($x \to \pm\infty$). In this limit, Long's steady flow approaches a uniform stream ($\overline{a},\ \overline{b} \to 0$), so $\overline{K}^c_{11},\ \overline{K}^c_{22} \to 1$ and $\overline{K}^c_{12},\ \overline{K}^c_{21} \to 0$ while the $x$-derivatives of the kernels go to zero. Consequently, equations (2.21) and the boundary condition (2.22) reduce to

$$\widetilde{a}_T + \widetilde{b}_{xY} = 0, \qquad \widetilde{b}_T - \widetilde{a}_{xY} = 0 \tag{2.23a, b}$$

and

$$\widetilde{a} = 0 \qquad (Y = 0). \tag{2.24}$$

This simplified system admits separable solutions,

$$\widetilde{a} = \sin mY \exp(\mathrm{i}\xi x + \sigma T), \qquad \widetilde{b} = \cos mY \exp(\mathrm{i}\xi x + \sigma T), \tag{2.25}$$

where $m$ is real and $\sigma = \mathrm{i}m\xi$. These modes correspond to internal-wave disturbances on a uniformly stratified stream over a flat rigid bottom; they are neutral propagating waves if $\xi$ is real and unstable evanescent waves if $\xi$ is complex.

Returning now to the full stability problem (2.21), (2.22), note that, even though both $T$ and $Y$ do not appear explicitly in equations (2.21) ($\overline{K}_{11}, \ldots, \overline{K}_{22}$ depend on $x$ alone), only the time dependence can be separated out; this complication arises from the boundary condition (2.22) on $Y = 0$ and is a consequence of the fact that Long's steady flow is not parallel for finite topography amplitude. Accordingly, we consider normal- mode disturbances proportional to $\exp(\sigma T)$ that are not separable in $Y$. As $x \to \pm\infty$, however, each of these modes may be expressed in terms of the (complete) set of separable solutions (2.25). Therefore, an unstable mode ($\mathrm{Re}\,\sigma > 0$) consists of evanescent waves ($\xi = -\mathrm{i}\sigma/m$ is complex) both far upstream and downstream, and a necessary condition for instability is the existence of modes that are trapped[†] over the topography (i.e., decay to zero as $x \to \pm\infty$).

On physical grounds, it is expected that no trapped modes exist when the topography is mild ($\epsilon \ll 1$) and the background flow deviates only slightly from a uniform stream. On the other hand, it would be interesting to know whether such modes become possible above a certain finite value of $\epsilon$ less than the critical overturning amplitude; in such a case, Long's steady flow would be unstable to modulations before static instability sets in.

This question is addressed by first looking for trapped modes of the stability equations

[†]These modes are distinct from the ones described by Laprise & Peltier (1989*a*) as trapped: in that study, the modes were trapped in the vertical direction between the ground and the steepest streamline.

(2.21) alone, ignoring the boundary condition (2.22), so the dependence on both $T$ and $Y$ can be separated out. It is then demonstrated that the critical value of $\epsilon$ for modulational instability obtained from this simplified modal analysis is somewhat lower than the critical topography amplitude predicted on the basis of the full stability problem (see §2.4).

We now seek separable normal-mode solutions of equations (2.21):

$$\left\{ \begin{array}{c} \widetilde{a} \\ \widetilde{b} \end{array} \right\} = \mathrm{Re} \left\{ \begin{array}{c} \mathcal{A}(x) \\ \mathcal{B}(x) \end{array} \right\} \mathrm{e}^{\mathrm{i}mY} \, \mathrm{e}^{\lambda m T}, \tag{2.26}$$

where $m$ is the (real) vertical wavenumber and $\sigma = \lambda m$ is the possibly complex growth rate. The system (2.21) is then transformed to

$$\overline{K}^c_{11}\mathcal{A} + \overline{K}^c_{12}\mathcal{B} - \mathrm{i}\frac{1}{\lambda}\mathcal{B}_x + \int_{-\infty}^{x} \mathrm{d}x' \left( \overline{K}_{11x}\mathcal{A}' + \overline{K}_{12x}\mathcal{B}' \right) = 0, \tag{2.27a}$$

$$\overline{K}^c_{21}\mathcal{A} + \overline{K}^c_{22}\mathcal{B} + \mathrm{i}\frac{1}{\lambda}\mathcal{A}_x + \int_{-\infty}^{x} \mathrm{d}x' \left( \overline{K}_{21x}\mathcal{A}' + \overline{K}_{22x}\mathcal{B}' \right) = 0. \tag{2.27b}$$

Furthermore, at a long distance from the topography, it follows from (2.23) that

$$\left\{ \begin{array}{c} \mathcal{A} \\ \mathcal{B} \end{array} \right\} \sim \left\{ \begin{array}{c} 1 \\ \pm\mathrm{i} \end{array} \right\} \mathrm{e}^{\pm\lambda x} \qquad (|x| \to \infty). \tag{2.28}$$

We thus have an eigenvalue problem for $\mathcal{A}(x)$ and $\mathcal{B}(x)$ with a possibly 'mixed' spectrum: for purely imaginary values of the eigenvalue parameter $\lambda$, equations (2.27) have solutions that correspond to neutrally stable radiating waves according to (2.26), (2.28) for all $\epsilon$. Apart from this continuous spectrum, however, when $\epsilon$ exceeds a certain critical value, there may exist a discrete spectrum comprising a finite number of complex eigenvalues (if $\lambda$ is an eigenvalue so is $-\lambda^*$) for which $\mathcal{A}(x)$ and $\mathcal{B}(x)$ decay exponentially as $|x| \to \infty$ and correspond to trapped modes; hence, the existence of a discrete spectrum is a necessary condition for instability.

A search for trapped modes was made by numerically solving equations (2.27), subject to the boundary conditions

$$\mathcal{A}(x) \to 0 \quad (x \to \infty), \qquad \mathcal{B}(x) \to 0 \quad (x \to -\infty). \tag{2.29}$$

The numerical procedure uses finite differences on a non-uniform grid, allowing for finer resolution close to the topography. The derivatives $\mathcal{A}_x$ and $\mathcal{B}_x$ are evaluated by first-order forward and backward differences respectively, and the boundary conditions (2.29) are imposed at the ends of the computational domain. The hydrostatic Long's steady state is determined from (2.18), (2.19) using the procedure described by Lilly & Klemp (1979), and the kernels are computed as follows. Based on the assumption that there is no breaking streamline, $y = y(\psi^{(0)}; a, b,)$ is first determined by inverting (2.5) numerically using Newton–Raphson iteration; all the quantities in the integrals over $\psi^{(0)}$ for the kernels (2.16) are then known as functions of $(\psi^{(0)}; a, b)$ and the integrals are evaluated by the trapezoidal rule. The $x$-derivatives of the kernels are evaluated using centred differences. Finally, the integrals in (2.27) are computed using the trapezoidal rule.

This leads to a standard generalized matrix eigenvalue problem,

$$[C]\{z\} = \lambda[E]\{z\}.$$

Estimates of the spectrum were first generated for several topography amplitudes using a global eigenvalue solver, to obtain a rough approximation to the critical value of $\epsilon$ and the discrete eigenvalues. More refined approximations to these eigenvalues were then found by inverse iteration with shifting (see Appendix A for details).

The real part of the most unstable (discrete) eigenvalue is plotted as a function of $\epsilon$ in figure 2-2. Indeed, there is a critical value of $\epsilon$, less than the overturning amplitude

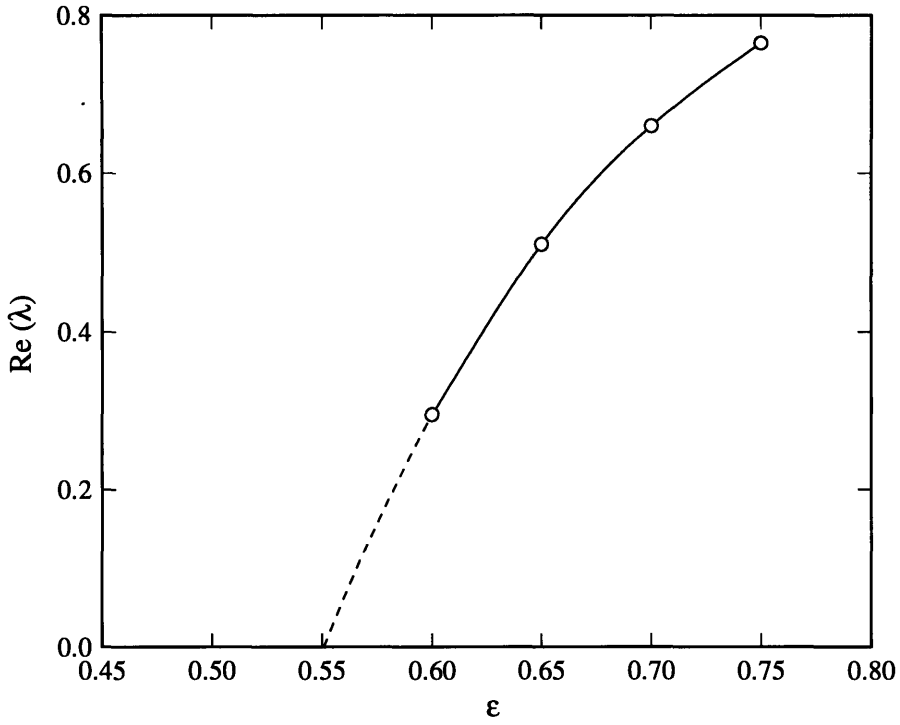


FIGURE 2-2. The real part of the most unstable eigenvalue $\lambda$ of the discrete spectrum (corresponding to a trapped mode) as a function of $\epsilon$.

$\epsilon = 0.85$, above which trapped modes become possible. The mode shapes $\mathcal{A}(x)$ and $\mathcal{B}(x)$ (normalized such that $\mathcal{A} = 1$ where $|\mathcal{A}|$ attains its maximum) for the case $\epsilon = 0.7$ are plotted in figure 2-3. Both the real and imaginary parts are clearly trapped close to the topography and they exhibit significant structure, especially on the upstream side of the obstacle. The scale over which the trapping occurs decreases rapidly with $\epsilon$. Close to conditions that instability sets in, the unstable modes are barely trapped, and determining the critical value of $\epsilon$ accurately is difficult. On the basis of figure 2-2, by extrapolation, we estimate that instability occurs for topography amplitudes above $\epsilon \approx 0.55$.

In terms of these trapped modes, it is straightforward to construct more general solutions to the perturbation equations (2.21) that represent locally confined unstable disturbances.

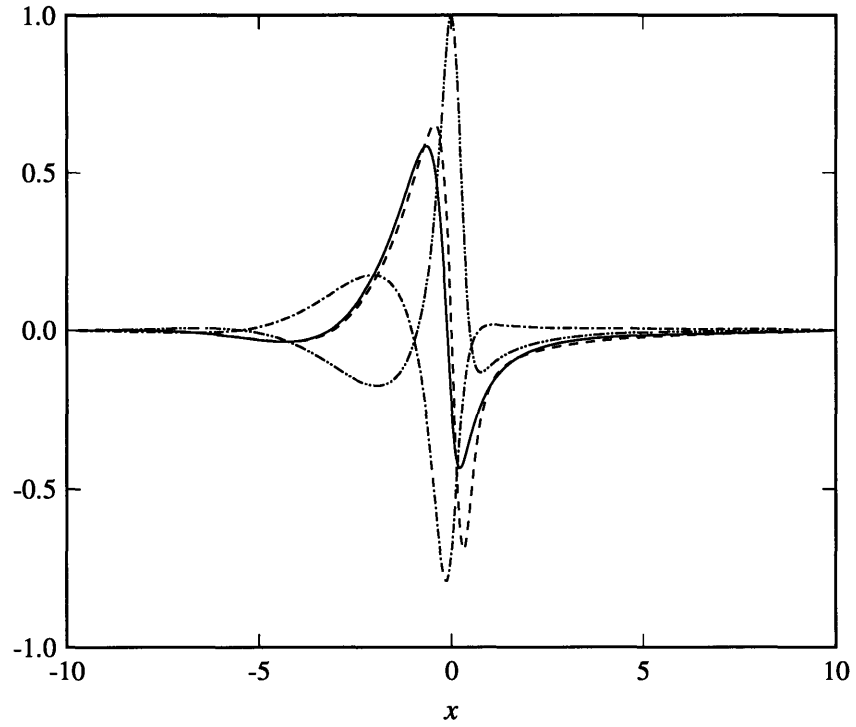


FIGURE 2-3. The dependence of the mode shapes $\mathcal{A}$ and $\mathcal{B}$ on $x$ when $\epsilon = 0.7$ ($\mathrm{Re}(\mathcal{A})$ : $-\cdots-$, $\mathrm{Im}(\mathcal{A})$: $---$, $\mathrm{Re}(\mathcal{B})$: ——, $\mathrm{Im}(\mathcal{B})$: $-\cdot-\cdot$). The trapping of the modes in the streamwise direction is evident.

For example, choosing a Gaussian distribution of vertical wavenumber $m$, superposition of the modes (2.26) yields

$$\left\{ \begin{array}{c} \widetilde{a} \\ \widetilde{b} \end{array} \right\} = \mathrm{Re} \left\{ \begin{array}{c} \mathcal{A}(x) \\ \mathcal{B}(x) \end{array} \right\} \int_{-\infty}^{\infty} \mathrm{d}m \, \mathrm{e}^{\lambda m T} \, \mathrm{e}^{-\frac{1}{4}m^2} \, \mathrm{e}^{-\mathrm{i}mY}. \tag{2.30}$$

It then follows that

$$\left\{ \begin{array}{c} \widetilde{a} \\ \widetilde{b} \end{array} \right\} \propto \mathrm{e}^{\lambda_r^2 T^2} \exp\left(-(\lambda_i T - Y)^2\right) \mathrm{Re} \left\{ \begin{array}{c} \mathcal{A}\mathrm{e}^{\mathrm{i}\phi} \\ \mathcal{B}\mathrm{e}^{\mathrm{i}\phi} \end{array} \right\},$$

where $\lambda = \lambda_r + \mathrm{i}\lambda_i$ and $\phi = 2\lambda_r T(\lambda_i T - Y)$. It may be shown that the kinetic energy of this perturbation grows like $\exp(2\lambda_r^2 T^2)$ at large $T$, so the flow can be violently unstable when $\epsilon$ exceeds the critical value above which trapped modes exist.

Expression (2.30) was also used to check the results of the modal analysis by imposing on

Long's steady state an initial disturbance that is Gaussian in $Y$ and whose variation along $x$ is given by the calculated trapped eigenmode. Using the numerical method outlined in the next section, this perturbation was then tracked in time and the result was found to agree very well with (2.30), verifying the computed modes and eigenvalues.

The critical topography amplitude for modulational instability ($\epsilon \approx 0.55$) deduced from modal analysis of equations (2.21) is well below the critical overturning amplitude $\epsilon = 0.85$. As already noted, however, the separable modes (2.26) are not consistent with the boundary condition (2.22) on the topography; moreover, it is not clear that they can be combined to satisfy (2.22) by superposition.

To examine the influence of the wall on the threshold for modulational instability, one may compute trapped modes of the full stability problem (2.21), (2.22). The associated eigenvalue problem is not separable in $Y$, however, and extensive numerical work is needed. Instead, we shall follow a more direct approach and solve (2.21), (2.22) numerically as an initial-value problem for a locally confined initial disturbance.

## 2.4 Evolution of a localized perturbation

### *2.4.1 Energy budget*

In tracking the development of a disturbance numerically, it is useful to monitor the energetics of the flow. This is achieved by means of an energy-balance equation which also adds to the understanding of the instability mechanism by bringing out the energy exchange between the perturbation and the background steady flow.

To derive the desired equation for the energy of the perturbation, we write the flow

variables as the sum of a steady mean representing Long's hydrostatic steady flow and a time-dependent small perturbation:

$$\boldsymbol{u} = \overline{\boldsymbol{u}} + \widetilde{\boldsymbol{u}}, \qquad \rho = \overline{\rho} + \widetilde{\rho}, \qquad p = \overline{p} + \widetilde{p}.$$

Upon substitution into the equations of motion (2.1)–(2.3), invoking the Boussinesq approximation ($\beta \to 0$), and linearizing, the following perturbation equations are obtained in the hydrostatic limit ($\mu \to 0$):

$$\boldsymbol{\nabla} \cdot \widetilde{\boldsymbol{u}} = 0, \tag{2.31}$$

$$\widetilde{\rho}_t + \overline{\boldsymbol{u}} \cdot \boldsymbol{\nabla}\widetilde{\rho} + \widetilde{\boldsymbol{u}} \cdot \boldsymbol{\nabla}\overline{\rho} = 0, \tag{2.32}$$

$$\widetilde{\boldsymbol{u}}_t + \overline{\boldsymbol{u}} \cdot \nabla\widetilde{u} + \widetilde{\boldsymbol{u}} \cdot \nabla\overline{u} = -\frac{1}{\beta}\widetilde{p}_x, \tag{2.33$a$}$$

$$\widetilde{\rho} = -\widetilde{p}_y, \tag{2.33$b$}$$

where $\overline{\boldsymbol{u}} = (\overline{u}, \overline{v})$ and $\widetilde{\boldsymbol{u}} = (\widetilde{u}, \widetilde{v})$.

Now, multiplying (2.33$a$) with $\widetilde{u}$, (2.33$b$) with $\widetilde{v}/\beta$ and adding, using (2.31), one has

$$\tfrac{1}{2}(\widetilde{u}^2)_t + \tfrac{1}{2}\boldsymbol{\nabla} \cdot (\overline{\boldsymbol{u}}\widetilde{u}^2) + \widetilde{u}(\widetilde{u}\overline{u}_x + \widetilde{v}\overline{u}_y) + \frac{1}{\beta}(\widetilde{\rho}\widetilde{v} + \boldsymbol{\nabla} \cdot (\widetilde{p}\widetilde{\boldsymbol{u}})) = 0.$$

Intergrating this equation over the entire fluid domain ($-\infty < x < \infty$, $\epsilon f < y < \infty$) and using the boundary conditions (the normal velocity must vanish on $y = \epsilon f$ and the perturbations vanish at infinity) then yields

$$\frac{\mathrm{d}}{\mathrm{d}t}(\mathrm{KE} + \mathrm{PE}) = \mathcal{R}, \tag{2.34}$$

where

$$\frac{\mathrm{d}}{\mathrm{d}t}\mathrm{KE} = \frac{1}{2}\frac{\mathrm{d}}{\mathrm{d}t}\int_{-\infty}^{\infty}\mathrm{d}x\int_{\epsilon f}^{\infty}\mathrm{d}y\,\widetilde{u}^2$$

is the rate of change of the kinetic energy of the perturbation and

$$\frac{\mathrm{d}}{\mathrm{d}t}\mathrm{PE} = \frac{1}{\beta}\int_{-\infty}^{\infty}\mathrm{d}x\int_{\epsilon f}^{\infty}\mathrm{d}y\,\widetilde{\rho}\widetilde{v}$$

is the rate of change of the potential energy of the perturbation. The term on the right-hand side of (2.34),

$$\mathcal{R} = -\int_{-\infty}^{\infty}\mathrm{d}x\int_{\epsilon f}^{\infty}\mathrm{d}y\,\widetilde{u}\,(\widetilde{u}\overline{u}_x + \widetilde{v}\overline{u}_y),$$

is the rate of work done by the Reynolds stresses. Depending on the sign of this term, power flows either from the mean flow to the perturbation or in the opposite direction.

Returning now to the asymptotic theory, equation (2.34) translates into an equivalent energy-balance equation in terms of the envelope variables. Specifically, with the same notation as in (2.20), one has to leading order in $\mu$ (consistent with the evolution equations (2.21) and the boundary condition (2.22))

$$\frac{\mathrm{d}}{\mathrm{d}t}\mathrm{KE} = \frac{\mathrm{d}}{\mathrm{d}T}\left\langle\widetilde{a}^2 + \widetilde{b}^2\right\rangle, \tag{2.35$a$}$$

$$\frac{\mathrm{d}}{\mathrm{d}t}\mathrm{PE} = -\frac{1}{2\pi}\left\langle\int_{-\infty}^{x}\mathrm{d}x'\int_0^{2\pi}\mathrm{d}\overline{\psi}\left(\widetilde{a}_x y_{\overline{a}} + \widetilde{b}_x y_{\overline{b}}\right)\left(\widetilde{a}'_T y'_{\overline{a}} + \widetilde{b}'_T y'_{\overline{b}}\right)\right\rangle, \tag{2.35$b$}$$

where

$$\langle\cdot\rangle \equiv \int_{-\infty}^{\infty}\mathrm{d}x\int_0^{\infty}\mathrm{d}Y(\cdot).$$

Similarly, the power-input term on the right-hand side of (2.34) takes the form

$$\mathcal{R} = -2\epsilon\int_{-\infty}^{\infty}\mathrm{d}x f_x\left(\widetilde{a}\sin\epsilon f + \widetilde{b}\cos\epsilon f\right)^2\Big|_{Y=0} + \langle P(x,Y,T)\rangle, \tag{2.35$c$}$$

where

$$P = \frac{1}{2\pi}\int_0^{2\pi}\mathrm{d}\overline{\psi}\,\overline{\psi}_y\overline{H}\left\{\left(\widetilde{a}_x\overline{b} - \widetilde{b}\overline{a}_x\right)y_{\overline{a}}^2 + \left(\widetilde{a}\overline{b}_x - \overline{a}\widetilde{b}_x\right)y_{\overline{b}}^2 - \left(\widetilde{a}_x\overline{a} - \overline{b}\widetilde{b}_x - \widetilde{a}\overline{a}_x + \widetilde{b}\overline{b}_x\right)y_{\overline{a}}y_{\overline{b}}\right\}$$

and

$$\overline{H} = -\frac{\partial}{\partial\overline{\psi}}\int_{-\infty}^{x}\mathrm{d}x'y'\left(\widetilde{a}'_T y'_{\overline{a}}+\widetilde{b}'_T y'_{\overline{b}}\right)-\int_{-\infty}^{x}\mathrm{d}x'\left(\widetilde{a}'_T y'_{\overline{a}}+\widetilde{b}'_T y'_{\overline{b}}\right)$$
$$+\,y\,\frac{\partial}{\partial\overline{\psi}}\int_{-\infty}^{x}\mathrm{d}x'\left(\widetilde{a}'_T y'_{\overline{a}}+\widetilde{b}'_T y'_{\overline{b}}\right).$$

Details of deriving expressions (2.35) are given in Appendix C.

In particular, when the topography amplitude is small ($\epsilon \ll 1$), it follows from (2.35$a,b$) that

$$\frac{\mathrm{d}}{\mathrm{d}t}\mathrm{PE} \sim \frac{\mathrm{d}}{\mathrm{d}t}\mathrm{KE},$$

while $\mathcal{R}$ is negligible according to (2.35$c$), to leading order. Hence, (2.34) implies that

$$\frac{\mathrm{d}}{\mathrm{d}T}\left\langle\widetilde{a}^2+\widetilde{b}^2\right\rangle = 0,$$

consistent with the simplified problem (2.23), (2.24).

### *2.4.2 Numerical solution*

We next turn our attention to the numerical treatment of the initial-value problem for the evolution of a perturbation. Equations (2.21) are discretized by an explicit finite-difference method combined with Euler forward time stepping. A grid with non-uniform spacing in both $x$ and $Y$ is used to capture the details of the disturbance close to the topography. The kernels are evaluated numerically as described in §2.3, taking great care to ensure that they are well resolved by the grid. All spatial derivatives are computed to second-order accuracy and the integrals are evaluated by the trapezoidal rule.

At each time step, the computation is commenced on $j = 1$, where $j$ denotes the grid node number along $Y$, $j = 0$ corresponding to the boundary $Y = 0$. Using the simplified equations (2.23) that are valid far upstream, the values of $\widetilde{a}$ and $\widetilde{b}$ at the left boundary are determined first, and the entire $x$–$Y$ plane ($j \geq 1$) is then covered by consecutive $x$-sweeps.

Numerical-stability constraints dictate that the boundary condition (2.22) be applied on $j = 0$ by an implicit method: by evaluating on $j = 1$ the terms involving $\widetilde{a}_{xY}$ and $\widetilde{a}_T$, $\widetilde{a}|_{j=0}$ is eliminated from (2.21*b*), and the resulting tridiagonal system is solved to obtain $\widetilde{b}|_{j=0}$; the boundary condition (2.22) is then used to calculate $\widetilde{a}|_{j=0}$. Despite the fact that this procedure was numerically stable for moderate values of $\epsilon$, small grid-scale oscillations were observed along $Y$ when $\epsilon$ was increased beyond 0.6 or so. Since this instability appeared to be very gentle, it was eliminated by using the 5-point smoothing stencil described by Shapiro (1975):

$$f_j = \tfrac{1}{16}(-f_{j-2} + 4f_{j-1} + 10f_j + 4f_{j+1} - f_{j+2}).$$

In a typical run of 2000 time steps, smoothing was applied every 100 steps. Moreover, the results were found to be virtually unaffected by cutting in half the number of times that smoothing was performed.

In implementing the above numerical procedure, the grid size used close to the topography varied from $\Delta X = 0.1$, $\Delta Y = 0.1$ for $\epsilon \leq 0.6$ to $\Delta X = 0.025$, $\Delta Y = 0.1$ for $\epsilon = 0.75$. The time step $\Delta T$ was chosen according to the stability condition $\Delta T \leq 0.1\ (\Delta X\ \Delta Y)$. Also, the finite computational domain was expanded as time increased to accommodate the spreading of the disturbance. This was done by monitoring the amplitudes $\widetilde{a}$ and $\widetilde{b}$ a few nodes away from the ends of the grid and adding a few points when the amplitudes exceeded a specified tolerance. The values of the amplitudes were set to zero at the ends of the grid. As a check of the accuracy of the numerical solution, the error in the energy budget (2.34) was typically less than 2%. Further details of the computational procedure are given in Appendix B.

### *2.4.3 Results*

Computations were carried out for several values of $\epsilon$ using the initial conditions

$$\widetilde{a} = a_0 \exp(-(x^2 + Y^2)), \quad \widetilde{b} = a_0 \exp(-(x^2 + Y^2)) \tan \epsilon f \qquad (T = 0), \tag{2.36}$$

$a_0$ being a normalization constant such that the kinetic energy of the disturbance $\langle \widetilde{a}^2 + \widetilde{b}^2 \rangle = 1$ at $T = 0$. This choice of initial disturbance is consistent with the boundary condition (2.22) and has its maximum close to the topography so the influence of the boundary on the stability characteristics is fully taken into account.

At low values of $\epsilon$, the flow is stable, as expected. There is little energy exchange between the perturbation and the background flow; the disturbance spreads out with time, more or less as predicted by the simplified system (2.23), (2.24) that ignores the presence of the topography. Figure 2-4($a$) illustrates the energy budget (2.34) as a function of $T$ for the moderately small value of $\epsilon = 0.5$. The rate of change of energy (potential and kinetic) of the perturbation increases from a positive value at $T = 0$ during the short time that most of the disturbance is still over the topography and can extract energy from the mean flow; at later times, when the disturbance has spread out, the energy budget exhibits a strongly damped oscillatory behaviour and the growth rate of the energy eventually decays to zero. This is also reflected in figure 2-5, where the kinetic energy of the disturbance is plotted as a function of $T$ for several values of $\epsilon$: for $\epsilon = 0.5$, the kinetic energy increases for a brief period of time and then approaches a constant value as the interaction with the mean flow ceases.

As the value of $\epsilon$ is increased, figure 2-5 shows that the kinetic energy of the perturbation grows for longer time, and there is a critical value of $\epsilon$ above which the energy appears to be

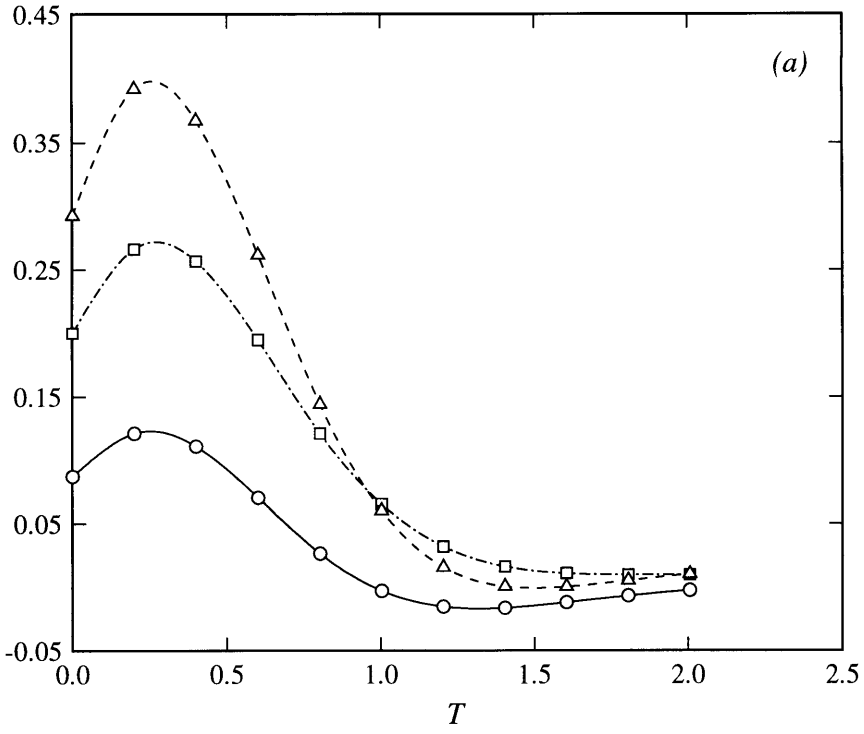


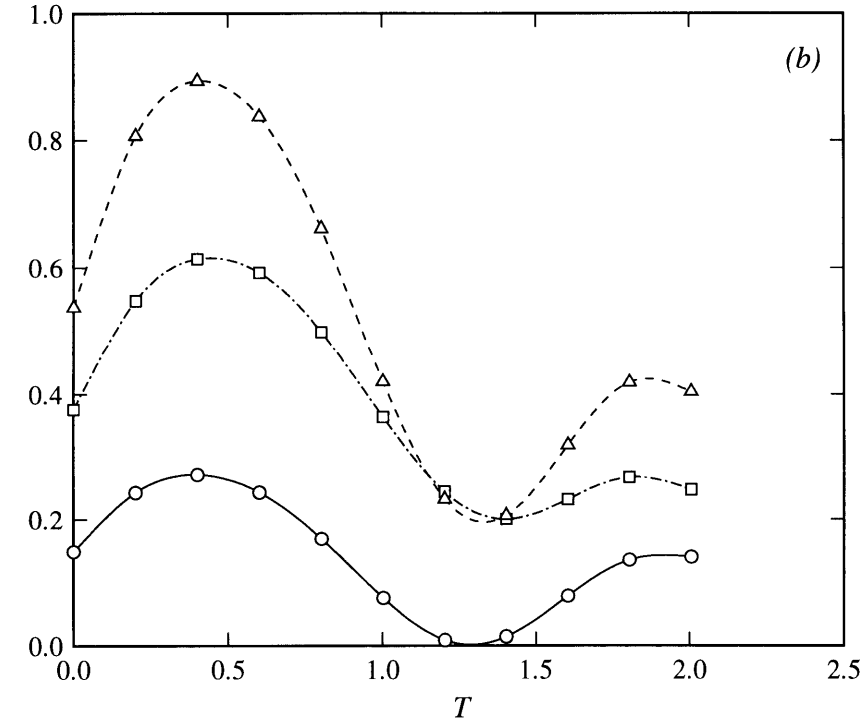


*(see caption overleaf)*

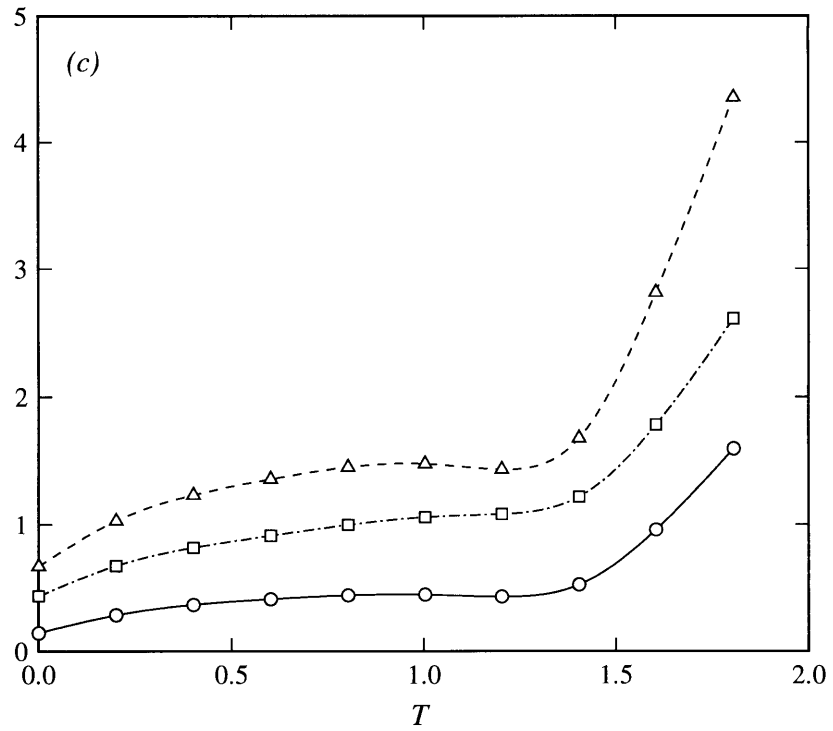


FIGURE 2-4. The energy budget for a small perturbation to Long's steady state for the cases (*a*) $\epsilon = 0.5$, (*b*) $\epsilon = 0.65$ and (*c*) $\epsilon = 0.7$. The circles and squares represent the rates of change of potential and kinetic energy respectively, while the triangles represent the rate of energy transfer from the mean flow to the perturbation.

growing indefinitely so the disturbance becomes unstable; the critical topography amplitude for instability appears to lie between $\epsilon = 0.6$ and $\epsilon = 0.65$. For values of $\epsilon$ in this transcritical range, the energy budget, as shown in figure 2-4(*b*) for $\epsilon = 0.65$, exhibits strong oscillations, the two opposing effects of spreading and energy extraction from the mean flow being more or less in balance.

In the unstable régime, on the other hand, the growth rates of the potential and kinetic energies of the perturbation eventually increase monotonically with time, as shown in figure 2-4(*c*) for $\epsilon = 0.7$. The power extracted from the mean flow by the perturbation also grows monotonically; hence, the perturbation grows at the expense of the mean flow. This continual energy transfer is facilitated by effectively trapping the disturbance over the

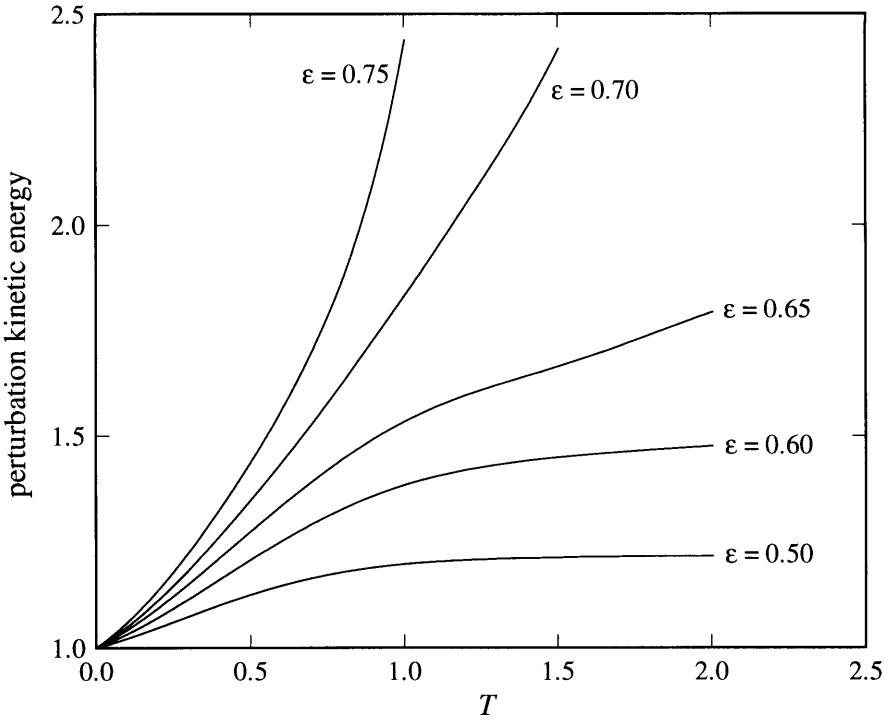


FIGURE 2-5. The perturbation kinetic energy as a function of $T$ at various $\epsilon$.

topography, where the streamlines of the mean flow are most steep and the action of the Reynolds stress is most pronounced.

It was noted earlier (see 2.35$a$) that $\langle|\widetilde{A}|^2\rangle = \langle\widetilde{a}^2 + \widetilde{b}^2\rangle$ measures the perturbation kinetic energy, so $|\widetilde{A}|^2$ may be interpreted as (averaged) kinetic energy density. To illustrate the significance of trapping in the instability mechanism, $|\widetilde{A}|^2$ is plotted in figure 2-6 as a function of $x$ and $Y$ at $T = 1.0$ for $\epsilon = 0.5$ and $\epsilon = 0.75$. At $T = 0$, $\langle|\widetilde{A}|^2\rangle = 1$ for both values of $\epsilon$ according to (2.36) and the initial conditions are similar. At $T = 1.0$, however, there are marked differences between the two disturbances: when no modulational instability is present ($\epsilon = 0.5$), the evolution is dominated by spreading of the initial disturbance, while in the unstable case $\epsilon = 0.75$ the rapid growth of the perturbation close to the topography overwhelms spreading in the streamwise direction. This is consistent with the conclusion

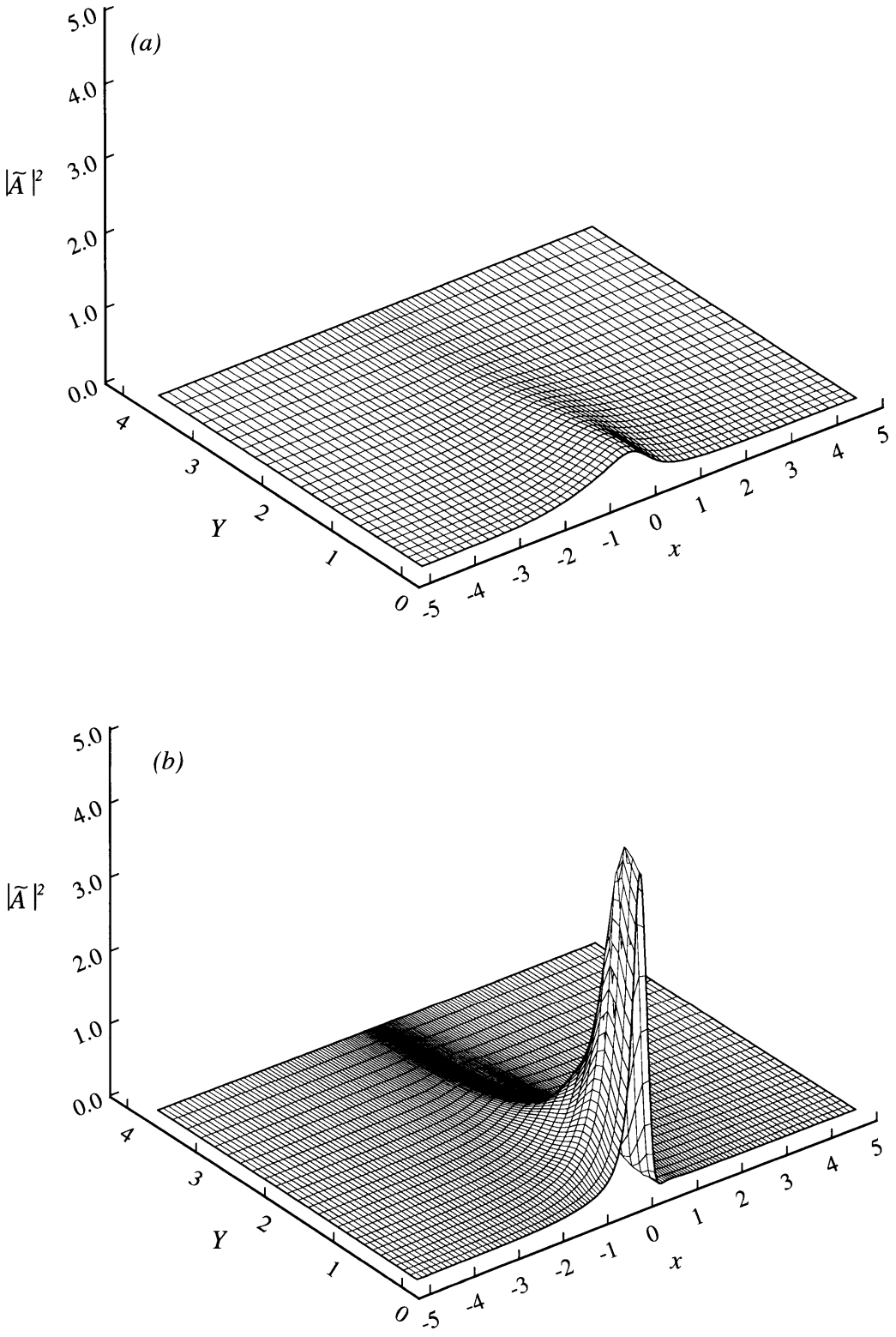


FIGURE 2-6. Perturbation kinetic energy density, $|\widetilde{A}|^2$, as a function of $x$ and $Y$ at $T = 1.0$ for ($a$) $\epsilon = 0.5$ and ($b$) $\epsilon = 0.75$, illustrating the contrast between the spreading and trapping mechanisms.

reached in §2.3 that a necessary condition for instability is the existence of trapped modes.

The critical topography amplitude for modulational instability obtained here, $\epsilon \approx 0.65$, is higher than the corresponding value of about 0.55 deduced from the modal analysis of equations (2.21) in §2.3. This difference must be attributed to the effect of the boundary condition (2.22) that is ignored in the modal analysis. To verify the role of the wall in inhibiting instability, we also tracked the evolution of an initial disturbance that was in the form (2.36) but was displaced from the boundary $Y = 0$ by a distance $Y_0 = 8$ such that the presence of the boundary took some time to be felt. For $\epsilon = 0.5$, that is well below critical in the presence of the boundary but is close to critical when the boundary is ignored, the energy budget (2.34) revealed a mild growth in the rate of change of the energy until the disturbance reached the boundary $Y = 0$ and this trend was reversed.

## 2.5 The transient problem

Based on the linear stability analysis presented above, Long's steady flow is unstable to infinitesimal modulations when the topography amplitude exceeds $\epsilon \approx 0.65$. Here we shall examine the transient development of the flow starting from rest, by solving the full nonlinear evolution equations (2.15), subject to the boundary condition (2.12), assuming that the topography is raised gradually to the specified amplitude. This way of establishing the flow mimics experimental conditions and avoids numerical difficulties associated with impulsive startup.

### *2.5.1 Energy balance equation*

As in §2.4, we first derive an energy budget that will aid in verifying the accuracy of the computation and will also provide a global description of the flow field. Denoting by $\widehat{\boldsymbol{u}} = (\widehat{u}, \widehat{v})$ the deviation of the velocity field from the uniform stream far upstream, and by $\widehat{\rho}$ and $\widehat{p}$ the deviations of the density and pressure, respectively, from their values far upstream, the governing equations (2.1)–(2.3) (in the hydrostatic limit $\mu \to 0$ and in the Boussinesq approximation $\beta \to 0$) take the form

$$\boldsymbol{\nabla} \cdot \widehat{\boldsymbol{u}} = 0, \tag{2.37}$$

$$\widehat{\rho}_t + \widehat{\rho}_x + \widehat{\boldsymbol{u}} \cdot \boldsymbol{\nabla} \widehat{\rho} = 0, \tag{2.38}$$

$$\widehat{u}_t + \widehat{u}_x + \widehat{\boldsymbol{u}} \cdot \boldsymbol{\nabla} \widehat{u} + \frac{1}{\beta} \widehat{p}_x = 0, \tag{2.39$a$}$$

$$\widehat{\rho} = -\widehat{p}_y. \tag{2.39$b$}$$

Proceeding as before, combining the momentum equations (2.39) and using (2.37) yields

$$\tfrac{1}{2}(\widehat{u}^2)_t + \tfrac{1}{2}(\widehat{u}^2)_x + \tfrac{1}{2}\boldsymbol{\nabla} \cdot (\widehat{\boldsymbol{u}}\widehat{u}^2) + \frac{1}{\beta}\left(\widehat{\rho}\widehat{v} + \boldsymbol{\nabla} \cdot (\widehat{p}\widehat{\boldsymbol{u}})\right) = 0.$$

Upon integrating this equation over the fluid domain using the boundary conditions ($\widehat{\boldsymbol{u}}$, $\widehat{\rho}$ and $\widehat{p}$ vanish in the far field and the component of velocity normal to the topography is zero), the following energy equation, analogous to (2.34), is obtained

$$\frac{\mathrm{d}}{\mathrm{d}t}(\mathrm{KE} + \mathrm{PE}) = \mathcal{R}; \tag{2.40}$$

here, as in (2.34),

$$\frac{\mathrm{d}}{\mathrm{d}t}\mathrm{KE} = \frac{1}{2}\frac{\mathrm{d}}{\mathrm{d}t}\int_{-\infty}^{\infty} \mathrm{d}x \int_{\epsilon f}^{\infty} \mathrm{d}y\, \widehat{u}^2$$

is the rate of change of kinetic energy and

$$\frac{\mathrm{d}}{\mathrm{d}t}\mathrm{PE} = \frac{1}{\beta}\int_{-\infty}^{\infty}\mathrm{d}x\int_{\epsilon f}^{\infty}\mathrm{d}y\,\widehat{\rho}\widehat{v}$$

is the rate of change of potential energy. The term on the right-hand side of (2.40),

$$\mathcal{R} = \frac{\epsilon}{\beta}\int_{-\infty}^{\infty}\mathrm{d}x f_x\,\widehat{p}|_{y=\epsilon f},$$

however, has a somewhat different interpretation from the corresponding term in (2.40); it is the rate of energy imparted to the flow by the force that is responsible for establishing the motion. Alternatively, if the obstacle were being towed in a stratified fluid, this term would be the power required to tow the obstacle.

The energy-balance equation (2.40) may be expressed in terms of the envelope variables (see Appendix D); to leading order in $\mu$, one has

$$\frac{\mathrm{d}}{\mathrm{d}t}\mathrm{KE} = \frac{\mathrm{d}}{\mathrm{d}T}\left\langle a^2 + b^2\right\rangle, \tag{2.41$a$}$$

$$\frac{\mathrm{d}}{\mathrm{d}t}\mathrm{PE} = -\frac{1}{2\pi}\left\langle\int_{-\infty}^{\infty}\mathrm{d}x'\int_0^{2\pi}\mathrm{d}\psi^{(0)}\left(a_x y_a + b_x y_b\right)\left(a'_T y'_a + b'_T y'_b\right)\right\rangle, \tag{2.41$b$}$$

$$\mathcal{R} = \epsilon\int_{-\infty}^{\infty}\mathrm{d}x f_x\left\{2\left(a\sin\epsilon f + b\cos\epsilon f\right)|_{Y=0} + \int_0^{\infty}\mathrm{d}Y Q(x,Y,T)\right\}, \tag{2.41$c$}$$

where

$$Q = \frac{1}{2\pi}\int_{-\infty}^{x}\mathrm{d}x'\int_0^{2\pi}\mathrm{d}\psi^{(0)}\frac{1}{\psi_y^{(0)}}\left\{a'_T\left(\left(y'y'_a\right)_{\psi^{(0)}} - yy'_{a\psi^{(0)}}\right) + b'_T\left(\left(y'y'_b\right)_{\psi^{(0)}} - yy'_{b\psi^{(0)}}\right)\right\}.$$

In the small-amplitude limit ($\epsilon \ll 1$), it follows from (2.41$a,b$) that

$$\frac{\mathrm{d}}{\mathrm{d}t}\mathrm{PE} \sim \frac{\mathrm{d}}{\mathrm{d}t}\mathrm{KE}.$$

Furthermore, (2.41$c$) gives

$$\mathcal{R} \sim 2\epsilon\int_{-\infty}^{\infty}\mathrm{d}x\, f_x\left(b - b^2\right)\Big|_{Y=0}.$$

Hence, to leading order, (2.40) implies that

$$\frac{\mathrm{d}}{\mathrm{d}T}\left\langle a^2+b^2\right\rangle \sim \epsilon \int_{-\infty}^{\infty} \mathrm{d}x\, f_x\left(b-b^2\right)\Big|_{Y=0},$$

which may also be derived directly from the linearized versions of the evolution equations (2.15) and the boundary condition (2.12).

### *2.5.2 Numerical method*

The overall strategy for solving the evolution equations (2.15) numerically parallels that described in §2.4 for the stability problem. A non-uniform grid with second-order approximation of the spatial derivatives by finite differences and forward Euler time stepping are used. One essential difference, however, is that the kernels here are no longer independent of $T$ (and $Y$) but change as the flow evolves, and have to be updated at every time step over the entire grid; this makes the computation much more expensive.

In order to reduce the cost, the following procedure was adopted. According to (2.16), the kernels are functions of $(a,b,a',b')$. When $a^2+b^2+a'^2+b'^2$ exceeded an upper threshold equal to 0.1, the kernels were evaluated numerically as in §2.4 whereas when this amplitude criterion was less than a lower threshold of 0.01, the linear limits $K_{11}=K_{22}=1$, $K_{21}=K_{12}=0$ were used. For intermediate values of the amplitudes, the kernels were evaluated using an analytic approximation: equation (2.5) for the streamfunction $\psi^{(0)}$ was inverted in terms of a power series to determine $y=y(\psi^{(0)};\,a,b)$ correct to eighth order in $a$ and $b$. With this approximation of $y$ and its derivatives inserted in (2.16), analytic expressions for the kernels, correct to sixth order in $(a,b,a',b')$, were obtained (Ramirez 1993). In a similar manner, the $x$-derivatives of the kernels were evaluated using

$$\frac{\partial}{\partial x}K_{mn}(x,x') = a_x\frac{\partial}{\partial a}K_{mn}(a,b,a',b') + b_x\frac{\partial}{\partial b}K_{mn}(a,b,a',b')$$

for $m,\ n = 1, 2$.

As in §2.4, the boundary condition (2.12) was applied implicitly: the values of $b$ on the boundary $Y = 0$ ($j = 0$) were determined from (2.15$b$) first (evaluating the kernels and the terms involving $a_T$ and $a_{xY}$ on $j = 1$) and then (2.12) was used to obtain $a$ on $j = 0$; details may be found in Appendix B. The grid size used (close to the topography) varied from $\Delta X = \Delta Y = 0.1$ for $\epsilon \leq 0.65$ to $\Delta X = 0.025,\ \Delta Y = 0.1$ for the highest topography amplitude $\epsilon = 0.75$ that we considered; the time step $\Delta T$ satisfied the stability condition $\Delta T \leq 0.1\,\Delta X\,\Delta Y$. Moreover, it was found necessary to apply smoothing in this case as well in order to eliminate a mild numerical instability along the vertical direction. Finally, the radiation condition was implemented by expanding the computational domain as before.

### *2.5.3 Results*

The transient problem was solved for values of $\epsilon$ ranging from 0.5 to 0.75. The forcing was turned on according to

$$f(x,T) = \frac{1}{1+x^2}(1 - \mathrm{e}^{-10T}),$$

so the topography achieved 99% of its maximum amplitude before $T = 0.5$. The results are presented in terms of the energy budget (2.40) and

$$d(x,T) \equiv \left(|A|^2_{Y=0} - |\overline{A}|^2\right) / |\overline{A}|^2_{\max}$$

where $\overline{A}(x)$ is the envelope corresponding to Long's steady flow and $|\overline{A}|_{\max}$ is the maximum value of $|\overline{A}|$. From the above definition, it is clear that $d(x,T)$ measures the local deviation of the transient flow from Long's steady state on the lower boundary.

The energy budget for $\epsilon = 0.5$ is shown in figure 2-7; the energy-balance equation (2.40)

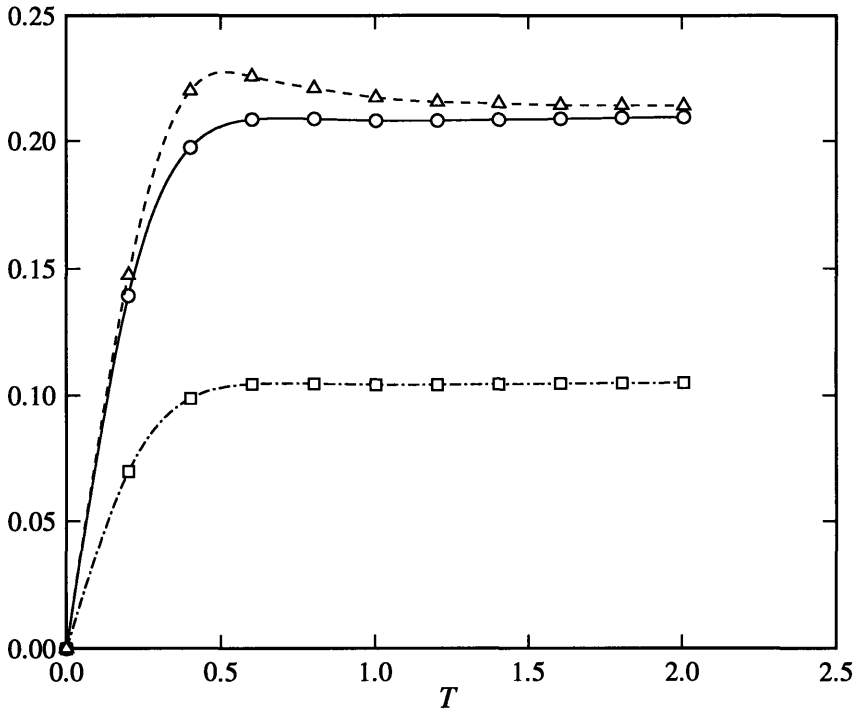


FIGURE 2-7. The energy budget for the transient response with $\epsilon = 0.5$. The squares represent the rate of change of potential energy while the circles represent the rate of change of total energy; the triangles denote the power input to the flow.

is satisfied to within 2%[†]. The rates of change of both the kinetic and potential energies as well as the external power input approach constant values shortly after the forcing has reached its maximum value, indicating that a steady state has been achieved. To check how close this steady state is to Long's steady flow, the quantity $d(x,T)$ is plotted in figure 2-8 as a function of $x$ at three different times. As measured by $d$, the deviation from Long's steady state is quite small (about 3%) and varies little with time; moreover, $d$ is more or less symmetric about $x = 0$ and decays rapidly to zero far from the topography at large $T$. Hence, it would seem that Long's steady state is achieved for $\epsilon = 0.5$. We recall that, for this value of $\epsilon$, Long's steady state is stable to infinitesimal modulations, and nonlinearity

[†]The error is larger during the time that the topography has not yet reached its maximum amplitude. This error can be reduced by turning on the topography more slowly.

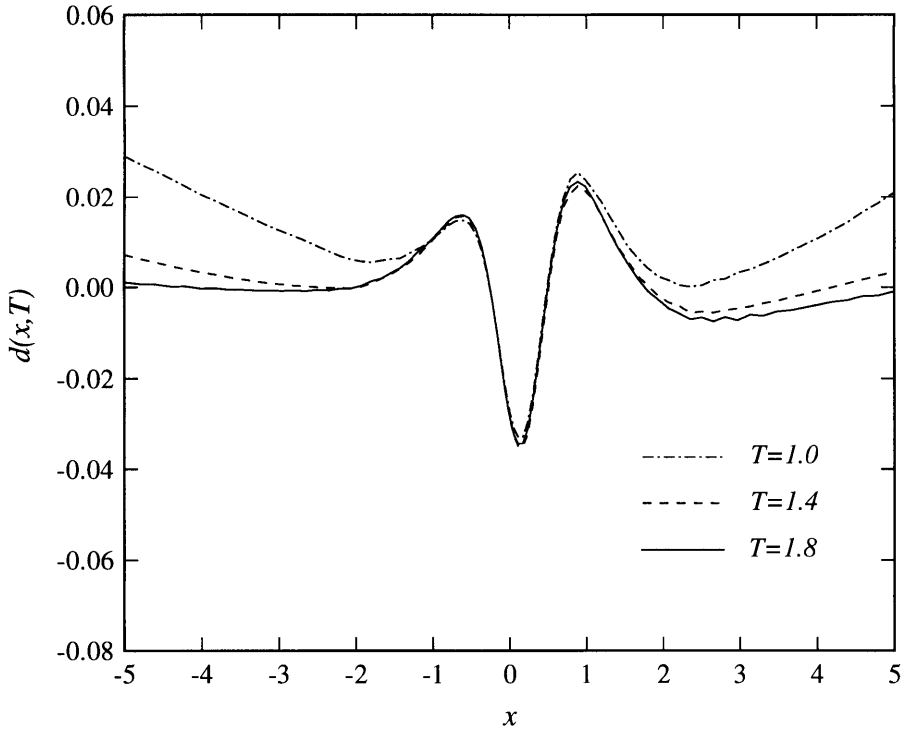


FIGURE 2-8. The deviation parameter $d(x,T)$ as a function of $x$ at $T = 1.0, 1.4$ and $1.8$ for $\epsilon = 0.5$.

does not turn out to have a destabilizing effect on the transient response.

When the topography amplitude is raised to a value of $\epsilon = 0.7$ for which the corresponding Long steady flow is linearly unstable, however, the energy budget is quite different in character. As shown in figure 2-9, the effect of nonlinearity here is to curtail the monotonic growth observed in the linear stability problem (figure 2-4($c$)), resulting in what appears to be a sustained oscillation in the energy budget. The oscillation occurs on an $O(1)$ timescale in terms of $T = \mu^2 t$, so the period of oscillation ($T \approx 1.5$) is very long, $O(1/\mu^2)$, in terms of the convective timescale. The response, in turn, exhibits a slowly varying transient behaviour rather than reaching steady state. The quantity $d(x,T)$ that measures the deviation from Long's steady flow is plotted in figure 2-10 as a function of $x$ at the same three times

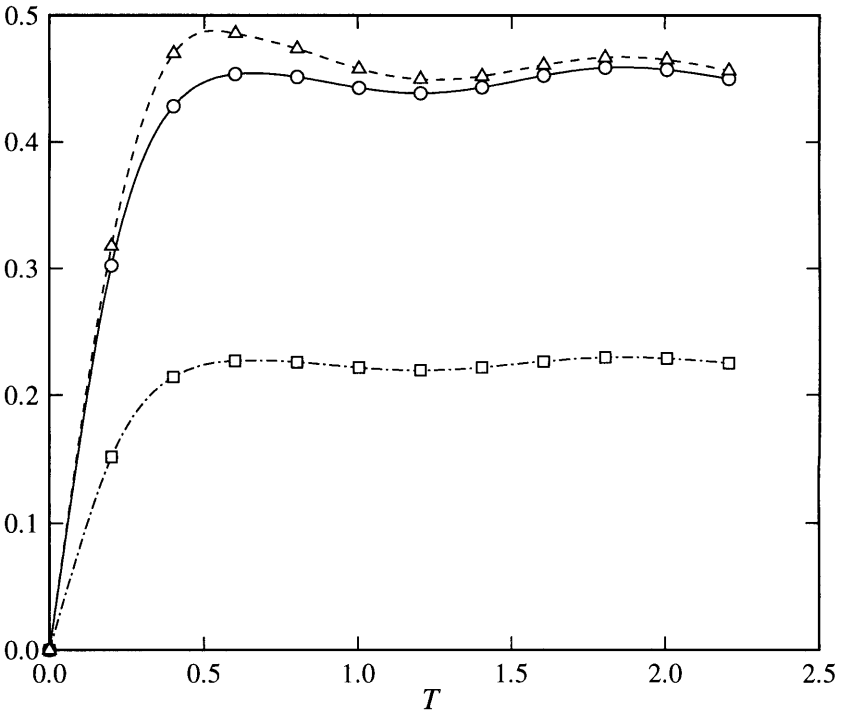


FIGURE 2-9. The energy budget for the transient response with $\epsilon = 0.7$. The squares represent the rate of change of potential energy while the circles represent the rate of change of total energy; the triangles denote the power input to the flow.

as in figure 2-8. While the values of $d$ are still fairly small (on the order of 6–7%), they are strongly dependent on $T$ in view of the transient nature of the flow; hence, the flow is different from that at Long's steady state but not substantially so. We remark that this transient flow behaviour is qualitatively similar to that found by Lamb (1994) in the corresponding finite-depth problem for values of the topography amplitude that no breaking occurs.

Comparing figure 2-10 with figure 2-8, it is also observed that in the case $\epsilon = 0.7$ where instability is present, the deviation of the transient reponse from Long's steady flow is markedly asymmetric about $x = 0$. Moreover, while the deviation downstream most likely goes to zero as $T$ increases, this does not seem to be the case on the upstream side.

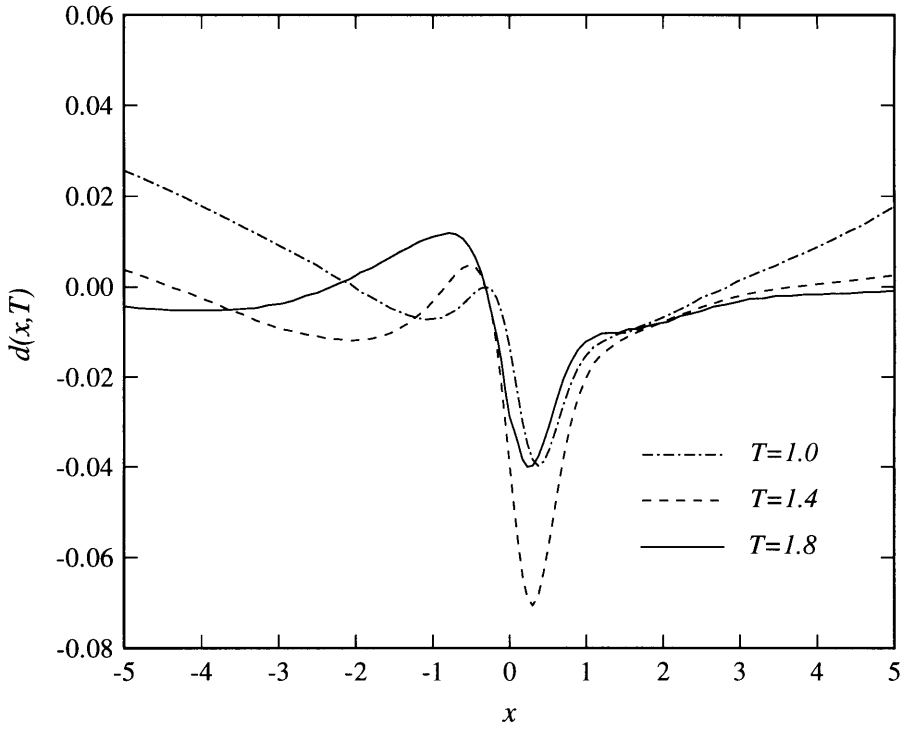


FIGURE 2-10. The deviation parameter $d(x,T)$ as a function of $x$ at $T = 1.0, 1.4$ and $1.8$ for $\epsilon = 0.7$.

Whether or not, ultimately, this causes upstream influence is not clear and would require carrying the computation to much larger values of $T$ in order to give a definitive answer. The amplitude of the upstream disturbance is quite small, however; certainly, there is no significant upstream influence comparable to that found near resonant flow conditions in the finite-depth problem (Grimshaw & Yi 1991).

The energy budget in figure 2-9 for $\epsilon = 0.7$ exhibits an overshoot shortly after the forcing achieves its maximum amplitude followed by a dip. It therefore seemed possible that the overshoot might lead to transient breaking at larger subcritical values of the mountain amplitude. To check this hypothesis, an abbreviated calculation was performed for $\epsilon = 0.75$ up to $T = 1.2$. While the amplitude of the fluctuation about Long's steady flow increases,

no evidence of transient breaking was found. Thus, if transient breaking does occur, it will most likely do so very close to the critical overturning amplitude of 0.85, consistent with the numerical results of Pierrehumbert & Bacmeister (1987). In conclusion, the modulational instability is rather mild in nature, causing the flow to go into a slowly varying transient state near Long's steady state without the occurence of transient breaking.

## 2.6 Discussion

In the present chapter, we have addressed the stability and realizability of Long's steady flow in the hydrostatic limit using the asymptotic theory of KA. For the algebraic mountain, this steady state is unstable to small-amplitude modulations for values of the topography steepness $\epsilon \gtrsim 0.65$, significantly below the critical overturning value of $\epsilon = 0.85$. This is clearly in contrast to the results of earlier investigations (Laprise & Peltier 1989*a*, Pierrehumbert & Wyman 1985, Clark & Peltier 1977), where it was found that the criteria for static and dynamic instabilities are simultaneously satisfied. These results are frequently justified by appealing to the Miles–Howard theorem, according to which the local Richardson Number $Ri$ has to be less than $\frac{1}{4}$ somewhere in the flow field for shear-flow instability to occur (Drazin & Reid 1981, p. 328), a condition that is first met at the critical amplitude for static instability (Lilly & Klemp 1979). However, it must be borne in mind that the above criterion applies to *parallel* flows, whereas the flows considered here ($\epsilon$ is finite) are strongly non-parallel, especially when the steepness approaches the critical value. This caveat of the Miles–Howard theorem has also been emphasized by Howard & Maslowe (1973) and the fact that $Ri < \frac{1}{4}$ at the critical steepness must therefore be regarded as fortuitous.

We have also demonstrated, using an eigenvalue analysis, that modes trapped near the

topography in the streamwise direction must exist for instability to occur. Physically, this condition ensures that disturbances can lodge in the region where the background shear is maximum so they can draw energy from the mean flow continually.

The effects of this instability on the realizability of Long's steady flow were studied by means of a transient calculation starting from rest. The stability boundary was found to agree with that of the linear stability problem. In the unstable régime $\epsilon \gtrsim 0.65$, the effect of nonlinearity causes the transient flow to fluctuate in the neighbourhood of Long's steady state. The transients evolve slowly—on a timescale $T = O(1)$ representing a large number of convective time units—which could explain why the modulational instability passed unnoticed in previous work. For example, in Laprise & Peltier (1989*b*), the simulations for $\mu = 0.1$ with $\epsilon = 0.95$ (a supercritical amplitude at which the authors found a dominant shear-flow instability) were carried out to 36 convective time units, corresponding to $T = 0.36$. The slow evolution of the response that we observe also supports the view that transient upstream motions could be mistaken for upstream influence at subcritical topography amplitudes.

We found no transient wave breaking even when $\epsilon$ was within 10% of the critical overturning value. We suspect that if subcritical transient breaking occurs, it must do so when the topography steepness is very close to the critical value predicted by Long's model. This is in stark contrast to the results found in the corresponding finite-depth problem where transient subcritical breaking is quite common (Grimshaw & Yi 1991, Lamb 1994).

Quantitative comparison of the present results with the experiments of Baines & Hoinka (1985) is difficult since their obstacles were significantly non-hydrostatic. We remark, however, that, according to Baines & Hoinka (1985), there is a range of moderately small topog-

raphy amplitudes for which the flow does not reach steady state but develops slowly without breaking; moreover, in this régime, their data indicates the presence of small-amplitude upstream motions that they interpret as upstream influence (if viscous effects were neglected). It would seem that this flow behaviour resembles, at least qualitatively, the slowly varying transient response found here when modulational instability is present. However, in making a detailed comparison between theory and experiment, non-hydrostatic and viscous effects (that may cause flow separation, among other things) could play an important part.

Finally, we remark that when the flow is transient, the density perturbation does not decay to zero far downstream according to (2.9), but rather gives rise to an $O(\mu^2)$ columnar disturbance that persists in the streamwise direction and is modulated in the vertical direction. The appearance of a similar 'shelf' owing to transient effects was also noted by Warn (1983) in his study of large-amplitude Rossby waves in a fluid of finite depth. It then becomes necessary to treat the flow field far downstream separately by rescaling the equations to account for the evolution of the shelf in the streamwise direction. This problem is discussed in detail in the following chapter. However, the appearance of these shelves does not alter the results of the present study, except for the finer details of the downstream flow field.

# CHAPTER 3

# SHELF GENERATION BY NONLINEAR LONG WAVES

## 3.1 Introduction

The theory of waveguides provides an excellent model for a variety of problems in geophysical fluid dynamics such as the propagation of internal waves in the oceanic thermocline. In these problems, nonlinear effects are of particular interest owing to the possibility of permanent-wave solutions which remain coherent over large distances and times. While two-dimensional, nonlinear internal waves in stratified fluids have been the subject of several theoretical studies in recent years (see, for example Grimshaw & Smyth 1986; Melville & Helfrich 1987; Grimshaw & Yi 1991; Kantzios & Akylas 1993), one aspect that appears to have escaped attention is the formation of shelves, which leads to considerable theoretical difficulties. It is precisely this aspect that we explore in some detail here. Shelves are streamwise structures of large extent and have been encountered before in the study of solitary surface-wave propagation over water of slowly varying depth (Leibovich & Randall 1973). However, as we will demonstrate, the mechanism by which shelves are formed in the present context is entirely different.

When the depth of the stratified layer is finite, the Korteweg-de Vries (KdV) equation describes the evolution of long internal waves of small, but not infinitesimal amplitude, wherein the effects of weak dispersion and nonlinearity balance. As the amplitude increases and the waves become shorter, the KdV equation becomes inadequate and higher order effects must be incorporated; a systematic procedure to accomplish this was developed by Benney (1966). For a linear density distribution, the nonlinear term in the KdV

equation vanishes identically so that the required balance between nonlinearity and dispersion does not obtain. Using a novel approach pioneered by Warn (1983), Grimshaw & Yi (1991, referred to hereinafter as GY) showed that the appropriate governing equation in this anomalous case is of the integro-differential type. This equation describes waves that are fully nonlinear, which explains why the KdV scaling breaks down.

The flow configuration examined by GY is the main focus of the present chapter. A detailed study of the far-field reveals that the nonlinear theory breaks down owing to the formation of an infinite shelf; it is found, moreover that mass is not conserved. It is shown in §3.3 that the nonlinear theory is valid in an 'inner region', while an 'outer region', corresponding to the far-field is described by linear theory. The mechanism of shelf formation is shown to be a nonlinear self-interaction of the main wave. The shelf itself is seen to have a large, but finite extent and its structure is obtained by matching the two regions. The analogous large-depth problem is examined in §3.4, where it is shown that although a shelf is formed, mass conservation is not affected.

In §3.5, shelf-generation in the weakly nonlinear, long wave limit is analysed and it is found that the shelf amplitude is considerably smaller than in the fully nonlinear case. The surprising feature here is the possibility that the shelf can extend upstream of the nonlinear wave. When the latter wave is generated through resonant forcing of a uniform flow by a submerged obstacle, the shelf would represent an upstream influence which is quite distinct from the one caused by solitary waves (Grimshaw & Smyth 1986). The analysis also demonstrates explicitly that the mechanism of shelf-formation is a transient, cubic self-interaction of the nonlinear wave.

The significance of shelves in stratified flows is examined in §3.6, where we also discuss

the present results in the context of related analytical and numerical work by McIntyre (1972) and Lamb (1994). In particular, it is found that the latter study contains evidence for shelf formation.

## 3.2 Review of asymptotic theory

We consider freely-propagating waves in an inviscid, incompressible, stratified fluid layer of depth $h$. Taking $L$ and $N_0$ to be characteristic values of the wavelength and Brunt–Väisälä frequency respectively, we have the following non-dimensional parameters:

$$\mu = \frac{h}{L}, \qquad \beta = \frac{N_0^2 h}{g}.$$

The long-wave parameter, $\mu$ is a measure of dispersive effects and $\beta$ is the Boussinesq parameter which measures stratification.

Scaling the streamwise coordinate $x$ with $L$, the vertical coordinate $y$ with $h$ and time $t$ with $\mu N_0$, the governing equations of incompressibility, mass conservation and momentum balance may be cast in the form

$$\boldsymbol{\nabla}\cdot\boldsymbol{u} = 0, \tag{3.1}$$

$$\rho_t + \boldsymbol{u}\cdot\boldsymbol{\nabla}\rho = 0, \tag{3.2}$$

$$\beta\rho(\boldsymbol{u}_t + \boldsymbol{u}\cdot\boldsymbol{\nabla}\boldsymbol{u}) = -(p_x, \mu^{-2}(\rho + p_y)), \tag{3.3}$$

where $\boldsymbol{u} = (u, v)$ is the velocity field and $p$ and $\rho$ are the pressure and density respectively. The fluid layer is assumed to be bounded above and below by impermeable walls so that

$$v = 0, \qquad y = 1, 0. \tag{3.4}$$

The density of the undisturbed fluid is $\overline{\rho}(y)$ and the Brunt–Väisälä frequency, $N(y)$ is defined by the relation

$$\beta\overline{\rho}N^2 = -\overline{\rho}_y. \tag{3.5}$$

Defining the streamfunction, $\Psi$ such that $u = \Psi_y$, $v = -\Psi_x$, the equations of motion (3.1)–(3.3) may, in the case of an infinitesimal perturbation, be combined to yield

$$\beta\left(\overline{\rho}\Psi_{ytt}\right)_y - \overline{\rho}_y\Psi_{xtt} = O(\mu^2). \tag{3.6}$$

Assuming further that the disturbance is wave-like and moves with a speed $c$, we may write

$$\Psi = A(x+ct)\phi(y), \tag{3.7}$$

where we have assumed unidirectional propagation. It is clear from (3.6) that the very long waves ($\mu \to 0$) are non-dispersive; upon making use of (3.7) and the boundary conditions (3.4), we obtain an eigenvalue problem for the structure of the long-wave modes, $\phi(y)$ and the corresponding phase speeds, $c$:

$$\left(\overline{\rho}\phi_y\right)_y - \frac{\overline{\rho}_y}{\beta c^2}\phi = 0, \tag{3.8$a$}$$

$$\phi(0) = \phi(1) = 0. \tag{3.8$b$}$$

In general, the wave-guide problem described by (3.8$a$,$b$) possesses an infinite number of modes. For the special case of uniform, Boussinesq stratification ($N = 1, \beta \to 0$), it is readily shown that the $n$-th mode, $\phi_n(y)$ and its speed, $c_n$ are given by

$$\phi_n(y) = \sin\frac{y}{c_n}; \qquad c_n = \frac{1}{n\pi} \tag{3.9}$$

We now consider long ($\mu \ll 1$), nonlinear waves in a uniformly stratified, Boussinesq fluid. As we have indicated earlier, these waves are described by the theory of GY, who

demonstrate that the wave-amplitude must be $O(1)$ to obtain a balance between dispersive and nonlinear effects. The background flow conditions assumed here imply that Long's model (Long 1953) is applicable. This model shows that the governing equations for a steady, nonlinear flow reduce to a linear form. Therefore, any solution of the nonlinear equations is also a solution of the linearized equations and the vertical structure of the large-amplitude wave must therefore be a linear mode shape. We assume here a mode-$n$ wave, travelling to the left. Then, choosing a reference frame moving along the $x$-axis at a speed of $-c_n$, we observe from (3.6) that dispersive corrrections are $O(\mu^2)$, implying that the nonlinear wave evolves on the slow timescale, $T = \mu^2 t$.

Next, we briefly review the salient features of the theory of GY; details may be found in the original paper. Defining the streamfunction, $\Psi$ as before, it is observed from (3.2) that the density, $\rho$ is conserved along streamlines to leading order in $\mu$. Hence, provided overturning does not occur, the vertical coordinate, $y$ may be replaced by $\Psi$ and (3.2), upon integration along a streamline yields

$$\rho = \overline{\rho}\left(\frac{\Psi}{c_n}\right) - \mu^2 \overline{\rho}_\Psi \int_{-\infty}^{x} \mathrm{d}x' \left.\frac{\Psi_T}{\Psi_y}\right|_\Psi , \tag{3.10}$$

where the subscript $|_\Psi$ indicates that $\Psi$ is held constant. Using (3.10), the momentum equation (3.3) may be manipulated to take the form

$$\Psi_{yy} + \frac{\Psi - c_n y}{c_n^2} = -\mu^2 \left[\Psi_{xx} + R\right], \tag{3.11}$$

where

$$c_n R = y \frac{\partial}{\partial \Psi} \int_{-\infty}^{x} \mathrm{d}x' \left.\frac{\Psi_T}{\Psi_y}\right|_\Psi - \frac{\partial}{\partial \Psi} \int_{-\infty}^{x} \mathrm{d}x' \left.\frac{y\Psi_T}{\Psi_y}\right|_\Psi + c_n \frac{\partial}{\partial \Psi} \int_{-\infty}^{x} \mathrm{d}x' \Psi_{yT}. \tag{3.12}$$

Following a multiple-scale perturbation procedure, the streamfunction $\Psi$ is expanded

according to

$$\Psi = \Psi^{(0)} + \mu^2 \psi^{(1)} + \cdots . \tag{3.13}$$

Defining $\psi^{(0)} = \Psi^{(0)} - c_n y$, and using (3.11) along with the boundary conditions (3.4), we find that

$$\psi^{(0)} = A(x,T) \sin n\pi y, \tag{3.14}$$

where $A(x,T)$ is an amplitude that remains to be determined.

At the next order in $\mu^2$, we obtain

$$\psi^{(1)}_{yy} + \frac{\psi^{(1)}}{c_n^2} = -\Psi^{(0)}_{xx} - R^{(0)}, \tag{3.15}$$

where $R^{(0)} = R(x, \Psi^{(0)}, T)$. The boundary conditions at this order, as at $O(1)$, are homogeneous. We now derive an evolution equation for $A(x,T)$ by imposing a solvability condition, which ensures that the right-hand side of (3.15) does not contain a mode-$n$ contribution. The result then is

$$\int_{-\infty}^{x} \mathrm{d}x' K(x,x') A'_T - \frac{1}{2} c_n^3 A_{xx} = 0. \tag{3.16}$$

The kernel $K(x,x')$ is defined by

$$K(x,x') = c_n \int_0^{c_n} \mathrm{d}\Psi y_A \left[ y'_A + c_n \left( y' y'_A \right)_\Psi - c_n y y'_{A\Psi} \right], \tag{3.17}$$

where $y = y(\Psi; A)$ is determined by inverting the streamfunction

$$\Psi = Vy + A \sin n\pi y, \tag{3.18}$$

which is just the expression in (3.13) to leading order. This inversion is possible only as long as

$$|A| \leq c_n^2; \tag{3.19}$$

when the magnitude of $A$ reaches the critical value of $c_n^2$, the flow features vertical streamlines and hence (3.19) represents a criterion for incipient breaking.

For small amplitudes, $|A| \ll c_n^2$, the relation (3.18) may be expanded in powers of $A$ to obtain an analytical expression for $y = y(\Psi; A)$, which when inserted into (3.17) yields the following small-amplitude expansion for the kernel:

$$K(x, x') = 1 + c_n^{-4}\left(-\frac{3}{4}A'^2 + 2AA' - \frac{3}{4}A^2\right) + \ldots; \tag{3.20}$$

substituting (3.20) into (3.16) and making use of the fact that $A_T = \frac{1}{2}c_n^3 A_{xxx} + O(A^3)$, we then obtain, correct to $O(A^5)$:

$$A_T + \frac{1}{4c_n}AA_xA_{xx} + \frac{1}{4c_n}A^2A_{xxx} - \frac{1}{2c_n}A_x^3 - \frac{1}{2}c_n^3A_{xxx} = 0. \tag{3.21}$$

## 3.3 Far-field response: shelf dynamics

We now commence our investigation of the flow dynamics far downstream of the obstacle. It is assumed, for simplicity that the nonlinear wave is mode-1; in what follows, this is referred to as the fundamental mode.

### *3.3.1 Breakdown of the nonlinear theory*

Since $A$ is locally confined, it follows that (3.15) reduces in the far field ($x \to \infty$) to

$$\psi_{yy}^{(1)} + \frac{\psi^{(1)}}{c_1^2} = -R_\infty^{(0)}, \tag{3.22}$$

where $R_\infty^{(0)} = \lim_{x\to\infty} R^{(0)}$ is, in general, non-zero. Hence, we find that $\psi^{(1)} \sim \psi_\infty^{(1)}(y, T)$ as $x \to \infty$; this implies that the streamfunction, $\Psi$, which is given by (3.13) features a uniform downstream shelf of $O(\mu^2)$. Furthermore, the $O(\mu^4)$ term in (3.13) grows linearly

with $x$, causing the expansion to break down when $x = O(\mu^{-2})$. A similar non-uniformity was observed by Warn (1983) in his study of finite-amplitude Rossby waves on weak shear.

Using (3.10) and (3.22), the expression for the density in the limit $x \to \infty$ may be written as

$$\rho = \overline{\rho}(y) + \mu^2 \frac{\overline{\rho}_y}{c_1} \left[ \delta + \psi^{(1)} \right], \tag{3.23}$$

where

$$\delta = \delta(y, T) = - \int_{-\infty}^{\infty} \mathrm{d}x' \left. \frac{\Psi_T}{\Psi_y} \right|_{\Psi^{(0)}} \tag{3.24}$$

is the vertical streamline displacement. Thus, it is observed that the density perturbation does not vanish in the far-field owing to the permanent distortion of the streamlines, brought about by transience. Considering a control volume extending from $x = -\infty$ to $x = +\infty$ and using (3.23), the net mass flux, $dM/dT$ out of the nonlinear wave is found to be given by

$$\frac{dM}{dT} = -\beta \int_0^1 \mathrm{d}y \, \delta, \tag{3.25}$$

from which it is evident that mass is not conserved.

These observations are reminiscent of the difficulties encountered in studies of the propagation of solitary surface waves in water of slowly-varying depth, described by the perturbed KdV equation (Leibovich & Randall 1973). In that case, the problems caused by the shelf were resolved by recognizing the existence of a reflected wave which moves in a direction opposite to that of the solitary wave and is therefore not correctly described by the perturbed KdV equation (Kaup & Newell 1978; Ko & Kuehl 1978; Knickerbocker & Newell 1980; Kodama & Ablowitz 1981). In the present problem, it will be seen that the resolution of the difficulty is somewhat more subtle, due in part to the fact that a stratified flow

possesses multiple modes in the vertical direction unlike the surface wave problem, where no such structure exists.

We now present a rational scheme to predict the flow field far downstream of the obstacle. From the earlier discussion, it is evident that the scales of the asymptotic theory break down when $x = O(\mu^{-2})$; moreover, the flow is governed by linear theory for large $x$ because $A(x,T)$ is locally confined. This suggests the use of matched asymptotic expansions, with the nonlinear theory being valid in an 'inner region' ($x \ll 1/\mu^2$) while the 'outer region' ($x \gg 1/\mu^2$) is described by linear theory. The specification of the flow field is then completed by matching the inner and outer expansions.

In view of the previous discussion, we define an outer streamwise coordinate, $\widetilde{X} = \mu^2 x$; correspondingly, the stretched time $T = \mu^2 t$ must also be used. It is interesting to note that the outer region evolves on the same timescale as the nonlinear wave.

### *3.3.2 Inner region*

We begin by examining the inner region where, as we have seen, the nonlinear theory of GY applies. However, anticipating the matching with the outer region that will follow, we concentrate on the extremity of the inner region, $x \to \mu^{-2}$, in the limit $\mu \to 0$. Integrating (3.21) over $x$, we find that

$$\frac{\mathrm{d}}{\mathrm{d}T}\int_{-\infty}^{\infty}\mathrm{d}x\left(A - \frac{1}{4c_1^4}A^3\right) = 0. \tag{3.26}$$

Next, the small-amplitude expansion procedure of §3.2 is used together with (3.24) to yield, correct to $O(A^5)$

$$\int_0^1 \mathrm{d}y\ \delta \sin \pi y = -\frac{1}{2c_1}\frac{\mathrm{d}}{\mathrm{dT}}\int_{-\infty}^{\infty}\mathrm{d}x\left(A - \frac{1}{8c_1^4}A^3\right). \tag{3.27}$$

It is evident from (3.26) and (3.27) that $\int_0^1 \mathrm{d}y\ \delta \sin \pi y \neq 0$, which implies that the density perturbation far downstream has a nonvanishing contribution from the first (fundamental) mode, $\phi_1 = \sin \pi y$. However, because the density and streamfunction perturbations are coupled, it is apparent that $\psi^{(1)}$ also contains a non-zero fundamental component. This result is surprising in view of the solvability condition imposed on (3.15) from which the evolution equation (3.16) follows. The reason for the appearance of downstream perturbations containing fundamental components will become clear later. For the moment, we note that in addition to the forced response due to $R_\infty^{(0)}$ in (3.22), a homogeneous solution of the form $G_1(T) \sin \pi y$ must also be included, where $G_1$ is thus far arbitrary. Decomposing $R_\infty^{(0)}$ into long-wave modes, the solution of (3.22) may be therefore written as

$$\psi^{(1)} = G_1(T) \sin \pi y + \sum_{m=2}^{\infty} \frac{G_m(T)}{\pi^2(m^2-1)} \sin m\pi y, \tag{3.28}$$

where

$$G_m(T) = 2 \int_0^1 \mathrm{d}y\ R_\infty^{(0)} \sin m\pi y. \tag{3.29}$$

Similarly, decomposing $\delta$ into long-wave modes, the expression (3.23) for the density may be written as

$$\rho = \overline{\rho}(y) - \frac{\mu^2 \beta}{c_1} \left[ (G_1 + P_1) \sin \pi y + \sum_{m=2}^{\infty} \left\{ \frac{G_m}{\pi^2(m^2-1)} + P_m \right\} \sin m\pi y \right], \tag{3.30}$$

where

$$P_m = 2 \int_0^1 \mathrm{d}y\ \delta \sin m\pi y. \tag{3.31}$$

### 3.3.3 *Outer region*

We now turn our attention to the outer region, $\widetilde{X} = O(1)$. Since the nonlinear wave is locally confined, we may write the streamfunction and density in the outer region respectively as

$$\Psi = c_1 y + \mu^2 \widehat{\psi}(\widetilde{X}, y, T); \qquad \rho = \overline{\rho}(y) + \mu^2 \beta \widehat{\rho}(\widetilde{X}, y, T).$$

Neglecting higher order dispersive effects, we find that

$$\left(\frac{\partial}{\partial T} + c_1 \frac{\partial}{\partial \widetilde{X}}\right)^2 \widehat{\psi}_{yy} + \widehat{\psi}_{\widetilde{X}\widetilde{X}} = 0; \tag{3.32}$$

the linearized version of (3.2) then yields the coupling between the density and streamfunction perturbations:

$$\left(\frac{\partial}{\partial T} + c_1 \frac{\partial}{\partial \widetilde{X}}\right) \widehat{\rho} = -\beta \widehat{\psi}_{\widetilde{X}}, \tag{3.33}$$

where we have again neglected the $O(\mu^2)$ terms. In addition, we have the conditions that $\widehat{\rho}$ and $\widehat{\psi}$ must vanish on $y = 0, 1$.

Motivated by the solution (3.28),(3.30) of the inner problem, we expand $\widehat{\psi}$ and $\widehat{\rho}$ so that the aforementioned boundary conditions on $y = 0, 1$ are satisfied:

$$\widehat{\psi} = \sum_{m=1}^{\infty} B_m(\widetilde{X}, T) \sin m\pi y, \tag{3.34a}$$

$$\widehat{\rho} = \sum_{m=1}^{\infty} R_m(\widetilde{X}, T) \sin m\pi y. \tag{3.34b}$$

From (3.32) and (3.34), we find that

$$\left(\frac{\partial}{\partial T} + c_m^+ \frac{\partial}{\partial \widetilde{X}}\right)\left(\frac{\partial}{\partial T} + c_m^- \frac{\partial}{\partial \widetilde{X}}\right) B_m = 0, \tag{3.35a}$$

where

$$c_m^{\pm} = c_1 \pm c_m. \tag{3.35b}$$

The implication of (3.35$a$) together with (3.34$a$) is that the outer region is composed of pairs of linear long-wave modes, one moving at a speed of $+c_m$ and the other at a speed of $-c_m$ relative to the background flow. The physical interpretation of the far-field behaviour of the inner region, described by (3.28),(3.30) is now clear: the fundamental, nonlinear wave—through a mechanism of transient self-interaction, manifested in the kernel (3.17)—generates higher harmonics. It is, moreover evident that these harmonics possess an asymptotically small amplitude ($O(\mu^2)$) and therefore travel at their linear long-wave speeds in both directions along the $x$-axis. After a time $t$, the two wave-fronts comprising the $m$-th harmonic will be located at $x = (c_1 \pm c_m)t$. Specifically, the fundamental mode extends between $x = 0$ and $x = 2c_1 t$, where the former wave-front corresponds to the nonlinear disturbance. However, since the timescale $t$ is related to the timescale $T$ of the nonlinear theory by $t = T/\mu^2$, we observe that in the limit $\mu \to 0$, the fundamental front stretches to $x = \infty$. This is the explanation for the appearance of a downstream shelf with fundamental components. In a similar manner, the observation that the higher harmonics also have an infinite extent in the long-wave limit explains their contributions to the shelf, seen in (3.28),(3.30). The preceding discussion also illustrates that the fundamental mode must be treated separately from the higher harmonics.

The structure of the outer region is now obtained by matching the streamfunction and density perturbations in the outer and inner regions:

$$\widehat{\psi}\Big|_{\widetilde{X}=0} = \psi^{(1)}\Big|_{x\to\infty}; \tag{3.36$a$}$$

$$\widehat{\rho}\Big|_{\widetilde{X}=0} = -\frac{\beta}{c_1}\left(\psi^{(1)} + \delta\right)\Big|_{x\to\infty}. \tag{3.36$b$}$$

In accordance with the previous discussion, we first determine the structure of the non-

fundamental modes. The general solution of (3.35$a$) may be written as

$$B_m(\widetilde{X},T) = B_m^+(\xi_m^+)H(\xi_m^+) + B_m^-(\xi_m^-)H(\xi_m^-); \qquad m \neq 1, \tag{3.37a}$$

where $H(x)$ is the Heaviside step function and the characteristics $\xi_m^{\pm}$ are defined by

$$\xi_m^{\pm} = T - \frac{\widetilde{X}}{c_m^{\pm}}.$$

Using (3.33) and (3.34$b$), we find that

$$R_m(\widetilde{X},T) = \frac{\beta}{c_m}\left[B_m^+(\xi_m^+)H(\xi_m^+) - B_m^-(\xi_m^-)H(\xi_m^-)\right]; \qquad m \neq 1. \tag{3.37b}$$

Employing the matching conditions (3.36) along with (3.37$a$,$b$) and solving the resulting linear system, we obtain the structure of a mode-$m$ shelf as

$$B_m^+(T) = \frac{1}{2}\left[\frac{G_m(T)}{m\pi^2(m+1)} - \frac{P_m}{m}\right], \qquad (m \neq 1), \tag{3.38a}$$

$$B_m^-(T) = \frac{1}{2}\left[\frac{G_m(T)}{m\pi^2(m-1)} + \frac{P_m}{m}\right], \qquad (m \neq 1). \tag{3.38b}$$

We now turn our attention to the fundamental mode. Equation (3.35$a$) yields, for $m = 1$,

$$\frac{\partial}{\partial T}\left(\frac{\partial}{\partial T} + 2c_1\frac{\partial}{\partial \widetilde{X}}\right)B_1 = 0, \tag{3.39}$$

while the matching condition (3.36$a$) yields

$$B_1(0,T) = G_1(T). \tag{3.40}$$

Solving (3.39) subject to the condition (3.40), we obtain

$$B_1(\widetilde{X},T) = G_1\left(T - \frac{\widetilde{X}}{2c_1}\right)H\left(T - \frac{\widetilde{X}}{2c_1}\right). \tag{3.41}$$

The function $G_1$ is finally determined by making use of the matching condition (3.36$b$) for the density together with (3.33), (3.34$b$) and (3.41), yielding

$$G_1 = -\frac{1}{2}P_1.$$

Hence, the streamwise structure of the fundamental mode is given by

$$B_1(\tilde{X},T) = -\frac{1}{2}P_1\left(T - \frac{\tilde{X}}{2c_1}\right)H\left(T - \frac{\tilde{X}}{2c_1}\right). \tag{3.42}$$

### *3.3.4 Conservation of mass*

We now demonstrate that the total mass of the system is conserved. The expression (3.25) for the net mass flux out of the inner region, corresponding to the nonlinear wave may be written in terms of the Fourier coefficients of the density perturbation in (3.30):

$$\frac{dM}{dT} = -2\beta\sum_{n=0}^{\infty} c_{2n+1}P_{2n+1}. \tag{3.43}$$

Turning now to the outer region, we calculate the excess mass, $\mathcal{M}_m(T)$ in a shelf corresponding to a non-fundamental mode, $m$:

$$\mathcal{M}_m(T) = \mu^2\beta(1-\cos m\pi)\left[\int_0^{c_m^+T}\mathrm{d}\tilde{X}B_m^+(\xi_m^+) - \int_0^{c_m^-T}\mathrm{d}\tilde{X}B_m^-(\xi_m^-)\right];$$

differentiating once with respect to $T$, the rate of change of mass within the mode-$m$ shelf is then given by

$$\frac{\mathrm{d}\mathcal{M}_m}{\mathrm{d}T} = \beta(1-\cos m\pi)\left[c_m^+B_m^+(T) - c_m^-B_m^-(T)\right]. \tag{3.44$a$}$$

Likewise, the rate of change of mass contained in the mode-1 shelf is determined to be

$$\frac{\mathrm{d}\mathcal{M}_1}{\mathrm{d}T} = -2\beta c_1P_1(T). \tag{3.44$b$}$$

The total rate of change of mass of the outer region is then calculated by summing the expressions in (3.44$a$,$b$) over $m$:

$$\frac{\mathrm{d}\mathcal{M}}{\mathrm{d}T} = 2\beta c_1P_1(T) + \beta\sum_{n=1}^{\infty}\left[c_{2n+1}^+B_{2n+1}^+(T) - c_{2n+1}^-B_{2n+1}^-(T)\right]. \tag{3.45}$$

Inserting the expressions (3.36$a$,$b$) and (3.42) for $B_m^{\pm}(T)$, it is found that (3.45) reduces to

$$\frac{\mathrm{d}\mathcal{M}}{\mathrm{d}T} = -2\beta \sum_{n=0}^{\infty} \frac{P_{2n+1}}{\pi(2n+1)},$$

which is the same as the mass flux out of the resonant wave (3.43). Therefore, the mass that leaves the resonant wave is exactly that required to create the shelves.

The preceding results have been derived assuming a mode-1 nonlinear wave; they are, nevertheless applicable when the modal structure of the nonlinear wave is arbitrary, say mode-$n$. In this eventuality, a shelf comprised of the fundamental mode, $n$ and its harmonics will be generated. Equation (3.9) shows that $c_m \propto m^{-1}$, from which it follows that the shelf will form exclusively on the downstream side of the nonlinear wave. Furthermore, since both the potential and kinetic energy of a wave-like disturbance are proportional to the square of its amplitude, averaged over the fluid domain, we observe that shelf carries a total energy that is $O(\mu^4)$. It is therefore evident that energy, unlike mass, is conserved to $O(\mu^2)$. Finally, we note that the shock-like nature of the fronts described by (3.38),(3.42) implies large spatial variations in their vicinity; dispersive effects are therefore significant there and will act to smooth the discontinuity.

## 3.4 Fully nonlinear flow of large depth

We now investigate nonlinear, weakly dipsersive waves in a vertically unbounded fluid with a uniform, Boussinesq stratification. This may be regarded as the infinite-depth limit of the problem treated by GY and is described by the asymptotic theory of Kantzios & Akylas (1993). Unlike the finite-depth flow, the spectrum here is continuous so that the linear long-wave speed, $c$ can take on any value. As in §3.2, we have the long-wave and

Boussinesq parameters; they are, however, defined somewhat differently:

$$\mu = \frac{c}{N_0 L}, \qquad \beta = \frac{N_0 c}{g}.$$

We also define the stretched coordinate, $Y = \mu^2 y$ in addition to the slow time, $T = \mu^2 t$. The governing equations are given by (3.1)–(3.3), where $y$ is now scaled with $c/N_0$. The boundary conditions are

$$v = 0, \qquad Y = 0, \infty.$$

We now follow the same general development as in §3.2 (see Kantzios & Akylas (1993) or Chapter 3 for details). The vertical coordinate, $y$ is replaced by the streamfunction, $\Psi$. The density is then given by (3.10) while $\Psi$ satisifes (3.11), with $c_n \equiv 1$. Adopting the perturbation expansion in (3.13), the lowest order solution is found to be

$$\Psi^{(0)} = y + 2(a\cos y - b\sin y),$$

where $a = a(x, Y, T)$ and $b = b(x, Y, T)$. At $O(\mu^2)$, we have

$$\psi^{(1)}_{yy} + \psi^{(1)} = H^{(0)} - \psi^{(0)}_{xx} - 2\psi^{(0)}_{yY}, \tag{3.46}$$

the boundary conditions at $Y = 0, \infty$ being homogeneous. By imposing solvability conditions on (3.46), Kantzios & Akylas (1993) derived evolution equations for $a$ and $b$, subject to a breaking criterion analogous to (3.19). Using (3.10) together with the expansion (3.13), the density in the far-field is found once again to be given by (3.23). Thus, following the reasoning of §3.3, it is clear that the present case also features a downstream shelf.

Next, we turn our attention to the issue of mass conservation. The net mass flux out of the resonant wave is given by

$$\frac{\mathrm{d}M}{\mathrm{d}T} = -\mu^2\beta \int_0^\infty \mathrm{d}Y \int_0^{2\pi} \mathrm{d}\Psi\delta + O(\mu^4), \tag{3.47}$$

It is readily shown that the inner integral in (3.47) vanishes since $\delta$ may be expanded in a Fourier series in $\Psi$. Thus, $\dfrac{\mathrm{d}M}{\mathrm{d}T} = O(\mu^4)$ and, unlike the finite-depth problem, mass is conserved. The reason for this is the absence of a physical upper boundary. The shelf amplitude here is $O(\mu^2)$ so that, following the same line of reasoning as in §3.3, the total energy carried therin is $O(\mu^4)$ and conservation of energy holds, correct to $O(\mu^2)$. This last result assumes some importance in view of the fact that in Chapter 2, we studied the modulational stability of infinite-depth flows and employed an energy budget that was crucial in interpreting the physics of the instability.

## 3.5 Weakly nonlinear flow in a waveguide

### *3.5.1 General stratification*

We now consider weakly nonlinear, long waves in an arbitrarily stratified fluid, described to leading order by the KdV equation (Benney 1966). We will show here that a shelf-formation is an inherent feature of this system as well.

Assuming a left-propagating, mode-$n$ wave of amplitude $\epsilon \ll 1$, we adopt the traditional KdV balance $\epsilon = \mu^2$, where the long-wave parameter, $\mu$ is defined in §3.2. Then, in a reference frame translating to the left at a speed of $c_n$, the streamfunction, $\Psi$ and density $\rho$ may be written as

$$\Psi = c_n y + \epsilon\psi, \tag{3.48a}$$

$$\rho = \overline{\rho}(y) + \epsilon q, \tag{3.48b}$$

where $T = \epsilon t$ as before. The equation of mass conservation (3.2) then takes the form

$$c_n q_x - \overline{\rho}_y \psi_x = \epsilon \left( q_y \psi_x - q_x \psi_y - q_T \right), \tag{3.49}$$

while the momentum equations (3.3) yield

$$c_n\left(q\psi_{yx}\right)_y - \frac{q_x}{\beta} = -\epsilon\left[c_n\overline{\rho}\psi_{xxx} + \left(\overline{\rho}\psi_{yT}\right)_y + \left\{\overline{\rho}(\psi_{yx}\psi_y - \psi_{yy}\psi_x) + c_n q\psi_{yx}\right\}_y\right]$$
$$-\epsilon^2\left[\left\{q(\psi_{yx}\psi_y - \psi_{yy}\psi_x)\right\}_y + c_n q\psi_{xx} - \left\{\overline{\rho}(\psi_{yx}\psi_x - \psi_{xx}\psi_y)\right\}_x + \left(q\psi_{yT}\right)_y\right]$$
$$+\epsilon^3\left[q(\psi_{yx}\psi_x - \psi_{xx}\psi_y)\right]_x . \tag{3.50}$$

The boundary conditions on the walls of the waveguide are

$$\psi = 0, \qquad y = 0, 1. \tag{3.51}$$

Following Benney (1966), we now expand $\psi$ and $q$ according to

$$\psi = A\phi^{(0,0)}(y) + \epsilon\psi^{(1)} + \epsilon^2\psi^{(2)} + \ldots, \tag{3.52a}$$

$$q = A\rho^{(0,0)}(y) + \epsilon\rho^{(1)} + \epsilon^2\rho^{(2)} + \ldots, \tag{3.52b}$$

where, in line with our earlier arguments, we have

$$\phi^{(0,0)} = \phi_n(y), \qquad \rho^{(0,0)} = \frac{\overline{\rho}_y}{c_n}\phi_n(y);$$

the amplitude $A = A(x,T)$ satisfies the equation

$$A_T = 2rAA_x + sA_{xxx} + \epsilon\left[\lambda_1(A^3)_x + \lambda_2 AA_{xxx} + \lambda_3 A_x A_{xx} + \lambda_4 A_{xxxxx}\right]$$
$$+\epsilon^2\left[\gamma_1(A^4)_x + \gamma_2 A^2 A_{xxx} + \gamma_3 AA_x A_{xx} + \gamma_4 A_x^3 + \gamma_5 AA_{xxxxx}\right.$$
$$\left. + \gamma_6 A_x A_{xxxx} + \gamma_7 A_{xx}A_{xxx} + \gamma_8 A_{xxxxxxx}\right] + O(\epsilon^3); \tag{3.53}$$

the constants $\lambda_1, \ldots, \lambda_4$ and $\gamma_1, \ldots, \gamma_8$ remain to be determined. It is evident that solutions of (3.53), like those of (3.16), are locally confined. In the development that follows, we use (3.49), (3.50) and (3.51) to derive a series of problems that enable the calculation of contributions to $\psi$ and $q$ at successive orders in $\epsilon$. For reasons that will become apparent

later, these contributions are not determined in their entirety; rather we focus on those that lead to cubic interactions.

We now define, for brevity, the operator $L$ such that

$$L\chi \equiv \frac{\mathrm{d}}{\mathrm{d}y}\left(\overline{\rho}\frac{\mathrm{d}\chi}{\mathrm{d}y}\right) - \frac{\overline{\rho}_y}{\beta c_n^2}\chi.$$

Then, the $O(1)$ problem is, by definition

$$L\phi^{(0,0)} = 0, \qquad \phi^{(0,0)}(0) = \phi^{(0,0)}(1) = 0. \tag{3.54}$$

The $O(\epsilon)$ contributions to $\psi$ and $q$ are given by

$$\psi^{(1)} = A^2\phi^{(1,0)} + A_{xx}\phi^{(0,1)}, \tag{3.55$a$}$$

$$\rho^{(1)} = A^2\rho^{(1,0)} + A_{xx}\rho^{(0,1)}, \tag{3.55$b$}$$

where

$$\rho^{(1,0)} = \frac{\overline{\rho}_y}{c_n}\phi^{(1,0)} + \frac{1}{2c_n^2}\overline{\rho}_{yy}\phi^{(0,0)^2} - \frac{r}{c_n^2}\overline{\rho}_y\phi^{(0,0)},$$
$$\rho^{(0,1)} = \frac{\overline{\rho}_y}{c_n}\phi^{(0,1)} - \frac{s}{c_n^2}\overline{\rho}_y\phi^{(0,0)},$$

and $\phi^{(1,0)}, \phi^{(0,1)}$ satisfy the boundary value problems

$$L\phi^{(1,0)} = E_1, \qquad \phi^{(1,0)}(0) = \phi^{(1,0)}(1) = 0, \tag{3.56$a$}$$

$$L\phi^{(0,1)} = E_2, \qquad \phi^{(0,1)}(0) = \phi^{(0,1)}(1) = 0, \tag{3.56$b$}$$

with $E_1$ and $E_2$ defined in Appendix E. Since the operators and boundary conditions in (3.56) and (3.54) are identical, it is necessary to impose the following conditions in order that (3.56$a$,$b$) possess solutions:

$$\int_0^1 \mathrm{d}y E_{1,2}\phi^{(0,0)} = 0,$$

which uniquely determine the constants $r, s$ in (3.53):

$$r = -\frac{3}{4I}\int_0^1 \mathrm{d}y\overline{\rho}\phi_y^{(0,0)^3}, \qquad s = \frac{c_n}{2I}\int_0^1 \mathrm{d}y\overline{\rho}\phi^{(0,0)^2},$$

where $I = \int_0^1 \mathrm{d}y\overline{\rho}\phi_y^{(0,0)^2}$.

Proceeding to the next order in $\epsilon$, we find that

$$\psi^{(2)} = A^3\phi^{(2,0)} + AA_{xx}\phi_1^{(1,1)} + A_x^2\phi_2^{(1,1)} + A_{xxxx}\phi^{(0,2)}, \tag{3.57a}$$

$$\rho^{(2)} = A^3\rho^{(2,0)} + AA_{xx}\rho_1^{(1,1)} + A_x^2\rho_2^{(1,1)} + A_{xxxx}\rho^{(0,2)}. \tag{3.57b}$$

The functions $\rho^{(2,0)}, \rho_1^{(1,1)}, \rho_2^{(1,1)}$ in (3.57$b$) are given by

$$\begin{aligned}
\rho^{(2,0)} &= \frac{\overline{\rho}_y}{c_n}\phi^{(2,0)} + P_1, \\
\rho_1^{(1,1)} &= \frac{\overline{\rho}_y}{c_n}\phi_1^{(1,1)} + P_2, \\
\rho_2^{(1,1)} &= \frac{\overline{\rho}_y}{c_n}\phi_2^{(1,1)} + \frac{1}{2}(P_3 - P_2).
\end{aligned}$$

We then have the following boundary value problems

$$L\phi^{(2,0)} = \frac{S_1}{c_n}, \qquad \phi^{(2,0)}(0) = \phi^{(2,0)}(1) = 0, \tag{3.58a}$$

$$L\phi_1^{(1,1)} = \frac{S_2}{c_n}, \qquad \phi_1^{(1,1)}(0) = \phi_1^{(1,1)}(1) = 0, \tag{3.58b}$$

$$L\phi_2^{(1,1)} = \frac{1}{2c_n}(S_2 - S_3), \qquad \phi_2^{(1,1)}(0) = \phi_2^{(1,1)}(1) = 0; \tag{3.58c}$$

the quantities $P_1, P_2, P_3, S_1, S_2, S_3$ are defined in Appendix E. As before, solvability conditions are applied to (3.58$a,b,c$), which lead to

$$\int_0^1 \mathrm{d}y\phi^{(0,0)}S_{1,2,3} = 0;$$

solution of these equations then determines the constants $\lambda_1, \lambda_2, \lambda_3$ in (3.53).

At $O(\epsilon^3)$, we have from (3.49), (3.52$b$) and the lower order solutions

$$\rho_x^{(3)} = \frac{\overline{\rho}_y}{c_n}\psi^{(3)} + R_2 A^2 A_{xxx} + R_3 A A_x A_{xx} + R_4 A_x^3 + \ldots, \tag{3.59}$$

where $R_1, R_2, R_3$ are displayed in Appendix E. Moreover, we may write

$$\psi^{(3)} = A^2 A_{xx}\phi_1^{(2,1)} + A A_x^2 \phi_2^{(2,1)} + \int_x \mathrm{d}x A_x^3 \phi_3^{(2,1)} + \ldots.$$

The functions $\phi_1^{(2,1)}, \phi_2^{(2,1)}, \phi_3^{(2,1)}$ are given by the boundary value problems

$$L\phi_1^{(2,1)} = \frac{Q_2}{c_n}, \qquad \phi_1^{(2,1)}(0) = \phi_1^{(2,1)}(1) = 0, \tag{3.60$a$}$$

$$L\phi_2^{(2,1)} = \frac{1}{2c_n}(Q_3 - 2Q_2), \qquad \phi_2^{(2,1)}(0) = \phi_2^{(2,1)}(1) = 0, \tag{3.60$b$}$$

$$L\phi_3^{(2,1)} = \frac{1}{2c_n}(2Q_2 + 2Q_4 - Q_3), \qquad \phi_3^{(2,1)}(0) = \phi_3^{(2,1)}(1) = 0, \tag{3.60$c$}$$

where the functions $Q_2, Q_3, Q_4$ are defined in Appendix E. Proceeding in the same manner as before, solvability conditions on (3.60$a,b,c$) yield

$$\int_0^1 \mathrm{d}y \phi^{(0,0)} Q_{1,2,3} = 0,$$

and thus the constants $\gamma_2, \gamma_3, \gamma_4$ in (3.53) are determined. Returning now to (3.49) and integrating over $x$, we find upon using (3.55$b$), (3.57$b$) and (3.59) that

$$c_n q - \overline{\rho}_y \psi\Big|_{-\infty}^{+\infty} = \epsilon^3 c_n \left(R_2 - \frac{1}{2}R_3 + R_4\right) \int_{-\infty}^{\infty} \mathrm{d}x A_x^3 + O(\epsilon^4), \tag{3.61}$$

where we have taken advantage of the fact that $A(x,T)$ is locally confined. Moreover, terms involving quadratic interactions make no contribution to the right-hand side of (3.61), which is why it was not required to determine *all* of the functions $\phi^{(i,j)}, \rho^{(i,j)}$ at the various levels of $\epsilon$. The same line of reasoning holds for the purely dispersive terms and for nonlinear terms such as $A^2 A_x$, which can be expressed as perfect differentials. Equation (3.61) clearly

indicates that a shelf exists, since the integral is not necessarily zero. However, it is important to bear in mind that this occurs only when the flow is transient. To illustrate this, we observe that under steady flow conditions, (3.53) yields, to leading order in $\epsilon$

$$A_{xx} = -\frac{r}{s}A^2. \tag{3.62}$$

Evaluating then the integral in (3.61) by parts and making use of (3.62), it is found that the right-hand side of (3.61) is $O(\epsilon^4)$. This aspect of the problem is emphasized by using (3.53) to express (3.61) in terms of temporal rather than spatial derivatives. Then, restoring the scaling of (3.48), we find that (3.61) is transformed to

$$c_n\rho - \overline{\rho}_y\Psi\Big|_{-\infty}^{+\infty} = \epsilon^4\frac{c_n}{3s}\left(R_2 - \frac{1}{2}R_3 + R_4\right)\frac{\mathrm{d}}{\mathrm{d}T}\int_{-\infty}^{\infty}\mathrm{d}xA^3 + O(\epsilon^5). \tag{3.63}$$

It is clear from Appendix E that $R_1, R_2, R_3$ are highly nonlinear functions of the vertical coordinate $y$ and are therefore likely to contain contributions from *all* modes, $\phi_m(y)$. Thus, an unsteady, nonlinear mode-$n$ wave will, in general produce a shelf with a broad-band modal structure. Consequently, mode-$m$ fronts with phase speed $c_m < c_n$ will propagate both upstream (towards $x = -\infty$) and downstream, while those with $c_m > c_n$ will only appear downstream of the main wave. The preceding analysis also shows that the mechanism by which the shelf is generated in the weakly nonlinear problem is also a transient, nonlinear (in this case, cubic) self-interaction of the main wave. However, owing to the complexity of the expressions in Appendix E, it is impossible to examine virtually any density-stratification, without resorting to numerical calculation of the boundary value problems.

### *3.5.2 Uniform Boussinesq limit*

We now apply the general results obtained earlier to a fluid with uniform, Boussinesq stratification:

$$\overline{\rho}_y = -\beta$$

As we have seen earlier, this problem is described by the fully nonlinear theory of GY; here, we consider the weakly nonlinear limit. It will be shown that the results obtained in this case agree with the limiting form of those of §3.3. In accordance with our earlier assumption, the nonlinear wave is taken to be mode-1.

The operator $L$ is then given by

$$L \equiv \frac{\mathrm{d}^2}{\mathrm{d}y^2} + \frac{1}{c_1^2},$$

so that $\phi^{(0,0)} = \sin \pi y$. Applying solvability conditions at $O(\epsilon)$, we find that $r = 0$, $s = -\frac{1}{2}c_n^3$. Solving the boundary value problems (3.56) then gives $\phi^{(1,0)} = \phi^{(0,1)} = 0$; additionally, we have $\rho^{(1,0)} = 0$, $\rho^{(0,1)} = \frac{\beta c_1}{2} \sin \pi y$.

Similarly, solvability conditions at $O(\epsilon^2)$ yield $\lambda_1 = \lambda_2 = \lambda_3 = 0, \lambda_4 = \frac{c_1^4}{8}$, with the result that

$$\phi^{(2,0)} = 0, \qquad \phi_1^{(1,1)} = \frac{1}{4} \sin 2\pi y, \qquad \phi_2^{(1,1)} = -\frac{1}{4} \sin 2\pi y,$$

and

$$\rho^{(2,0)} = 0, \qquad \rho_1^{(1,1)} = -\frac{\beta}{2c_1} \sin 2\pi y, \qquad \rho_2^{(1,1)} = \frac{\beta}{2c_1} \sin 2\pi y.$$

Proceeding now to $O(\epsilon^3)$, it is readily shown that $\gamma_1 = \gamma_5 = \gamma_6 = \gamma_7 = 0$ and

$$\gamma_2 = \gamma_3 = -\frac{1}{4c_1}, \qquad \gamma_4 = \frac{1}{2c_1}.$$

The constants $\lambda_1, \ldots, \lambda_4$ and $\gamma_1, \ldots, \gamma_8$ are thus known and (3.53) reduces to

$$A_T - \frac{1}{2}c_n^3 A_{xxx} - \frac{\epsilon c_1^4}{8}A_{xxxxx} + \frac{\epsilon^2}{4c_1}A^2 A_{xxx} + \frac{\epsilon^2}{4c_1}AA_xA_{xx} - \frac{\epsilon^2}{2c_1}A_x^3 + \frac{\epsilon^3 c_1^8}{32}A_{xxxxxxx} = 0. \tag{3.64}$$

We observe that (3.21), upon rescaling $A$ with $\epsilon$, is the same as (3.65), with the exception of the higher-order dispersive terms. This discrepancy is to be expected because the theory of GY only accounts for the leading effects of dispersion.

Next, we find using (3.63) that

$$c_1\rho + \beta\Psi|_{-\infty}^{+\infty} = \epsilon^4 \frac{\beta}{8c_1^5}(\sin\pi y + 3\sin 3\pi y)\frac{\mathrm{d}}{\mathrm{dT}}\int_{-\infty}^{\infty}\mathrm{d}xA^3 + \ldots. \tag{3.65}$$

Returning to the fully nonlinear problem and again scaling $A$ with $\epsilon$, we observe from (3.26) that

$$\int_{-\infty}^{\infty}\mathrm{d}xA_T = \frac{\epsilon^3}{4c_1^4}\frac{\mathrm{d}}{\mathrm{d}T}\int_{-\infty}^{\infty}\mathrm{d}xA^3 + O(\epsilon^5). \tag{3.66}$$

Then, using (3.23) and expanding the integral in (3.24) by small-amplitude expansions, we find that

$$c_1\rho + \beta\Psi|_{-\infty}^{+\infty} = \epsilon^2\frac{\beta}{c_1^2}\sin\pi y\int_{-\infty}^{\infty}\mathrm{d}xA_T - \epsilon^4\frac{\beta}{8c_1^5}(\sin\pi y - 3\sin 3\pi y)\frac{\mathrm{d}}{\mathrm{d}T}\int_{-\infty}^{\infty}\mathrm{d}xA^3 + O(\epsilon^5). \tag{3.67}$$

From (3.66), it is evident that the right-hand sides of (3.65) and (3.67) are identical. Of course, the lower limit of the left-hand side of (3.67) is zero owing to the fact that no shelves can propagate upstream. This would be true even if the main wave were not mode-1 because nonlinear self-interactions of sinusoids do not generate lower harmonics. Thus the case of uniform, Boussinesq stratification is pathological since almost any other density distribution

can be expected to lead to the generation of lower harmonics, causing the appearance of upstream shelves.

## 3.6 Discussion

This chapter has addressed the problem of shelf formation in the context of internal waves in stratified flows. We examined fully nonlinear waves in a uniformly stratified fluid of finite depth and showed that a downstream shelf of asymptotically small amplitude exists when the flow is unsteady, which renders the nonlinear theory of GY invalid far downstream and causes a net efflux of mass. While this was not accounted for by GY, it does not alter the results obtained therein, which pertain to the near-field of the forcing. The far-field must be treated separately since the scales of the nonlinear theory no longer apply; when this is done, it is found that mass is indeed conserved. The downstream shelf is found to consist of pairs of linear waveguide modes propagating in both streamwise directions at their linear long-wave speeds.

The present results would also apply when the nonlinear wave is generated by resonant flow past topography. Allowing the background flow speed, $V$ to differ from the long-wave speed of the resonant mode (assumed to be the $n$-th mode), it is readily shown that the mode-$m$ fronts predicted in §3.3 now travel at speeds $V \pm c_m$ relative to the topography. This was, in fact, the scenario examined numerically by Lamb (1994), who considered a case where the flow is close to a mode-1 resonance. He discovered that long mode-2 waves are formed far downstream, in addition to the dominant mode-1 response as observed in figure 3-1, which is adapted from his figure 9. Lamb proposed that the mode-2 waves are caused by a nonlinear mechanism involving self-interaction of the mode-1 wave and interactions

between mode-1 and mode-2 waves. In the light of the present investigation, it is seen that this expalanation is only partially correct. Flow transience causes nonlinear coupling, which leads to the formation of pairs of *linear* harmonics of the resonant response; the two mode-$m$ harmonics that are generated evolve on the (unstretched) timescale, $t = T/\mu^2$ so that their streamwise extent is large. In Lamb's simulations, the mode-2 wave is observed to possess two downstream fronts. Using his data (see figure 3-1), we calculated the speeds of these fronts to be $V \pm c_2$, in agreement with our prediction. The obstacle used by Lamb was fairly narrow and this precludes further quantitative comparison. However, we note that his mode-2 waves are an order of magnitude smaller than the resonant mode-1 wave, which is in qualitative agreement with the present theory.

Physically, the presence of shelves in the downstream flow implies the existence of columnar disturbances with a high degree of spatial and temporal persistence. Moreover, since the theory of GY may be regarded as a prototype for large-amplitude waves in arbitrarily stratified fluids, one may expect shelves to be generated in an arbitrarily stratified fluid layer as the amplitude of the wave becomes large. In fact, our analysis of the weakly nonlinear flow indicates that shelves of fourth order in amplitude are formed. We have also shown that these latter shelves will, in general, contain components that propagate upstream of the main wave. Since this occurs continuously in a transient flow, it constitutes an upstream influence of a type that has not been considered hitherto.

The problem of upstream influence has been examined in detail by McIntyre (1972) in the context of finite-depth flows with uniform, Boussinesq stratification with a weakly nonlinear topographic forcing of amplitude $\epsilon$; however, unlike the present investigation, the horizontal scale of the forcing is arbitrary. By solving the transient problem using a

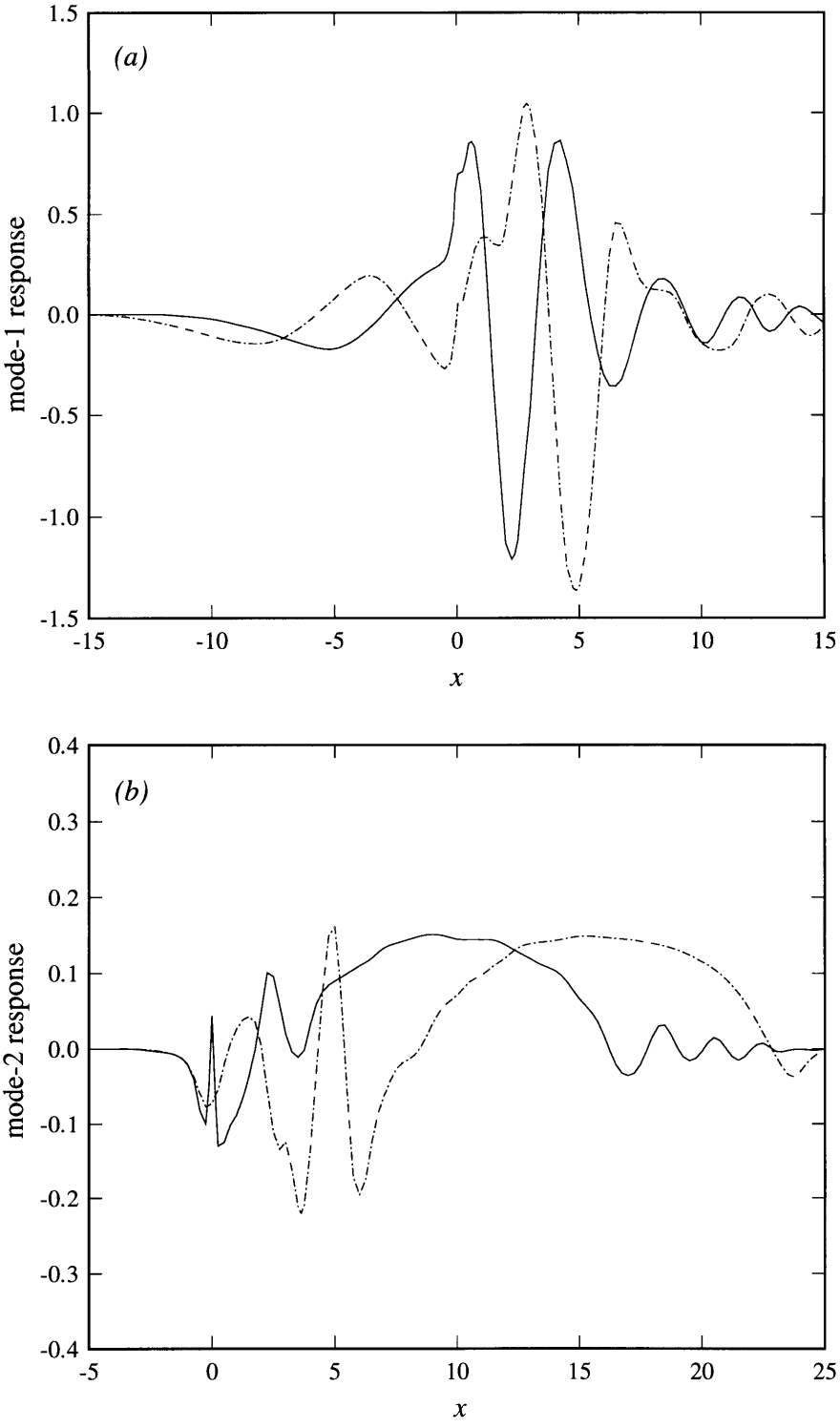


FIGURE 3-1. Data adapted from the numerical simulations of Lamb (1994), illustrating shelf formation. The mode-1 and mode-2 responses are plotted in ($a$) and ($b$) respectively at time, $t = 35$ (——) and $t = 50$ ($-\cdot-\cdot$).

perturbation expansion in terms of the small parameter $\epsilon$, McIntyre demonstrated that upstream-propagating disturbances of $O(\epsilon^2)$ may be generated by nonlinear interactions of the transient 'tails' of the (short) lee waves. Furthermore, the primary contribution to these disturbances is from even-numbered modes, signifying that self-interaction of the lee waves dominates the interactions. In contrast, the shelves in the present study are of $O(\epsilon^4)$ and are caused by self-interaction of the (main) nonlinear long wave. Parenthetically, we observe that in the case of uniform, Boussinesq stratification, there are no upstream shelves.

Finally, we note that although the shelves predicted here are asymptotically small, they can be significant for short obstacles of finite amplitude, as illustrated by Lamb's simulations. Indeed, the shelves there are seen to be only one order of magnitude smaller than the resonant wave, a fact that was alluded to earlier. In geophysical flows, these shelves would act to enhance scalar and momentum transport, thereby increasing the drag force on the obstacle and altering, for example the temperature distribution . In addition, their presence implies reduced towing times in tank experiments, compared with values that might be anticipated based on linear theory. Similar considerations would apply to the appropriateness of boundary conditions that may be used in direct simulations.

# CHAPTER 4

# RESONANT GENERATION OF FULLY NONLINEAR WEAKLY THREE-DIMENSIONAL LONG WAVES

## 4.1 Introduction

It is now generally accepted that the Korteweg–de Vries (KdV) equation and its variants provide the correct theoretical description of two-dimensional (straight-crested), weakly nonlinear waves in arbitrarily stratified, shallow fluid layers (Benney 1966; Grimshaw & Smyth 1986; Melville & Helfrich 1987; Clarke & Grimshaw 1994). The study of three-dimensional waves, where variations occur in both the streamwise and transverse directions has commanded somewhat less attention. The analogous surface wave problem with a forcing consisting of a travelling weakly three-dimensional pressure distribution was shown by Katsis & Akylas (1987*a*) to be governed by a forced Kadomtsev–Petviashvili (fKP) equation, in which three-dimensional effects are represented by a linear term and the basic KdV scaling holds. As Hanazaki (1994) has pointed out, the fKP equation may also be used to describe internal waves. By numerically solving the fKP problem for waves in a channel, Katsis & Akylas (1987*a*) showed that close to resonance (*i.e.*, when the speed of the forcing approaches the linear long-wave speed), upstream-propagating solitary waves which eventually become straight-crested are generated, in agreement with the experimental observations of Ertekin, Webster & Wehausen (1984). The mechanism by which this two-dimensionalization takes place has been a controversial issue. Pedersen (1988) has explained it as being due to a nonlinear (Mach) reflection process, while Tomasson & Melville (1991) argue that it occurs because of differences in the group velocities of the linear trans-

verse modes. However, in recent simulations of the Navier–Stokes equations for a two-layer stratification, Hanazaki (1994) has demonstrated convincingly that the process of Mach reflection does indeed occur.

The KdV and KP families of equations are valid only as long as the stipulation of weak nonlinearity holds. To be sure, higher order corrections may be included in the manner outlined by Benney (1966), but this procedure becomes cumbersome beyond the second order. It is nevertheless known, both from field observations and laboratory measurements that the wave amplitude can be so large as to cause breaking (overturning). While these large-amplitude waves can be studied using direct simulation (Hanazaki 1993; Lamb 1994; Rottman, Broutman & Grimshaw 1996), a theoretical description is useful in providing insight into the flow physics. The first theoretical study of finite-amplitude internal waves was conducted by Grimshaw & Yi (1991, referred to hereinafter as GY), who considered the two-dimensional, finite-depth flow past submerged topography of a fluid with a uniform background flow speed and linearly-varying density distribution. This type of stratification is the one that is most commonly used in laboratory experiments. When the background flow speed coincides with one of a discrete number of linear long-wave speeds, a resonance obtains and nonlinear waves are generated. However, under the aforementioned flow conditions, the coefficient of the nonlinear (quadratic) term in the fKdV equation vanishes. Indeed, it is found that the coefficients of purely nonlinear terms at *all* orders are identically zero. The disappearance of the nonlinear term is not surprising in view of the fact that this occurs in the corresponding steady problem, where it is known as Long's model. It was first shown by Long (1953) that the Euler equations for steady flow past topography can be reduced to a Helmholtz equation for the streamline displacement when the flow

far upstream of the obstacle satisfies precisely the same conditions as those assumed in the Grimshaw–Yi theory. The absence of a nonlinear term in the forced, unsteady problem implies that the required KdV balance between nonlinearity and dispersion does not obtain. It was demonstrated by GY that the flow is governed by an integro-differential equation which is valid until breaking takes place. Although this theory applies in the case of a very special, albeit particularly relevant type of stratification and might therefore appear restrictive, it serves as a prototype for any highly nonlinear wave system and the results therefore have a much wider qualitative applicability. It may be noted that similar analytical investigations have been carried out in other contexts: Warn (1983) and Yi & Warn (1987) examined Rossby waves on a weak shear while Kantzios & Akylas (1993) and Prasad, Ramirez & Akylas (1996) employed analogous techniques to study the modulational stability of two-dimensional internal waves in vertically unbounded fluids.

However, as Hanazaki (1994) has observed, there has been no attempt to study three-dimensional, fully nonlinear waves. Developing a theory for fully nonlinear waves with weak spanwise modulations in the special case of a linearly-varying background density forms the central theme of the present investigation. We consider a forcing that is due to an obstacle at the bottom of a channel instead of the pressure distribution used by Katsis & Akylas (1987*a*). It will be shown in §4.3 that the flow is governed by an integro-differential equation, wherein three-dimensional effects are incorporated *via* a highly nonlinear term, the presence of which leads to certain complications. Specifically, we will demonstrate in §4.4 that the solution of the evolution equation must satisfy an integral constraint in order to remain locally confined. This is not surprising in view of a similar constraint that applies to KP-type problems (Grimshaw 1985; Katsis & Akylas 1987*b*).

In Chapter 3, it has been demonstrated that transient, nonlinear internal waves in two-dimensional flows are accompanied by the formation of shelves. We show in §4.5 that this occurs in the present problem as well, causing the nonlinear theory to break down in the far field, with the result that neither mass nor energy is conserved. This necessitates a separate treatment of the shelf region, described in §4.6, where a procedure for constructing the far-field solution is outlined. In §4.7, the nonlinear theory developed here is employed to study the flow past an obstacle in a straight-walled channel. A few numerical solutions of the evolution equation are presented. The behaviour of the breaking time is also examined.

## 4.2 Formulation

We consider the flow of an inviscid, incompressible density-stratified fluid of depth $h$ past an obstacle that lies at the bottom of a channel, as illustrated in figure 4-1. The streamwise and spanwise coordinates are respectively $x$ and $z$, while the vertical direction is $y$. The flow far upstream of the obstacle is assumed to possess a uniform streamwise speed, $U$. Taking $\rho_0$, $N_0$ and $L$ to be typical values of the density, Brunt–Väisälä frequency and wavelength respectively, we choose the following dimensionless (primed) variables:

$$x = Lx', \quad y = hy', \quad z = Lz', \quad t = t'/(\mu N_0),$$

$$u = N_0 h u', \quad v = \mu N_0 h v', \quad w = N_0 h w', \quad \rho = \rho_0 \rho', \quad p = \rho_0 g h p',$$

where $\boldsymbol{u} = (u, v, w)$ is the velocity field, $p$ is the pressure, $\rho$ is the density and the dispersion parameter $\mu = h/L$ is a measure of dispersive effects. Dropping the primes, the governing equations of incompressibility, mass conservation and momentum may be written as

$$\boldsymbol{\nabla} \cdot \boldsymbol{u} = 0, \tag{4.1}$$

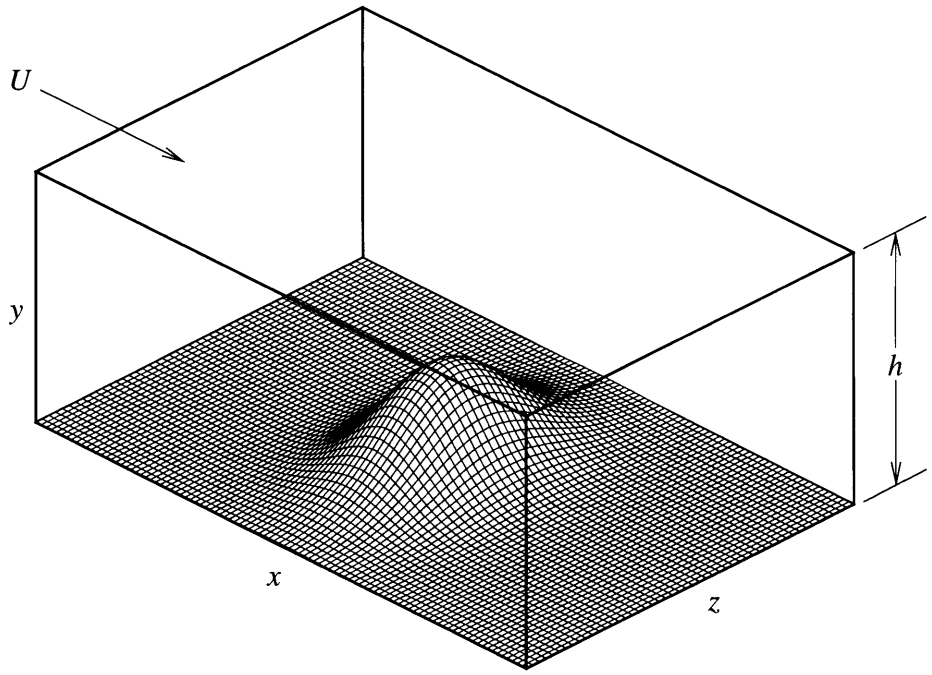


FIGURE 4-1. Schematic of flow configuration for three-dimensional flow.

$$\rho_t + \boldsymbol{u} \cdot \boldsymbol{\nabla}\rho = 0, \tag{4.2}$$

$$\beta\rho(\boldsymbol{u}_t + \boldsymbol{u} \cdot \boldsymbol{\nabla}\boldsymbol{u}) = -\left(p_x,\ \mu^{-2}(\rho + p_y), -p_z\right), \tag{4.3}$$

where the Boussinesq parameter, $\beta$ is defined by

$$\beta = \frac{N_0^2 h}{g}.$$

The Brunt–Vaisala frequency, $N$ is defined in terms of the density, $\overline{\rho} = \overline{\rho}(y)$ of the background flow by

$$\beta\overline{\rho}N^2 = -\overline{\rho}_y. \tag{4.4}$$

We assume here that $N$ is nearly constant with height; following conventional terminology, the condition of constant $N$ is referred to as a uniform stratification. Furthermore, the fluid

layer is assumed to be bounded above by a rigid lid, which leads to the condition

$$v = 0, \qquad y = 1. \tag{4.5}$$

On the bottom topography, we have the boundary condition

$$v = \epsilon \left( u f_x + w f_z \right), \qquad y = \epsilon f, \tag{4.6}$$

where $\epsilon$ is a small parameter that measures the amplitude of the topography in comparison with the depth of the fluid layer.

We now examine the dynamics of a linear flow ($\epsilon = 0$) with a uniform stratification, $N = 1$, in the Boussinesq approximation ($\beta \to 0$). The linearized forms of (4.1)–(4.3) may be combined to yield

$$\left( \frac{\partial}{\partial t} + V \frac{\partial}{\partial x} \right)^2 \left[ v_{yy} + \mu^2 \left( v_{xx} + v_{zz} \right) \right] + \left( \frac{\partial^2}{\partial x^2} + \frac{\partial^2}{\partial z^2} \right) v = 0, \tag{4.7}$$

where $V$ is an inverse Froude number defined by

$$V = \frac{U}{Nh}.$$

The linearized versions of the boundary conditions (4.5), (4.6), with (4.7) then lead to an eigenvalue problem for $v_m(y)$, the vertical structure of $v$, the solution of which is given by

$$v_m(y) = \sin \frac{y}{c_m}, \qquad c_m = \frac{1}{m\pi}, \qquad m = 1, 2, 3 \ldots, \tag{4.8$a, b$}$$

where the $c_m$ are the eigenvalues and represent the speeds corresponding to the long-wave modes, $v_m$. Using these modes, it follows from (4.7) that the linear dispersion relation satisfied by a wave-like disturbance proportional to $v_m \exp[i(kx + my + lz - \omega t)]$ is given by

$$\omega = Vk \pm c_m \left( k^2 + l^2 \right)^{\frac{1}{2}} \left[ 1 - \frac{1}{2} \mu^2 c_m^2 \left( k^2 + l^2 \right) \right] + O(\mu^4). \tag{4.9}$$

In the limit $\mu \to 0$, we observe from (4.9) that weakly three-dimensional disturbances with $l/k = O(\mu)$ are stationary relative to the topography when the background flow speed is such that $V = c_m + O(\mu^2)$. The group velocity also vanishes under these conditions, implying that the flow is resonant. The resulting accumulation of energy close to the obstacle causes the amplitude of the response to increase continuously with time, necessitating the use of a nonlinear theory.

The linear dispersion relation (4.9) also indicates that under resonant conditions, the flow evolves on a slow timescale $t = O(\mu^{-2})$. In order to accommodate this slow temporal development as well as the weak spanwise variation introduced earlier, the stretched coordinates $T$ and $Z$ are defined:

$$T = \mu^2 t; \qquad Z = \mu z \tag{4.10}$$

Furthermore, the background flow speed is taken as

$$V = c_n \left(1 + \mu^2 \sigma\right), \tag{4.11}$$

in accordance with the condition for a mode-$n$ resonance; additionally, we allow for small departures from a uniform background stratification:

$$N^2(y) = 1 + \mu^2 \overline{q}(y). \tag{4.12}$$

Here, both $\sigma$ and $\overline{q}(y)$ are both $O(1)$ quantities.

We now define two streamfunctions $\Psi$ and $\phi$ such that

$$u = \Psi_y + \mu^2 \mathcal{U}, \tag{4.13a}$$

$$v = -\Psi_x + \mu^2 \mathcal{V}, \tag{4.13b}$$

$$w = \mu \mathcal{W}, \tag{4.13c}$$

where

$$(\mathcal{U}, \mathcal{V}, \mathcal{W}) = \boldsymbol{\nabla}\Psi \times \boldsymbol{\nabla}\phi. \tag{4.14}$$

From the definitions of $\Psi$ and $\phi$, it is clear that $\Psi$ describes an almost two-dimensional flow while $\phi$ accounts for weakly three-dimensional effects and, moreover, that the condition of incompressibility (4.1) is automatically satisfied. The equation of mass conservation (4.2) then yields

$$J(\rho, \Psi) = -\mu^2 \left(\rho_T + \mathcal{U}\rho_x + \mathcal{V}\rho_y + \mathcal{W}\rho_Z\right), \tag{4.15}$$

where the jacobian is defined by $J(a, b) \equiv a_x b_y - a_y b_x$. Equation (4.15) implies that the density $\rho$ is conserved along lines of constant $\Psi$ to leading order in $\mu$. The coordinate $y$ may therefore be replaced by $\Psi$:

$$(x, y, Z, T) \longrightarrow (x, \Psi, Z, T); \tag{4.16}$$

this is possible provided $\Psi$ is a single-valued function of $y$, which implies that wave-breaking (overturning) has not occurred. Using the transformation (4.16), it is readily shown that

$$\mathcal{U}\rho_x + \mathcal{V}\rho_y + \mathcal{W}\rho_Z = O(\mu^2);$$

thus (4.15) may be integrated to yield

$$\rho = \Gamma(\Psi) - \mu^2 \overline{\rho}_\Psi \int_{-\infty}^{x} \mathrm{d}x' \left.\frac{\rho_T}{\Psi_y}\right|_\Psi, \tag{4.17}$$

where the notation $|_\Psi$ signifies that $\Psi$ is held constant. The function $\Gamma(\Psi)$ is determined by requiring that $\rho$ approach the background flow density far upstream:

$$\rho = \overline{\rho}(y), \qquad x \to -\infty. \tag{4.18}$$

Given that the flow is uniform far upstream, we find, using (4.11) that

$$y = \frac{\Psi}{c_n}\left(1 - \mu^2\sigma\right), \qquad x \to \infty. \tag{4.19}$$

In view of (4.18) and (4.19), equation (4.17) yields

$$\rho = \overline{\rho}\left(\frac{\Psi}{c_n}\right) - \mu^2\overline{\rho}_\Psi\left[\sigma\Psi + \int_{-\infty}^{x} \mathrm{d}x' \left.\frac{\Psi_T}{\Psi_y}\right|_\Psi\right]. \tag{4.20}$$

Next, manipulating the momentum equations (4.3) and assuming a uniform, Boussinesq background stratification, we obtain, correct to $O(\mu^2)$

$$\beta J(\Psi_y, \Psi) = -p_x - \mu^2\beta\left[\Psi_{yT} + J(\mathcal{U}, \Psi) + Q\right], \tag{4.21a}$$

$$\beta J(\Psi, \Psi_x) = -\frac{p_y}{\mu^2} - \frac{\rho}{\mu^2}, \tag{4.21b}$$

$$\beta J(\mathcal{W}, \Psi) = -p_Z, \tag{4.21c}$$

where

$$Q = \mathcal{U}\Psi_{yx} + \mathcal{V}\Psi_{yy} + \mathcal{W}\Psi_{yZ}. \tag{4.22}$$

Eliminating $p$ from (4.21$a$,$b$), it is found that

$$\beta J(S, \Psi) = \frac{1}{\beta}\left(\rho_x|_\Psi\, y\right)_y + \mu^2\overline{\rho}\left\{-\Psi_{yyT} - J(\Psi_{xx}, \Psi) - \left[J(\mathcal{U}, \Psi_y)\right]_y - Q_y\right\}, \tag{4.23}$$

where

$$S = \Psi_{yy} + \rho_\Psi\frac{y}{\beta}. \tag{4.24}$$

From (4.23), it is clear that $S$, like $\rho$, is conserved to leading order along lines of constant $\Psi$. Simplifying the expression for $Q$ in (4.22) and using (4.14), we obtain

$$Q = \phi_Z|_\Psi\, J(\Psi_y, \Psi) + \phi_x|_\Psi\left(\Psi_Z\Psi_{yy} - \Psi_y\Psi_{yZ}\right). \tag{4.25}$$

We now integrate (4.23) with respect to $x$ to obtain

$$S = \Omega(\Psi) + \frac{1}{\beta}\frac{\partial}{\partial\Psi}\int_{-\infty}^{x} \mathrm{d}x' \rho_x\, y|_\Psi \\ + \mu^2\overline{\rho}\left[\Psi_{xx} + \frac{\partial}{\partial\Psi}\int_{-\infty}^{x} \mathrm{d}x'\, \Psi_{yT}|_\Psi + \frac{\partial}{\partial\Psi}\int_{-\infty}^{x} \mathrm{d}x'\, (\mathcal{U}_x\Psi_y + Q)|_\Psi\right]. \tag{4.26}$$

The function $\Omega(\Psi)$ is then determined by imposing the condition that

$$S = -\overline{\rho}\frac{\Psi}{c_n^2}\left[1 + \mu^2(\overline{q} - 2\sigma)\right], \qquad x \to -\infty.$$

Then, making use of (4.19), (4.20) and (4.24), it is found that (4.26) simplifies to

$$\Psi_{yy} + \frac{\Psi - Vy}{c_n^2} = -\mu^2\left[\Psi_{xx} + R + \frac{\partial}{\partial\Psi}\int_{-\infty}^{x} \mathrm{d}x'\, (\mathcal{U}_x\Psi_y + Q)|_\Psi \right. \\ \left. + \frac{\Psi - Vy}{c_n^2}(\overline{q} - 2\sigma)\right], \tag{4.27}$$

where

$$c_n R = y\frac{\partial}{\partial\Psi}\int_{-\infty}^{x} \mathrm{d}x' \left.\frac{\Psi_T}{\Psi_y}\right|_\Psi - \frac{\partial}{\partial\Psi}\int_{-\infty}^{x} \mathrm{d}x' \left.\frac{y\Psi_T}{\Psi_y}\right|_\Psi + c_n\frac{\partial}{\partial\Psi}\int_{-\infty}^{x} \mathrm{d}x'\Psi_{yT}. \tag{4.28}$$

An examination of (4.27) indicates that it reduces to Long's equation when the flow is steady and two-dimensional, as expected. In addition, it is clear that the first three terms on the right hand side account for non-hydrostatic, unsteady and three-dimensional effects, while the fourth term represents the effects of non-uniform stratification and deviation from exact resonance.

The boundary conditions on (4.27) follow from (4.5) and (4.6): on the upper boundary, we have

$$\Psi_x = \mu^2\mathcal{V}, \qquad y = 1, \tag{4.29}$$

while the boundary condition on the topography (4.6), after expanding about $y = 0$, may be expressed as

$$\Psi_x + \epsilon\Psi_y f_x - \mu^2\mathcal{V} = O(\mu^2\epsilon), \qquad y = 0. \tag{4.30}$$

Finally, we eliminate $p$ from (4.21$a$,$c$) to obtain

$$[J(\mathcal{W},\Psi)]_x = [-\Psi_{yy}\Psi_x + \Psi_{yx}\Psi_y]_Z\,,$$

which, upon use of (4.27), may be integrated to give

$$J(\mathcal{W},\Psi) = \Psi_{yZ}\Psi_y - \Psi_{yy}\Psi_Z. \tag{4.31}$$

The definition of $\mathcal{W}$ in (4.14) then yields an equation for $\phi$:

$$J(\phi,\Psi) = -\mathcal{W}. \tag{4.32}$$

The form of (4.31) reveals that $\mathcal{W}$ (and therefore $\phi$) does not evolve independently in time but is slaved to $\Psi$; this is a consequence of the assumption that the spanwise dependence is weak. As stated earlier, our interest here is centred on the flow past an obstacle lying at the bottom of a channel. The transverse velocity must therefore vanish on the channel walls, located at $Z = \pm W$. Assuming further that the obstacle is symmetric about the centre-plane of the channel, $Z = 0$, we have

$$\mathcal{W} = 0, \qquad Z = 0, W. \tag{4.33}$$

Alternatively, (4.33) may be considered as describing a flow through a constriction in a straight-walled channel.

The ensuing analysis is developed on the basis of (4.27), (4.31) and the boundary conditions (4.29), (4.30) and (4.33). The governing equations (4.27) and (4.31) may also be derived as outlined in Appendix F by an alternative, perhaps more physical approach, which is based on the properties of the vorticity and Bernoulli function.

## 4.3 Evolution equation

We now derive an equation that describes the evolution of the resonant mode. The form of (4.27) suggests pertubation expansions of the form

$$\Psi = Vy + \psi^{(0)} + \mu^2\psi^{(1)} + \ldots; \qquad \phi = \phi^{(0)} + \mu^2\phi^{(1)} + \ldots. \tag{4.34a, b}$$

At the lowest order in $\mu$, (4.27) yields

$$\psi^{(0)}_{yy} + \frac{\psi^{(0)}}{c_n^2} = 0, \tag{4.35a}$$

while the boundary conditions (4.29) and (4.30) reduce to their linear form

$$\psi^{(0)} = 0, \qquad y = 0, 1. \tag{4.35b}$$

The solution of the system (4.35$a$,$b$) is given by

$$\psi^{(0)} = Av_n = A\sin n\pi y,$$

where $v_n$, defined in (4.8$a$), is the vertical structure of the resonant mode and $A = A(x, Z, T)$ is an amplitude that remains to be determined. For later mathematical convenience, we also define

$$\Psi^{(0)} = Vy + A\sin n\pi y. \tag{4.36}$$

Next, from (4.31) and (4.34), it is found that

$$\mathcal{W}^{(0)}_x\Big|_\Psi \Psi^{(0)}_y = -\Psi^{(0)}_{yy}\Psi^{(0)}_Z + \Psi^{(0)}_{yZ}\Psi^{(0)}_y, \tag{4.37}$$

where $\mathcal{W}^{(0)} = \mathcal{W}(x, \Psi^{(0)}, Z, T)$. Integrating (4.37) with respect to $x$, we obtain

$$\mathcal{W}^{(0)} = \int_{-\infty}^{x} \mathrm{d}x' \left(\Psi^{(0)}_{yZ} - \frac{\Psi^{(0)}_{yy}\Psi^{(0)}_Z}{\Psi^{(0)}_y}\right)\Bigg|_\Psi. \tag{4.38}$$

It then follows, from (4.32) and (4.34$b$) that

$$\phi^{(0)} = -\int_{-\infty}^{x} \mathrm{d}x' \left. \frac{\mathcal{W}^{(0)}}{\Psi_y^{(0)}} \right|_{\Psi}. \tag{4.39}$$

Returning to the expansion (4.34$a$) for $\Psi$, we have at the next order in $\mu^2$

$$\psi_{yy}^{(1)} + \frac{\psi^{(1)}}{c_n^2} = -\Psi_{xx}^{(0)} - R^{(0)} - \mathcal{H}^{(0)} - \frac{\Psi^{(0)} - Vy}{c_n^2}(\overline{q} - 2\sigma), \tag{4.40}$$

where

$$\mathcal{H}^{(0)} = \frac{\partial}{\partial \Psi} \int_{-\infty}^{x} \mathrm{d}x' \left( \mathcal{U}_x^{(0)}\Big|_{\Psi} \Psi_y^{(0)} + Q^{(0)} \right)\Big|_{\Psi}, \tag{4.41}$$

where $Q^{(0)}$ is obtained from (4.25 and the superscript $^{(0)}$ signifies evaluation at $\Psi = \Psi^{(0)}$. Then, integrating the first term in (4.41) by parts and using (4.38),(4.39) to simplify the expression for $Q^{(0)}$, we find that

$$\mathcal{H}^{(0)} = \mathcal{U}_y^{(0)} + \phi_Z^{(0)}\Big|_{\Psi} \Psi_{yy}^{(0)} + \mathcal{W}^{(0)}\mathcal{W}_{\Psi}^{(0)}. \tag{4.42}$$

Invoking the definition of $\mathcal{V}$ in (4.14)and the fact that $\psi^{(1)}\Big|_{x\to\infty} = 0$, the upper boundary condition (4.29) reduces to

$$\psi^{(1)} = 0, \qquad y = 1, \tag{4.43}$$

while the boundary condition on the topography (4.30) yields

$$\psi^{(1)} = -\frac{\epsilon}{\mu^2}\left(c_n + \frac{A}{c_n}\right) f, \qquad y = 0. \tag{4.44}$$

It is evident from (4.44) that nonlinear and dispersive effects will balance when $\epsilon = O(\mu^2)$. Therefore, we may, without loss of generality set $\epsilon = \mu^2$ in the subsequent development of the theory.

The left-hand side of (4.40) is the same as that of the lowest order problem (4.35$a$). It is therefore necessary to impose a solvability condition, which is derived by multiplying (4.40)

by $\sin n\pi y$ and integrating over $y$. Upon using (4.43) and (4.44), these operations result in the equation

$$-\int_0^1 \mathrm{d}y R^{(0)} \sin n\pi y - \frac{1}{c_n^2}\int_0^1 \mathrm{d}y A \sin^2 n\pi y(\overline{q}-2\sigma) - \frac{1}{2}A_{xx} - \int_0^1 \mathrm{d}y \mathcal{H}^{(0)} \sin n\pi y + \left(1+\frac{A}{c_n^2}\right) f = 0. \tag{4.45}$$

The integration over $y$ in the first term may be replaced with one over $\Psi$, in line with the reasoning that led to (4.16). The order of integration over $\Psi$ and $x$ may then be interchanged. Further, we assume a linear variation of $\overline{q}$ with the vertical coordinate:

$$\overline{q}(y) = q_0 y,$$

where $q_0$ is a constant. With these simplifications, equation (4.45) reduces to the form

$$\int_{-\infty}^{x} \mathrm{d}x' K(x,x') A_T' + \lambda_1 c_n A - \frac{c_n}{2}\lambda_2 A^2 - \frac{1}{2}c_n^3 A_{xx} + c_n^3 \int_0^{c_n} \mathrm{d}\Psi \mathcal{H}^{(0)} y_A + c_n^3\left(\frac{A}{c_n^2}+1\right) f = 0, \tag{4.46}$$

with

$$\lambda_1 = \frac{1}{2}(q_0 - \sigma), \qquad \lambda_2 = \frac{4}{3}q_0(1-\cos n\pi).$$

Making use of the fact that $y_A = -\sin \pi y/\Psi_y$, the kernel $K(x,x')$ is defined by

$$K(x,x') = c_n \int_0^{c_n} \mathrm{d}\Psi y_A \left[y_A' + c_n \left(y' y_A'\right)_\Psi - c_n y y_{A\Psi}'\right]. \tag{4.47}$$

The form of the kernel $K(x,x')$ is seen to be identical to the one derived by GY for the corresponding two-dimensional problem. We now differentiate (4.46) once with respect to $x$ in preparation for its numerical solution; this also has the effect of yielding a more recognizable form:

$$K^c A_T + \int_{-\infty}^{x} \mathrm{d}x' K_x A_T' + \lambda_1 c_n A_x - c_n \lambda_2 A A_x - \frac{1}{2}c_n^3 A_{xxx}$$

$$+ c_n^3 \int_0^{c_n} \mathrm{d}\Psi \left(\mathcal{H}^{(0)} y_A\right)_x\Big|_\Psi + c_n^3 \left[\left(\frac{A}{c_n^2}+1\right) f\right]_x = 0, \qquad (4.48)$$

with $K^c(x) = K(x,x)$.

The first two terms in (4.48) represent unsteady effects while the terms involving $\lambda_1$ and $\lambda_2$ arise from non-uniform stratification and departure from exact resonance. The third order dispersive term is caused by non-hydrostatic effects and is familiar from KdV-type problems. The sixth term in (4.48), which is nonlinear involves quantities that arise only as a result of transverse variations in the flow and therefore represents three-dimensional effects. Finally, the last term arises from the forcing due to the bottom topography and also appears in the two-dimensional problem of GY.

We now turn our attention to the transverse boundary conditions. From (4.36) and (4.38), it is seen that (4.33) is equivalent to

$$A_Z = 0, \qquad Z = 0, W; \qquad (4.49)$$

this similar to the boundary condition used by Katsis & Akylas (1987*a*) in their forced Kadomtsev–Petviashvili (fKP) model for resonant generation of three-dimensional surface waves in a channel.

Equation (4.48), together with the boundary condition (4.49) and appropriate initial conditions fully determines the amplitude $A(x, Z, T)$. However, it is crucial to bear in mind that the theory is valid only as long as the transformation (4.16) is possible. This implies that $\Psi_y \neq 0$, which leads to the condition

$$|A| < c_n^2. \qquad (4.50)$$

This condition imposes a limit on the magnitude of $A$, above which the flow features reversed density gradients which eventually lead to wave-breaking. For this reason, we shall refer to

(4.50) as the breaking criterion. It may be noted that (4.50) is identical to the breaking criterion derived by GY, after the necessary change of variables has been made.

We now proceed to examine an important property of the evolution equation (4.48). For solutions of the form $A = A(x + pZ, T)$, it may be shown (see Appendix G) that

$$-c_n^3 \int_0^{c_n} \mathrm{d}\Psi \, \mathcal{H}^{(0)} y_A \Big|_\Psi = \frac{c_n}{2} p^2 A. \tag{4.51}$$

In addition, as shown by GY, the kernel satisfies the following property

$$\int_{-\infty}^{x} \mathrm{d}x' K(x, x') A_x = c_n A, \tag{4.52}$$

The implication of (4.51) and (4.52) is that for steady, oblique travelling wave solutions in the absence of a forcing term, (4.48) becomes linear when $\lambda_2 = 0$. This is not surprising, for the conditions of Long's model are then met. Thus the presence of three-dimensionality and transience intorduces nonlinearity, as expected. When $\lambda_2 \neq 0$, (4.48) reduces to the steady KdV equation and therefore possesses solitary wave solutions.

When the transformation (4.16) is valid, we may invert (4.36)

$$y = y(\Psi^{(0)}; A).$$

For small amplitudes, $|A| \ll c_n^2$, this relation for $y$ may be expanded in powers of $A$, with $\Psi^{(0)}$ as a parameter. All functions of the vertical coordinate can then be determined in terms of $A$ and $\Psi^{(0)}$. Thus, we find that the kernel and the three-dimensional term yield, upon expansion

$$K(x, x') = 1 + \frac{1}{c_n^4} \left( -\frac{3}{4} A'^2 + 2AA' - \frac{3}{4} A^2 \right) + O(A^4), \tag{4.53a}$$

$$\int_0^{c_n} \mathrm{d}\Psi \left( \mathcal{H}^{(0)} y_A \right)_x \Big|_\Psi = \frac{1}{2} \int_{-\infty}^{x} \mathrm{d}x' A'_{ZZ} + O(A^3); \tag{4.53b}$$

thus, to lowest order in $A$, the evolution equation (4.48) reduces to the form

$$A_T + c_n\lambda_1 A_x - \frac{1}{2}c_n^3 A_{xxx} + \frac{1}{2}c_n^3 \int_{-\infty}^{x} \mathrm{d}x' A'_{ZZ} + c_n^3 f_x = 0,$$

which is just the linearized fKP equation and is consistent with the dispersion relation (4.9).

Finally, we note that in the absence of spanwise modulations, the three-dimensional term in (4.48) vanishes and the evolution equation of GY is recovered.

## 4.4 Integral constraint

We now turn our attention to the crucial issue of whether or not solutions of (4.48) are locally confined. In the case of equations of the KP type, Grimshaw (1985) has shown that certain integral contraints must be satisfied for the waves to be locally confined. Specifically, in the case of the KP equation, the constaint takes the form

$$\int_{-\infty}^{\infty} \mathrm{d}x A(x, Z, T) = 0. \tag{4.54}$$

Katsis & Akylas (1987*b*) have demonstrated that (4.54) is exactly consistent with the linear dispersion relation (4.9): when (4.54) is violated, the amplitude $A$ possesses components with streamwise wavenumber, $k = 0$ and nonzero spanwise wavenumber. According to (4.9), the group velocities of these components is infinite. Consequently, they travel downstream to $x = +\infty$ instantaneously, thus rendering the wave non-locally confined. However, the scaling in (4.10) (which is identical to the fKP problem) assumes that $l/k = O(\mu)$, which excludes components with finite $l$ and $k = 0$. In the eventuality that an initial condition which does not satisfy (4.54) is imposed, the problem must be treated in terms of asymptotically matched 'time layers' in which the 'outer layer' corresponds to the fKP model and the 'inner

layer' is the linear, transient problem (Grimshaw & Melville 1989; Ablowitz & Wang 1995). For a flow that is started from rest, the condition (4.54) is satisfied trivially at $T = 0$ and it is easy to show that it continues to hold for all $T$.

We now examine the asymptotic behaviour of $\mathcal{W}^{(0)}$ as $x \to \infty$. Following the procedure used to obtain (4.53$a$,$b$), the expression in (4.37) may be expanded in the small-amplitude limit, $|A| \ll c_n^2$ to give

$$\mathcal{W}_\infty^{(0)}(\Psi, Z, T) = \frac{1}{c_n} \cos\frac{\Psi}{c_n^2} \int_{-\infty}^{\infty} \mathrm{d}x A_Z + \frac{1}{c_n^3} \sin^2\frac{\Psi}{c_n^2} \int_{-\infty}^{\infty} \mathrm{d}x \left(A^2\right)_Z - \frac{3}{2c_n^5} \sin^2\frac{\Psi}{c_n^2} \cos\frac{\Psi}{c_n^2} \int_{-\infty}^{\infty} \mathrm{d}x \left(A^3\right)_Z + O(A^4), \tag{4.55}$$

where $\mathcal{W}_\infty^{(0)}(\Psi, Z, T) = \lim_{x\to\infty} \mathcal{W}^{(0)}$. It is evident from (4.55) that $\mathcal{W}^{(0)}$ does not vanish as $x \to \infty$ and since $\mathcal{W}^{(0)}$ is related to $A$ through (4.38) it therefore appears that that the solution does not remain locally confined.

In order to clarify this issue, we formally derive a constraint analogous to (4.54), which guarantees a locally confined solution of the evolution equation (4.48). This is done by setting $x = \infty$ in (4.48); assuming further that $A$ and its derivatives decay to zero sufficiently fast for large $x$, we obtain the condition

$$\lim_{x\to\infty} \int_0^{c_n} \mathrm{d}\Psi y_\Psi \cos n\pi y \, \phi_{xZ}^{(0)}\Big|_\Psi = 0,$$

which, upon using (4.39) and the boundary condition (4.49) simplifies to

$$\int_0^{c_n} \mathrm{d}\Psi \cos\frac{\Psi}{c_n^2} \mathcal{W}_\infty^{(0)}(\Psi, Z, T) = 0. \tag{4.56}$$

The constraint (4.56) must therefore be satisfied if $A$ is to remain locally confined. It is trivially satisifed when $\mathcal{W}_\infty^{(0)} = 0$, which is true for two-dimensional flow or in the linear limit, $|A| \ll c_n^2$. However, (4.56) indicates that the solution for $A$ can remain locally confined

even when $\mathcal{W}_\infty^{(0)}$ is non-zero, provided it is orthogonal to $\cos(\Psi/c_n^2)$; physically, this means that the transverse velocity far downstream must not contain a component corresponding to the resonant mode. Since the evolution equation (4.48) reduces to the linearized fKP equation when $|A| \ll c_n^2$, it is clear that $A$ is locally confined for small $T$. That it continues to remain so is not obvious since, unlike the fKP case, it cannot be proven that (4.56) is satisfied for all $T$ when it holds at $T = 0$. We therefore adopt the following procedure to verify if (4.56) is satisified for $T \gg 1$.

The small-amplitude expansion for $\mathcal{W}_\infty^{(0)}$ in (4.55), when substituted into the constraint (4.56) yields

$$\int_{-\infty}^{\infty} \mathrm{d}x A - \frac{3}{8c_n^4}\int_{-\infty}^{\infty} \mathrm{d}x A^3 + \frac{5}{192c_n^8}\int_{-\infty}^{\infty} \mathrm{d}x A^5 + O(A^7) = 0. \tag{4.57}$$

To lowest order in $A$, it is clear that (4.57) is just the constraint (4.54) for the fKP equation. We now define

$$C_1 = \int_0^W \mathrm{d}Z \int_{-\infty}^{\infty} \mathrm{d}x A, \tag{4.58a}$$

$$C_3 = C_1 - \frac{3}{8c_n^4}\int_0^W \mathrm{d}Z \int_{-\infty}^{\infty} \mathrm{d}x A^3, \tag{4.58b}$$

$$C_5 = C_3 + \frac{5}{192c_n^8}\int_0^W \mathrm{d}Z \int_{-\infty}^{\infty} \mathrm{d}x A^5, \tag{4.58c}$$

corresponding respectively to the constraint (4.57), correct to first, third and fifth order respectively, averaged over the width of the channel. The evolution equation (4.48) is solved numerically using the method described in §4.7, assuming that the solution is locally confined. The integrals in (4.58) are evaluated numerically, using the trapezoidal rule and are displayed in figure 4-2 as functions of $T$. For $T \ll 1$, the integrals are all small and nearly identical. As $T$ increases, $C_1$ begins to deviate significantly from zero, while $C_3$ and $C_5$ remain small, which shows that the constraint (4.56) is satisfied beyond the linear

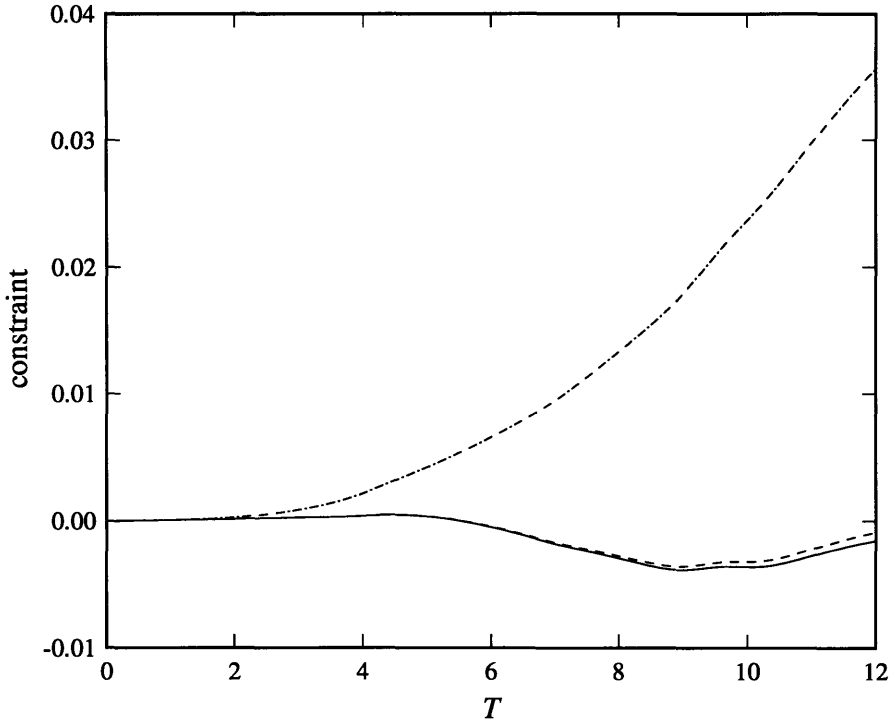


FIGURE 4-2. Demonstration that the integral constraint for locally confined solutions is satisfied. The lines represent $C_1$ ($-\cdot-\cdot$), $C_3$ (——), and $C_5$ ($-\,-\,-$) respectively as functions of $T$.

limiting case of the KP constraint (4.54). This suggests that the solution will indeed be locally confined, a point that is of pivotal importance in the development of the far-field solution, as we shall see later.

## 4.5 Far-field response: shelf formation

We now examine the details of the the flow field far downstream of the obstacle. For simplicity, it is assumed that the background straification is exactly uniform and that the flow speed, $V$ coincides with $c_1$, the linear long-wave speed of the first mode, $v_1 = \sin \pi y$; in what follows, this is referred to as the fundamental mode. These assumptions imply that $\lambda_1 = \lambda_2 = 0$ in (4.48). There is however no loss of generality for, as we shall see, the two

integral terms contain the underlying physics. The developments in this and the following section rely heavily on the earlier study of the two-dimensional analogue of the present problem (see Chapter 3).

### *4.5.1 Breakdown of the nonlinear theory*

We begin by studying the asymptotic behaviour of the transverse velocity $\mathcal{W}$ in the far field. In line with the expansions (4.34*a*,*b*), we may write

$$\mathcal{W} = \mathcal{W}^{(0)} + \mu^2 \mathcal{W}^{(1)} + \ldots. \tag{4.59}$$

From (4.55), $\mathcal{W}^{(0)} \to \mathcal{W}_\infty^{(0)}(\Psi, Z, T)$ as $x \to \infty$, implying that $\mathcal{W}$ possesses a shelf of $O(1)$. As a result, we have from (4.39)

$$\phi_\infty^{(0)} \sim -\frac{\mathcal{W}^{(0)}}{c_1} x, \tag{4.60}$$

where $\phi_\infty^{(0)} = \lim_{x\to\infty} \phi^{(0)}$. It was shown in §4.4 that the lowest order solution $\psi^{(0)}$ is locally confined in $x$. Since $\mathcal{U} = \phi_Z|_\Psi \Psi_y$, it follows from (4.42) and (4.60) that $\mathcal{H}^{(0)} \sim x$ for $x \gg 1$. In addition, $R^{(0)}\Big|_{x\to\infty} = O(1)$ and therefore the leading behaviour of $\psi^{(1)}$ for large $x$ is found from (4.40) to be given by

$$\psi^{(1)} \sim x.$$

Then, using (4.31), we find

$$\mathcal{W}_x^{(1)} = \psi_{yZ}^{(1)}; \qquad x \to \infty,$$

so that

$$\mathcal{W}^{(1)} \sim x^2; \qquad x \to \infty. \tag{4.61}$$

From (4.61), it is evident that the expansion (4.59) fails when $x = O(\mu^{-1})$ owing to the formation of an $O(1)$ shelf. In contrast, it was observed in Cahpter 3 that the two-dimensional

problem features a downstream shelf of $O(\mu^2)$, causing breakdown to occur at $x = O(\mu^{-2})$.

We now turn our attention to the issue of mass conservation. The expression (4.20) for the density, upon using (4.34$a$) yields, in the limit $x \to \infty$

$$\rho = \overline{\rho}(y) + \frac{\mu^2}{c_1}\left[\delta + \psi^{(1)}\right], \tag{4.62}$$

where

$$\delta = \delta(y, Z, T) = -\int_{-\infty}^{\infty} \mathrm{d}x' \left.\frac{\Psi_T}{\Psi_y}\right|_{\Psi(0)}. \tag{4.63}$$

Then considering a control volume extending from $x = -\infty$ to $x = \infty$ and spanning the width and height of the channel, the overall mass flux out of the resonant wave is given by

$$\frac{dM}{dt} = \int_0^W \mathrm{d}Z \int_0^1 \mathrm{d}y \left(\rho u|_{x\to\infty} - \overline{\rho} c_1\right).$$

The boundary condition (4.49) implies that $\mathcal{U}^{(0)}\big|_{x\to\infty} = 0$ on $Z = 0, W$. Using this result together with (4.43),(4.44), the expression for the net mass flux reduces to

$$\frac{dM}{dT} = -\beta \int_{-W}^{W} \mathrm{d}Z \int_0^1 \mathrm{d}y\, \delta(y, Z, T). \tag{4.64}$$

It is somewhat surprising that the mass flux defect is $O(1)$ as in the two-dimensional problem (Cahpter 3) although the magnitude of the shelf here is much larger. The reason for this will become apparent in §4.6.

### *4.5.2 Energy budget*

An energy balance equation is now derived for the nonlinear response. In addition to providing insight into the physics of the flow, it also proves to be of value in assessing the accuracy of the numerical solution in §4.7. In accordance with the earlier result that the asymptotic theory becomes invalid when $x = O(\mu^{-1})$, we confine our attention to the

region $-\infty < x \ll 1/\mu$. Introducing the variables $\widetilde{\boldsymbol{u}} = (\widetilde{u}, \widetilde{v}, \widetilde{w})$ to denote the deviation of the velocity field from the uniform upstream flow and $\widetilde{\psi}, \widetilde{\rho}$ and $\widetilde{p}$ to denote respectively the deviations of the streamfunction $\Psi$, density and pressure from their values far upstream, the governing equations (4.1) and (4.2) take the form

$$\boldsymbol{\nabla} \cdot \widetilde{\boldsymbol{u}} = 0, \tag{4.65}$$

$$\widetilde{\rho}_t + c_1 \widetilde{\rho}_x + \widetilde{\boldsymbol{u}} \cdot \boldsymbol{\nabla} \widetilde{\rho} = 0, \tag{4.66}$$

while (4.3) yields

$$\widetilde{u}_t + c_1 \widetilde{u}_x + \widetilde{\boldsymbol{u}} \cdot \boldsymbol{\nabla} \widetilde{u} = -\frac{1}{\beta} \widetilde{p}_x, \tag{4.67a}$$

$$\widetilde{v}_t + c_1 \widetilde{v}_x + \widetilde{\boldsymbol{u}} \cdot \boldsymbol{\nabla} \widetilde{v} = -\frac{1}{\beta \mu^2} \left( \widetilde{p}_y + \widetilde{\rho} \right), \tag{4.67b}$$

$$\widetilde{w}_t + c_1 \widetilde{w}_x + \widetilde{\boldsymbol{u}} \cdot \boldsymbol{\nabla} \widetilde{w} = -\frac{1}{\beta} \widetilde{p}_z. \tag{4.67c}$$

We now multiply (4.67) by $\widetilde{u}$, (4.67) by $\mu^2 \widetilde{v}$ and (4.67) by $\widetilde{w}$ and add; the resulting equation, upon using (4.65) simplifies to

$$\frac{\partial E_K}{\partial t} + c_1 \frac{\partial E_K}{\partial x} + \boldsymbol{\nabla} \cdot (\widetilde{\boldsymbol{u}} E_K) + \frac{\widetilde{\rho} \widetilde{v}}{\beta} = -\frac{1}{\beta} \boldsymbol{\nabla} \cdot (\widetilde{\boldsymbol{u}} \widetilde{p}), \tag{4.68}$$

where $E_K$ is the kinetic energy density and is defined by

$$E_K = \frac{1}{2} \left( \widetilde{u}^2 + \widetilde{w}^2 + \mu^2 \widetilde{v}^2 \right).$$

The boundary conditions on the deviation variables are that they decay to zero far upstream, that the component of $\widetilde{\boldsymbol{u}}$ normal to the topography and to the channel walls must vanish and that $\widetilde{v}, \widetilde{p} \to 0$ far downstream. Defining the operator $\langle \cdot \rangle$ by

$$\langle \cdot \rangle \equiv \int_{-\infty}^{\infty} \mathrm{d}x \int_0^W \mathrm{d}Z \, ( \cdot ),$$

we now integrate (4.68) over the volume of fluid, with the understanding that the upper limit of integration in the streamwise direction is $x \to 1/\mu$. Then, using the boundary conditions stated earlier, we obtain, correct to $O(\mu^2)$

$$\frac{\mu^2}{2}\frac{\partial}{\partial T}\left\langle \int_{\epsilon f}^{1} \mathrm{d}y \widetilde{\psi}_y^2 \right\rangle + \frac{1}{\beta}\left\langle \int_{\epsilon f}^{1} \mathrm{d}y \widetilde{\rho}\widetilde{v} \right\rangle = \frac{\mu^2 c_1}{\beta}\left\langle f_x \, \widetilde{p}|_{y=\epsilon f} \right\rangle - \frac{\mu^2}{2}\int_0^W \mathrm{d}Z \int_0^{c_1} \mathrm{d}\Psi \, \mathcal{W}^2\Big|_{x\to\infty}. \qquad (4.69)$$

In the energy balance expressed by (4.69), the first two terms represent respectively the rates of change of kinetic and potential energy within the fluid. Similarly, the first term on the right hand side is the rate at which energy is imparted to the flow by the force that drives the motion. In the experimental context, for instance, where an obstacle is towed at the bottom of a tank, this term would represent the power required to drag the obstacle. Finally, the last term is seen to be a flux of kinetic energy out of the resonant wave at $x = \infty$ and arises because of the shelf in the transverse velocity.

In the two-dimensional limit, $\mathcal{W} \equiv 0$ and this flux term is absent, implying that to $O(\mu^2)$, the evolution equation conserves energy. Thus, we see that the presence in three-dimensional flows of an $O(1)$ shelf leads to more severe problems: neither mass nor energy is conserved. We will outline in §4.6 how these difficulties may be reconciled by accounting for the presence of different scales in the downstream flow.

## 4.6 Shelf dynamics

We now demonstrate how a solution for the downstream flow field may be constructed. Following Chapter 3, the method of matched asymptotic expansions is employed, with the nonlinear theory being valid in an 'inner region', $x \ll \mu^{-1}$, which is deduced from the

earlier discussion. Consequently, we define an outer streamwise coordinate $X = \mu x$ and a corresponding stretched time $\tau = \mu t$. Since the integral constraint (4.56) has been shown to hold, a locally confined solution for $A(x, Z, T)$ is guaranteed. This is of crucial importance because it implies that that the outer region, $X = O(1)$, may be described by linear theory.

### *4.6.1 Inner region*

Focusing our attention on the inner region, (4.40) yields, in the limit $x \to \infty$

$$\psi^{(1)}_{yy} + \frac{\psi^{(1)}}{c_1^2} = -\mathcal{R}, \tag{4.70}$$

where

$$\mathcal{R} = \left(R^{(0)} + \mathcal{U}^{(0)}_y\right)\Big|_{x\to\infty} + \frac{1}{2}\frac{\partial}{\partial\Psi}\left(\mathcal{W}^{(0)2}_\infty\right).$$

In order to satisfy the boundary condition (4.49), we write $A(x, Z, T)$ in terms of transverse modes:

$$A \sim \cos\alpha_l Z; \qquad \alpha_l = \frac{l\pi}{W}; \qquad l = 0, 1, 2 \ldots.$$

The solution to (4.70) therefore takes the form

$$\psi^{(1)} = \sum_{l=0}^{\infty} G_{l1}(T)\cos\alpha_l Z \sin\pi y + \sum_{l=0}^{\infty}\sum_{m=2}^{\infty} \frac{G_{lm}(T)}{\pi^2(m^2-1)}\cos\alpha_l Z \sin m\pi y. \tag{4.71}$$

It is seen that modes with $l = 0$ do not possess a spanwise structure. Hence, in what follows, they will be referred to as two-dimensional modes. It may also be noted that the fundamental vertical mode ($m = 1$) is included in (4.71); this represents the homogeneous solution and must be present for the reasons detailed in Chapter 3. Hence, the coefficients $G_{l1}$ are unknown and are expected to be $O(1)$ whereas we have, for $m \neq 1$

$$G_{lm} = \frac{2}{W}\int_0^W \mathrm{d}Z \int_0^1 \mathrm{d}y \mathcal{R}\cos\alpha_l Z \sin m\pi y. \tag{4.72}$$

It is therefore evident that the modes with a fundamental $y$-dependence require separate treatment. Owing to the transverse boundary condition (4.49), the expression (4.72) yields

$$G_{0m} = -\frac{1}{W}\frac{m\pi}{c_1}\int_0^W \mathrm{d}Z \int_0^1 \mathrm{d}y \mathcal{W}_\infty^{(0)2} \cos m\pi y + \frac{2}{W}\int_0^W \mathrm{d}Z \int_0^1 \mathrm{d}y\, R^{(0)}\Big|_{x\to\infty} \sin m\pi y. \tag{4.73a}$$

Similarly, using the fact that $\mathcal{R}$ is dominated by the term $\mathcal{U}_y$, which grows linearly with $x$, we have

$$G_{lm} = -\frac{4m\pi c_1}{W}\int_0^W \mathrm{d}Z \int_0^1 \mathrm{d}y \phi_{\infty Z}^{(0)} \cos\alpha_l Z \cos m\pi y + O(1). \tag{4.73b}$$

Thus, we see that for the non-fundamental vertical modes, $G_{0m} = O(1)$ and $G_{lm} = O(\mu^{-1})$. Next, we decompose $q = q(y, Z, T)$ into transverse and vertical modes:

$$q = \sum_{l=0}^{\infty}\sum_{m=1}^{\infty} P_{lm} \sin m\pi y \cos\alpha_l Z, \tag{4.74}$$

where

$$P_{lm} = \frac{2}{W}\int_0^W \mathrm{d}Z \int_0^1 \mathrm{d}y q \sin m\pi y \cos\alpha_l Z.$$

Hence, the expression (4.62) for the density becomes

$$\rho = \overline{\rho}(y) - \frac{\mu^2\beta}{c_1}\left[\sum_{l=0}^{\infty}(G_{l1} - P_{l1})\sin\pi y + \sum_{l=0}^{\infty}\sum_{m=2}^{\infty}\left\{\frac{G_{lm}}{\pi^2(m^2-1)} - P_{lm}\right\}\cos\alpha_l Z \sin m\pi y\right] \tag{4.75}$$

The unknown functions $G_{l1}$ will be determined by matching the inner and outer expansions. We now study the outer region using transverse and vertical modes; in accordance with our earlier remarks, the modes with a fundamental vertical structure are considered separately from the higher $y$-harmonics.

### *4.6.2 Outer region: non-fundamental modes*

Here we consider the downstream structure of modes with $m \neq 1$. The difference between the scales of the coefficients $G_{0m}$ and $G_{lm}$ points to the fact that the two-dimensional modes ($l = 0$) behave differently from the three-dimensional modes ($l \geq 1$). Indeed, this is to be expected since the results of Chapter 3 indicate that the two-dimensional theory breaks down when $x = O(\mu^{-2})$ while the reasoning of §4.5 demonstrates that this occurs when $x = O(\mu^{-1})$ for the three-dimensional problem. Consequently, it is necessary to adopt the outer coordinates $(\widetilde{X}, T)$ for the two-dimensional modes, whereas the outer coordinates $(X, \tau)$ apply for modes with $l \geq 1$.

We first consider the two-dimensional modes, for which the flow may therefore be described in terms of the streamfunction $\Psi = c_1 y + \mu^2 \widehat{\psi}(\widetilde{X}, y, T)$. Hence, the outer problem for these modes is similar to that of the two-dimensional flow, examined in Chapter 3; using the results therein, we find that

$$\widehat{\psi} = \sum_{m=2}^{\infty} \left[ B_m^+(\xi_m^+) H(\xi_m^+) + B_m^-(\xi_m^-) H(\xi_m^-) \right] \sin m\pi y, \tag{4.76}$$

where $H(x)$ is the Heaviside step function, the characterisics $\xi_m^{\pm}$ are defined by

$$\xi_m^{\pm} = T - \frac{\widetilde{X}}{c_m^{\pm}}, \tag{4.77}$$

and

$$c_m^{\pm} = c_1 \pm c_m. \tag{4.78}$$

Making use of the matching conditions on streamfunction and density perturbations employed in Chapter 3, it is found that

$$B_m^+(T) = \frac{1}{2} \left[ \frac{G_{0m}(T)}{m\pi^2(m+1)} - \frac{P_{0m}}{m} \right], \tag{4.79a}$$

$$B_m^-(T) = \frac{1}{2}\left[\frac{G_{0m}(T)}{m\pi^2(m-1)} + \frac{P_{0m}}{m}\right]. \tag{4.79b}$$

Turning now to the three-dimensional modes, the scaling of the coefficients $G_{lm}$ and equation (4.71) reveal that the flow variables in the far-field may be written as

$$u = c_1 + \mu\hat{u}; \qquad v = \mu^2\hat{v}; \qquad w = \mu\hat{w}; \qquad \rho = \overline{\rho} + \mu\beta\hat{\rho},$$

where, as before, $\hat{u}, \hat{v}, \hat{w}, \hat{\rho}$ are all $O(1)$. Using linear theory and neglecting higher order dispersive effects, we find that $\hat{u}$ satisfies the equation

$$\left(\frac{\partial}{\partial\tau} + c_1\frac{\partial}{\partial X}\right)^2 \hat{u}_{yy} + \left(\frac{\partial^2}{\partial X^2} + \frac{\partial^2}{\partial Z^2}\right)\hat{u} = 0, \tag{4.80}$$

while the density and transverse velocity are coupled to $\hat{u}$ through

$$\frac{\partial\hat{\rho}}{\partial X} = \beta\left(\frac{\partial}{\partial\tau} + c_1\frac{\partial}{\partial X}\right)\frac{\partial\hat{u}}{\partial y}, \tag{4.81a}$$

$$\frac{\partial\hat{w}}{\partial X} = \frac{\partial\hat{u}}{\partial Z}. \tag{4.81b}$$

We then use separation of variables as before and write

$$\hat{u} = \sum_{l=1}^{\infty}\sum_{m=2}^{\infty} U_{lm}(X,\tau)\cos\alpha_l Z\cos m\pi y, \tag{4.82a}$$

$$\hat{\rho} = \sum_{l=1}^{\infty}\sum_{m=2}^{\infty} R_{lm}(X,\tau)\cos\alpha_l Z\sin m\pi y, \tag{4.82b}$$

$$\hat{w} = \sum_{l=1}^{\infty}\sum_{m=2}^{\infty} W_{lm}(X,\tau)\sin\alpha_l Z\cos m\pi y, \tag{4.82c}$$

so that (4.80) yields

$$\left(\frac{\partial}{\partial\tau} + c_m^+\frac{\partial}{\partial X}\right)\left(\frac{\partial}{\partial\tau} + c_m^-\frac{\partial}{\partial X}\right)U_{lm} + c_m^2\alpha_l^2 U_{lm} = 0, \tag{4.83}$$

where $c_m^{\pm}$ is defined by (4.78). In the two-dimensional limit, (4.83) has the two non-dispersive propagating-wave solutions determined earlier in (4.79). The presence of transverse variations is seen to have a dispersive effect; it is nevertheless clear that (4.83) also admits

two independent solutions. The streamwise group velocities of these solutions are readily determined using the linear dispersion relation (4.9) to be

$$c_g = c_1 \pm c_m \left( \frac{k}{k^2 + l^2} \right)^{\frac{1}{2}},$$

from which it is seen that the shelves must stretch between $X = c_m^- \tau$ and $X = c_m^+ \tau$; hence the nearest and farthest waves in the downstream shelf are two-dimensional. Neither of the two solutions of (4.83) can be rejected on physical grounds and therefore two conditions are necessary to uniquely determine each solution. The first condition is obtained by matching the streamwise velocities in the inner and outer regions. Owing to the fact that $\tau = T/\mu$, we observe that the outer region is forced by the inner region in a quasi-steady manner. The velocity matching condition is therefore

$$\left( \psi_y^{(1)} + \mathcal{U}^{(0)} \right) \Big|_{x \to \infty} = \lim_{\tau \to \infty} \widehat{u}|_{X=0} \,. \tag{4.84}$$

Using the expansions proposed earlier, this is found to reduce to

$$\frac{G_{lm}}{\pi(m^2 - 1)} = U_{lm}(0, \infty). \tag{4.85}$$

We now attempt to derive a second condition by matching the density perturbations in the two regions:

$$\left( \psi^{(1)} + q \right) \Big|_{x \to \infty} = \lim_{\tau \to \infty} \widehat{\rho}|_{X=0} \,.$$

Employing the $\widehat{\rho}$–$\widehat{u}$ coupling in (4.81) and the expansions (4.71), (4.74) and (4.82) along with the fact that $P_{lm}$ is subdominant compared with $G_{lm}$, it is found that the above matching condition reduces to (4.85). Hence, the velocity matching condition (4.84) ensures that the density perturbations in the inner and outer regions are also matched.

It is not clear how the required closure condition might be obtained. One possibility is to make use of the property of the vorticity that for an inviscd flow that is started from rest,

$$\boldsymbol{\omega} \cdot \boldsymbol{\nabla} \rho = 0, \tag{4.86}$$

where $\boldsymbol{\omega} = \boldsymbol{\nabla} \times \boldsymbol{u}$ is the vorticity. It is evident that this is automatically satisfied by the two-dimensional modes. The vorticity for the three-dimensional modes is given by

$$\boldsymbol{\omega} = (\mu \widehat{w}_y, 0, -\mu \widehat{u}_y) + O(\mu^2),$$

and (4.86) together with the expansions (4.82$a$,$c$) yields

$$W_{lm} \frac{\partial R_{lm}}{\partial X} - \alpha_l U_{lm} R_{lm} = 0, \tag{4.87}$$

where $W_{lm}$ and $R_{lm}$ are related to $U_{lm}$ are related to $U_{lm}$ through (4.81$a$,$b$). Thus, (4.87) and (4.85) determine the amplitude of the two independent solutions of (4.80).

### *4.6.3 Outer region: fundamental modes*

The behaviour of downstream modes with $m = 1$ is now examined, following a procedure similar to that of §4.6.2. We first observe that because the integral constraint (4.56) is satisifed in the inner region, $\mathcal{U}$ for these modes is finite as $x \to \infty$. Therefore, the streamwise velocity and density at the extremity, $x \to \infty$, of the inner region are given by

$$u = c_1 + \mu^2 \pi G_{01} \cos \pi y + \mu^2 \sum_{l=1}^{\infty} (\pi G_{l1} + Q_{l1}) \cos \pi y \cos \alpha_l Z, \tag{4.88$a$}$$

$$\rho = \overline{\rho} - \frac{\mu^2 \beta}{c_1} \sum_{l=0}^{\infty} (G_{l1} + P_{l1}) \sin \pi y \cos \alpha_l Z, \tag{4.88$b$}$$

where $Q_{l1}$ is an $O(1)$ quantity defined by

$$Q_{l1} = \frac{4}{W} \int_0^W \mathrm{d}Z \int_0^1 \mathrm{d}y \mathcal{U} \cos \pi y \cos \alpha_l Z.$$

The flow quantitites for the fundamental modes in the outer region may therefore be rescaled in terms of the circumflexed $O(1)$ variables as follows:

$$u = c_1 + \mu^2 \widehat{u}, \qquad v = \mu^3 \widehat{v}, \qquad w = \mu^2 \widehat{w}, \qquad \rho = \overline{\rho} + \mu^2 \beta \widehat{\rho}.$$

The determination of the structure of the two-dimensional modes ($\widehat{w} = 0$) is relatively straightforward: the relevant outer coordinates are $\widetilde{X}, T$ and the streamfunction is scaled according to (4.76), where

$$\widehat{\psi} = B_1(\widetilde{X}, T) \sin \pi y, \qquad B_1 = G_{01}\left(T - \frac{\widetilde{X}}{2c_1}\right) H\left(T - \frac{\widetilde{X}}{2c_1}\right). \tag{4.89$a, b$}$$

Following Chapter 3 and matching the inner and outer solutions, the unknown function $G_{01}$ is then determined:

$$G_{01}(T) = -\frac{1}{2} P_{01}(T). \tag{4.90}$$

In the case of the three-dimensional modes, $\widehat{u}$ and $\widehat{\rho}$ satisfy (4.80) and (4.81); decomposing as before into transverse and vertical modes, we have

$$\widehat{u} = \sum_{l=1}^{\infty} U_{l1}(X, \tau) \cos \alpha_l Z \cos \pi y, \tag{4.91$a$}$$

$$\widehat{\rho} = \sum_{l=1}^{\infty} R_{l1}(X, \tau) \cos \alpha_l Z \sin \pi y; \tag{4.91$b$}$$

from (4.80), it is then found that

$$\frac{\partial}{\partial \tau}\left(\frac{\partial}{\partial \tau} + 2c_1 \frac{\partial}{\partial X}\right) U_{l1} + \frac{\alpha_l^2}{\pi^2} U_{l1} = 0. \tag{4.92}$$

Matching the streamwise velocity in the inner and outer regions, we obtain

$$U_{l1}(0, \infty) = \pi G_{l1} + Q_{l1}, \tag{4.93}$$

where it is assumed that $G_{l1} = G_{l1}(T)$. Defining the Laplace transform with respect to the scaled time, $\tau$ by

$$\widetilde{(\cdot)} \equiv \int_0^\infty \mathrm{d}\tau(\cdot)\mathrm{e}^{-s\tau},$$

the solution in transform space of (4.92) subject to the condition (4.93) is given by

$$\widetilde{U}_{l1}(X;s) = \frac{1}{s}(\pi G_{l1} + Q_{l1}) \exp\left[-\left(\frac{s}{2c_1} + \frac{l^2}{2c_1 W^2 s}\right) X\right]. \tag{4.94}$$

Now using (4.88), (4.91) and (4.81), we attempt to match the density perturbations in the inner and outer regions. Again working with the Laplace transform, we find that density matching requires that

$$-\frac{\beta}{c_1}(G_{l1} + P_{l1}) = -\beta(\pi G_{l1} + Q_{l1}) \lim_{s\to 0} \frac{s^2W^2 - l^2}{s^2W^2 + l^2}. \tag{4.95}$$

However, it may be shown using small amplitude expansions that $\pi P_{l1} \neq Q_{l1}$ and it is therefore not possible to satisfy (4.94).

The only solution to this impasse appears to be to reject the hypothesis that $G_{l1}$ is a function of the nonlinear slow time, $T$ and to replace it with the postulate that $G_{l1} = G_{l1}(\tau)$. Equation (4.93) is then transformed to

$$\widetilde{U}_{l1}(X;s) = \left(\pi\widetilde{G}_{l1} + \frac{Q_{l1}}{s}\right) \exp\left[-\left(\frac{s}{2c_1} + \frac{l^2}{2c_1 W^2 s}\right) X\right],$$

and the matching condition for density then determines $G_{l1}$:

$$\widetilde{G}_{l1}(s) = -\frac{W^2}{2\pi^2 l^2 s}\left[Q_{l1}\left(s^2 - \frac{l^2}{W^2}\right) + \pi P_{l1}\left(s^2 + \frac{l^2}{W^2}\right)\right].$$

The assumption that $G_{l1} = G_{l1}(\tau)$ implies that the non-stationary wave with a fundamental vertical structure evolves on a faster timescale than the resonant wave. Physically, it is not clear why this should be the case; however, the underlying scales are not violated because

the assumption of long waves is still valid. Finally, we note that $\boldsymbol{\omega} \cdot \boldsymbol{\nabla}\rho = O(\mu^2)$ for the fundamental modes, which to leading order is consistent with the vorticity constraint (4.85).

### *4.6.4 Mass conservation*

We now demonstrate that the system described by the matched asymptotic solutions determined earlier conserves mass. Substituting the expansion (4.74) for $q$ into (4.64), the mass flux out of the inner region is found to be

$$\frac{dM}{dT} = -2\beta W \sum_{n=0}^{\infty} c_{2n+1} P_{0,2n+1}. \tag{4.96}$$

In the outer region, the excess mass, $\mathcal{M}_{lm}$ contained in a three-dimensional mode ($l \geq 1$) with a vertical structure corresponding to the $m$-th harmonic is given by

$$\mathcal{M}_{lm} = \int_0^W \mathrm{d}Z \int_0^1 \mathrm{d}y \int_0^\infty \mathrm{d}X P_{lm}(X,\tau) \cos \alpha_l Z \sin m\pi y.$$

It is evident that $\mathcal{M}_{lm} = 0$ and therefore the three-dimensional modes do not carry any excess mass. All of the mass that is transferred from the inner region to the outer region must therefore be contained in the two-dimensional modes. This explains why the mass flux defect in three-dimensional flows is of the same order as it is in the corresponding two-dimensional problem, despite the larger magnitude of the shelves in the former case. Following the calculation in Chapter 3 for the two-dimensional modes, the rate of change of mass in the outer region is found to be

$$\frac{d\mathcal{M}}{dT} = -2c_1\beta P_{01}(T) + \beta \sum_{n=1}^{\infty} \left[ c^+_{2n+1} B^+_{2n+1}(T) - c^-_{2n+1} B^-_{2n+1}(T) \right],$$

where $B^\pm_m$ are given by (4.79$a$,$b$). Consequently, it is seen that

$$\frac{d\mathcal{M}}{dT} = -2\beta \sum_{n=0}^{\infty} \frac{P_{0,2n+1}}{\pi(2n+1)}; \tag{4.97}$$

from (4.96) and (4.97) the mass flux out of the inner region is identical to the rate of change of mass in the outer region and mass is therefore conserved.

It may also be noted that the solutions for the outer region indicate that the rate of change of kinetic energy outer region in $O(\mu^2)$, in agreement with the energy budget (4.69). Unfortunately, an exact analytical evaluation of this quantity is precluded by the complexity of the expressions for the outer region.

## 4.7 The transient problem

In this section, we investigate the time evolution of a flow that is started from rest, focusing our attention on the flow field close to the obstacle, which is described by (4.48). The far-field may then, in principle, be calculated using the method outlined in §4.6.

It is assumed that the background flow speed is such that a mode-1 resonance obtains. The quantities in (4.48), (4.38) and (4.39) are rescaled as follows:

$$x^* = \frac{3^{-\frac{1}{3}}}{c_1}x; \quad Z^* = \frac{3^{-\frac{1}{6}}}{c_1}Z; \quad \mathcal{W}^* = 3^{-\frac{1}{6}}\mathcal{W}; \quad \phi^* = \frac{3^{-\frac{1}{2}}}{c_1}\phi;$$
$$\lambda_1^* = 3^{-\frac{1}{3}}\lambda_1; \quad \lambda_2^* = 3^{-\frac{1}{3}}\lambda_2.$$

Rewriting (4.48) in terms of the rescaled variables and dropping the asterisks, we obtain

$$K^c A_T + \int_{-\infty}^{x} \mathrm{d}x' K_x A_T' + \lambda_1 A_x - \lambda_2 A A_x - \frac{1}{6}A_{xxx} - \int_0^1 \mathrm{d}y \frac{\partial}{\partial x}\left(\mathcal{H}^{(0)}\sin\pi y\right)\Big|_{\Psi} + \left[\left(\frac{A}{c_n^2}+1\right)g\right]_x = 0, \tag{4.98}$$

where

$$g = 3^{-\frac{1}{3}}c_1^2 f$$

and $\mathcal{H}^{(0)}$ is given by (4.42) and $\mathcal{W}^{(0)}$ and $\phi^{(0)}$ are determined using (4.38) and (4.39)

respectively. Equation (4.98) is solved numerically, subject to the boundary condition (4.49) and quiescent initial conditions. We also solve, for purposes of comparison, the KP analogue of (4.98):

$$A_T + \lambda_1 A_x - \lambda_2 A A_x - \frac{1}{6} A_{xxx} - \frac{1}{2} \int_{-\infty}^{x} \mathrm{d}x' A'_{ZZ} + g_x = 0. \tag{4.99}$$

However, it must be remembered that these latter solutions have no physical meaning since (4.99) is not a valid description of the fully nonlinear flow.

### *4.7.1 Energy balance equation*

Owing to the complexity of (4.98), it proves beneficial to employ the energy budget derived in §4.6.2 to assess the accuracy of the numerical solution. In order to do this, (4.69) must be expressed in terms of the amplitude $A(x, Z, T)$. We begin by simplifying the first term of (4.69):

$$\frac{\mu^2}{2} \frac{\partial}{\partial T} \left\langle \int_{\epsilon f}^{1} \mathrm{d}y \widetilde{\psi}_y^2 \right\rangle = \frac{\mu}{4c_n^2} \left\langle A^2 \right\rangle_T + O(\mu^3). \tag{4.100}$$

Next, we turn our attention to the second term in (4.69) which represents the rate of change of potential energy. By definition, $\widetilde{\rho} = \rho - \overline{\rho}(y)$, so that

$$\widetilde{\rho} = -\frac{\beta}{c_n} \widetilde{\psi} + \mu^2 \frac{\beta}{c_n} \int_{-\infty}^{x} \mathrm{d}x' \left. \frac{\psi'_T}{\psi'_y} \right|_{\Psi}, \tag{4.101}$$

while $\widetilde{v} = \widetilde{\psi}_x + \mu^2 (\Psi_Z \phi_x - \psi_x \phi_Z)$. We therefore have

$$\begin{aligned} \frac{1}{\beta} \left\langle \int_{\epsilon f}^{1} \mathrm{d}y \widetilde{\rho} \widetilde{v} \right\rangle = {} & \frac{1}{2c_n} \left\langle \int_{\epsilon f}^{1} \mathrm{d}y \frac{\partial}{\partial x} \left( \widetilde{\psi}^2 \right) \right\rangle - \frac{\mu^2}{c_n} \left\langle \int_{-\infty}^{x} \mathrm{d}x' \int_{\epsilon f}^{1} \mathrm{d}y \left. \frac{\widetilde{\psi}_x \Psi'_T}{\Psi'_y} \right|_{\Psi} \right\rangle \\ & - \frac{\mu^2}{2c_n^2} \left\langle \int_{\epsilon f}^{1} \mathrm{d}y \left[ \left( \widetilde{\psi}^2 \phi_x \right)_Z - \left( \widetilde{\psi}^2 \phi_Z \right)_x \right] \right\rangle. \end{aligned} \tag{4.102}$$

Using the boundary condition $\widetilde{\psi}|_{y=\epsilon f} = \epsilon f$, it is found that the first term on the right-hand side of (4.102) vanishes. Similarly, making use of the fact that $\phi = 0$ on $Z = 0, W$ as a

consequence of the boundary condition (4.49), the third term is also zero. Hence, (4.102) reduces to

$$\frac{1}{\beta}\left\langle \int_{\epsilon f}^{1} \mathrm{d}y \widetilde{\rho}\widetilde{v} \right\rangle = -\frac{\mu^2}{c_n}\left\langle \int_{-\infty}^{x} \mathrm{d}x' \int_{0}^{c_n} \mathrm{d}\Psi \left. \frac{\widetilde{\psi}_x \Psi'_T}{\Psi_y \Psi'_y} \right|_{\Psi} \right\rangle + O(\mu^2). \tag{4.103}$$

We now focus our attention on the third term in (4.69), which represents the rate of work done on the fluid. From (4.67), it is seen that

$$\widetilde{p}_y = -\widetilde{\rho} - \mu^2 \left[ \Psi_x^{(0)} \Psi_{xy}^{(0)} - \Psi_{xx}^{(0)} \Psi_y^{(0)} \right] + O(\mu^3). \tag{4.104}$$

Integrating (4.104) over $y$, we have

$$\widetilde{p}_y = -\left. \widetilde{p} \right|_{y=1} + \int_{y}^{1} \mathrm{d}y \widetilde{\rho} + O(\mu^2). \tag{4.105}$$

Next, we make use of the property (F 10) derived in Appendix F that the Bernoulli function is conserved along streamlines, to leading order: $H = \overline{H}(\Psi) + O(\mu^2)$, where $H$ is defined by (F 2). This leads to the result that

$$\left. \widetilde{p} \right|_{y=1} + \frac{1}{2}\beta \left( u^2 - c_1^2 \right) \Big|_{y=1} = O(\mu^2).$$

By definition, $u = c_1 + \widetilde{\psi}_y + \mu^2 \mathcal{U}$, and hence we find that

$$\left. \widetilde{p} \right|_{y=1} = -\frac{1}{2}\beta \left[ \frac{A^2}{c_1^2} + 2A + 2\mu^2 \left( c_1 - \frac{A}{c_1} \right)^2 \mathcal{U}|_{y=1} \right]. \tag{4.106}$$

Combining (4.105),(4.106) and using (4.101) to simplify the integral term, we obtain

$$\left. \widetilde{p} \right|_{y=\epsilon f} = -\frac{1}{2}\beta \left[ \frac{A^2}{c_1^2} + 2A + 2\mu^2 \left( c_1 - \frac{A}{c_1} \right)^2 \phi_Z|_{\Psi=c_1} \right].$$

Thus the power input term is given by

$$\left\langle f_x \left. \widetilde{p} \right|_{y=\epsilon f} \right\rangle = -\frac{1}{2}\beta \left\langle f_x \left( \frac{A^2}{c_1^2} + 2A \right) \right\rangle - \mu^2 \beta \left\langle f_x \left( c_1 - \frac{A}{c_1} \right)^2 \phi_Z|_{\Psi=c_1} \right\rangle. \tag{4.107}$$

It may be shown by integrating by parts that the second term in (4.107) is $O(\mu^2)$. Finally, combining (4.100),(4.103),(4.107) and implementing the scaling used to obtain (4.98), we have the following energy balance equation, correct to $O(\mu^2)$:

$$\frac{1}{4}\left\langle A^2\right\rangle_T - c_1\left\langle \int_{-\infty}^{x} \mathrm{d}x' \int_0^{c_1} \mathrm{d}\Psi \left.\frac{\widetilde{\psi}_x \Psi'_T}{\Psi_y \Psi'_y}\right|_\Psi \right\rangle = \\ -\frac{1}{2}\left\langle f_x\left[\frac{A^2}{c_1^2}+2A\right]\right\rangle - \frac{1}{2}c_n\int_0^W \mathrm{d}Z\int_0^{c_1}\mathrm{d}\Psi \mathcal{W}_\infty^2. \tag{4.108}$$

### *4.7.2 Numerical method*

The evolution equation (4.98) was solved using finite-difference discretizations in space and time. All spatial derivatives are evaluated by centred second-order difference schemes on a uniform grid, while the integrals are computed using the trapezoidal rule. The kernel $K(x,x')$ is determined using a procedure similar to the one used in Chapter 3. From (4.47), the kernel is seen to depend on $A(x,Z,T)$. Therefore, in order to reduce the computational cost, the linear limit $K=1$ is used when $|A|<0.005$, while for $|A|>0.04$, the following algorithm was employed: the relation (4.36) is numerically inverted using Newton–Raphson iteration to obtain $y=y(\Psi;A)$ at discrete values of $\Psi$; the integrand in (4.47) is thus known and the required integration to determine the kernel is accomplished using the trapezoidal rule. For intermediate values of $|A|$, an analytical approximation to $K$, computed to fifth order in $A$ using the method outlined in §4.3 is used.

Time-stepping is achieved by means of a forward Euler scheme, modified by the addition of a sixth-order derivative term that provides the necessary numerical damping to ensure stability and is motivated by a similar term that appears when the KdV equation is solved by the Lax-Wendroff method. The scheme to advance the amplitude $A(x,Z,T)$ in time

takes the form

$$A^{(n+1)} = A^{(n)} + A_T^{(n)}\Delta T + \frac{1}{72}(\Delta T)^2 \left[\frac{A_{xxxxxx}^{(n)}}{K(x,x) + \frac{\Delta x}{2}K_x(x,x)}\right], \tag{4.109}$$

where $A_T^{(n)}$ is computed using (4.98). Equation (4.109) describes a fully explicit scheme with first-order temporal accuracy; it is found to be conditionally stable provided

$$\Delta T \leq \min(\Delta x^3, \Delta Z^2/\Delta x); \qquad \Delta Z > 2\Delta x. \tag{4.110}$$

Although the scheme worked well for moderate times, grid-scale instabilities along the transverse direction were found to occur at large $T$ far downstream . The cause for this instability was traced to the function $\phi$, which grows linearly with $x$ in the far field and appears as a product with $A$ and its derivatives in the three-dimensional term. Since $A$ is locally confined, the three-dimensional term ought to decay to zero for large $x$. However, it turns out that the large values of $\phi$ cause numerical errors in $A$ to be amplified, leading to instability. In order to remedy this situation, the growing function $\phi$ was truncated at a sufficiently large downstream location and held constant with $x$.[†] This *ad hoc* procedure introduces a new source of error and it is vital to gauge its effect on the accuracy of the computation. This is done by monitoring the energy budget at frequent time intervals. The maximum error in the energy budget was found not to exceed 10%, which was considered acceptable. Furthermore, in presenting our results, we reject most of the flow field downstream of the truncation point.

Next, we turn our attention to the boundary conditions. The condition (4.49) on the channel walls is used to calculate $\mathcal{W}$ and $\phi$ and the boundary values of $A$ were then advanced using the time-stepping scheme described earlier. In addition to the transverse boundary

[†]It was also necessary in some cases to apply occasionally the 5-point filter of Shapiro (1975), along the $Z$-direction.

conditions, numerical boundary conditions along the streamwise direction are also required. There are no waves upstream of the obstacle and we therefore set $A = A_x = A_{xx} = 0$ at $x = -\infty$. Similarly, following Katsis & Akylas (1987*a*), we also set $A$ and its first two $x$-derivatives to zero at $x = \infty$. As noted earlier, this is permissible only as long as $A$ is locally confined. Finally, the radiation condition at the upstream and downstream boundaries is implemented by expanding the grid when $|A|$ exceeds 0.5–1% of the breaking amplitude.

The finite-difference scheme described here was tested by applying it in two limiting scenarios: the fKP problem and the two-dimensional equation of GY. In the former case, the solution was found to agree very well with that of Katsis & Akylas (1987*a*). The solution for the two-dimensional problem was found in general to agree with that of GY although in significant differences were observed in some cases, particularly in the prediction of the breaking time. However, the energy budget was satisfied to an accuracy of better than 1% and the breaking times we obtained agreed with the results of Lamb (1994), enabling us to develop some confidence in the present numerical scheme. Moreover, our results are in excellent agreement with those of Broutman *et al.*(1996) where it has been shown that some of the results of GY are in error due to insufficient resolution of the kernel.

### *4.7.3 Results*

We now present numerical solutions of (4.98) for some specific flow configurations. Rather than conduct an exhaustive survey of the parameter space, the aim here is to highlight some of the principal phenomena. Choosing the forcing to be the product of two Gaussians with streamwise and transverse length scales $L_x$ and $L_z$ respectively, we have

$$f\left(\frac{x}{\mu}\frac{h}{L_x}, \frac{Z}{\mu^2}\frac{h}{L_z}\right) = F_0 \exp(-\kappa^2 x^2) \exp(-\zeta^2 Z^2),$$

where $F_0 = O(1)$ is the peak height of the topography and

$$\kappa = \frac{1}{\mu}\frac{h}{L_x}; \qquad \zeta = \frac{Z}{\mu^2}\frac{h}{L_z}.$$

We set $\kappa = 0.25$ and $F_0 = 0.33$; $\zeta$ varies over the range 0, 0.375. In addition, we set the width of the channel, $W = 10$. For this choice of parameters, the spanwise grid spacing, $\Delta Z$ varied between 0.517 and 0.833, while $\Delta x$ and $\Delta T$ were chosen in accordance with the criteria (4.110) for numerical stability. Next, we define the relative blockage, $\eta$ and relative breaking time, $\theta$ as

$$\eta = \frac{S}{S_{2d}}; \qquad \theta = \frac{\mathcal{T}}{\mathcal{T}_{2d}}, \tag{4.111}$$

where $S$ and $\mathcal{T}$ represent the blockage coefficient[†] and the breaking time respectively for a given three-dimensional obstacle; the subscript '2d' denotes the corresponding value of the quantity for a two-dimensional obstacle of the same shape and peak height. Clearly $\eta$ is related to $\zeta$ and is therefore a measure of three-dimensional effects. In addition to $\eta$, there are two other free parameters: $\lambda_2$, which quantifies the quadratic nonlinearity caused by departures from uniform stratification and $\lambda_1$, which for fixed $\lambda_2$ measures the detuning from exact resonance.

A typical response is illustrated in figure 4-3*a*, where $-A$ is plotted as a function of $x$ and $Z$ at $T = 108$, with $\lambda_1 = 0$, $\lambda_2 = -3.0$ and $\eta = 0.354$. A solitary wave is observed to form upstream of the obstacle. This wave emerges as a three-dimensional disturbance but becomes straight-crested upon feeling the influence of the wall, a process that is reminiscent of Mach reflection. It is seen that $|A|$ has its maximum value across the crest of the solitary wave. With increasing time, the solitary wave grows in amplitude and breaking occurs at

[†]The blockage coefficient is frequently used in naval hydrodynamics and is defined as the ratio of the maximum cross-sectional area of the obstacle to the wetted crossectional area.

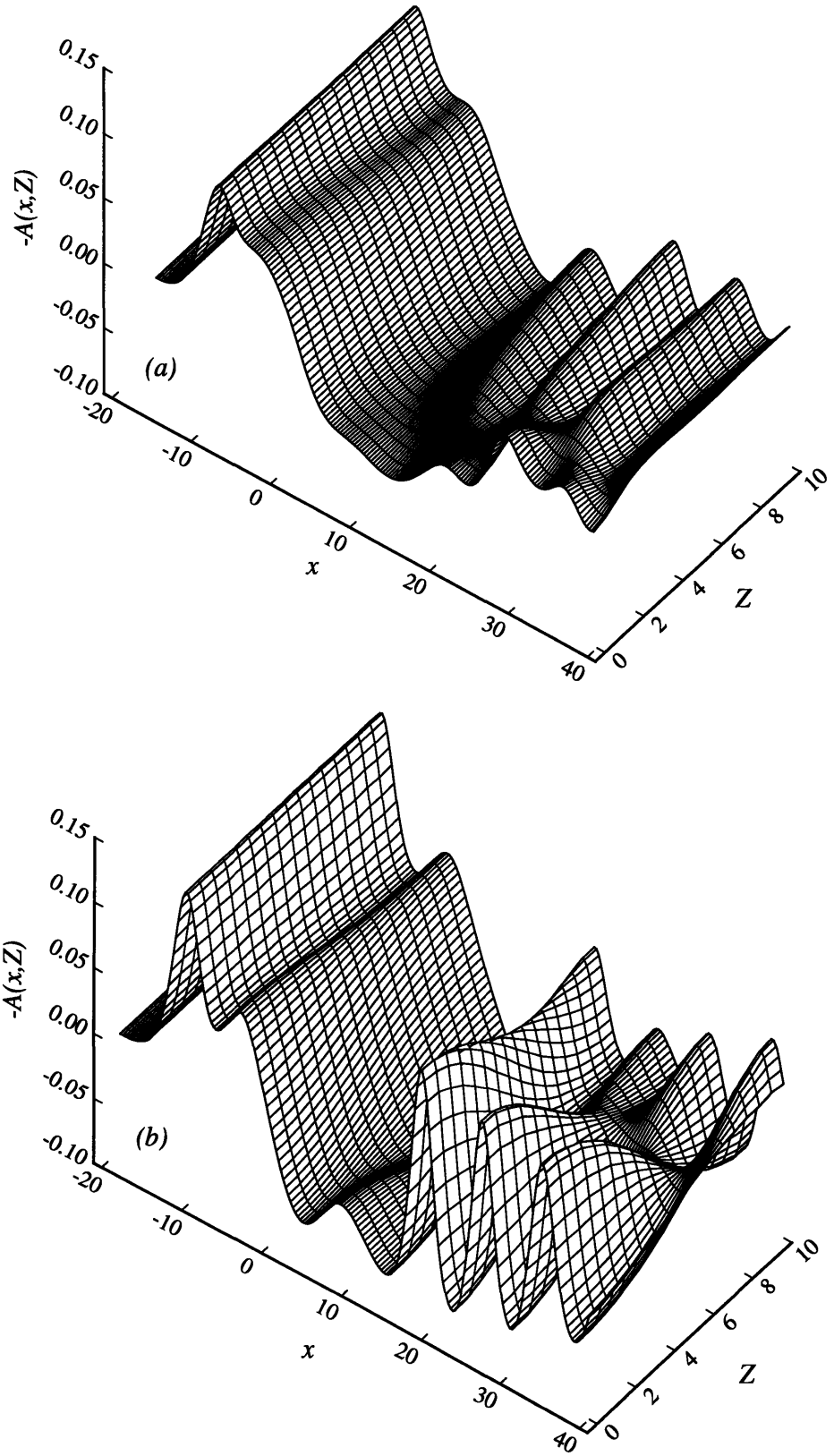


FIGURE 4-3. The response $-A$, as a function of $x$ and $Z$ at $T = 108$ of ($a$) the nonlinear evolution equation and ($b$) the analogous fKP equation. The obstacle is located at $x = 0$.

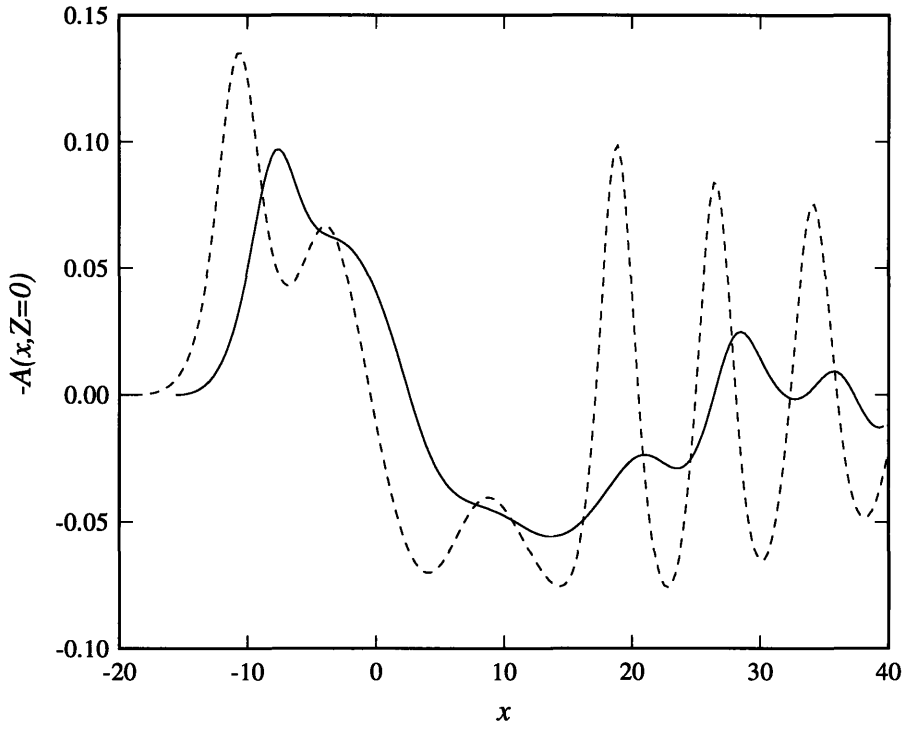


FIGURE 4-4. Variation of the response at $T = 108$ along the centre-plane of the channel, $Z = 0$ for the fKP equation (– – –) and the nonlinear evolution equation (——), illustrating the significantly larger solitary wave amplitude predicted by the fKP equation.

$T = 113$. We also observe that a second solitary wave just begins to form behind the first one, which would presumably be radiated away eventually, if breaking did not take place. The upstream wave of elevation is followed by a long depression and a lee-wave field in which spanwise modulations appear to be restricted to a relatively small region near the centre-plane, $Z = 0$.

The solution of the fKP equation (7.2) for the same choice of parameters is shown in figure 4-3*b*. As in figure 4-3*a*, the presence of the quadratic nonlinearity causes a solitary wave to appear upstream. However, the amplitude in this case is substantially different. This is exemplified in figure 4-4, in which the response along the centre-plane, $Z = 0$ corresponding to figures 4-3*a,b* is shown. The effect of enhanced nonlinearity is to attenuate the response,

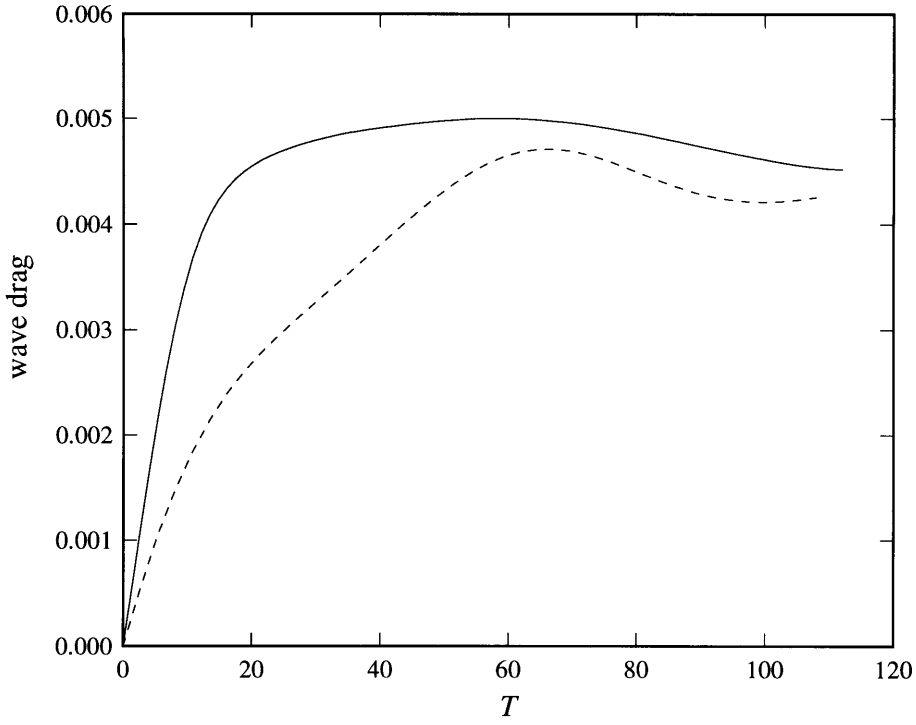


FIGURE 4-5. Temporal development of the wave drag for the fKP problem (– – –) and the fully nonlinear problem (——).

as expected. Consequently, the fKP solitary wave travels faster, as is evident from figure 4-4. This also permits the second solitary wave to be developed to a larger extent than the fully nonlinear case. The most striking difference between the two solutions displayed in figures 4-3*a,b* is however in the downstream flow field, where the fKP response is observed to be large in magnitude and more strongly modulated in the spanwise direction. The temporal development of the obstacle drag for both the fully nonlinear and fKP problems is shown in figure 4-5. Despite the fact that the upstream solitary wave at large times in the latter case is larger in amplitude, it is seen that the nonlinear flow develops more rapidly. Nevertheless, the ultimate drag force does not differ substanitally between the two cases.

The formation (and eventual two-dimensionalization) of the solitary wave in figure 4-3*a*

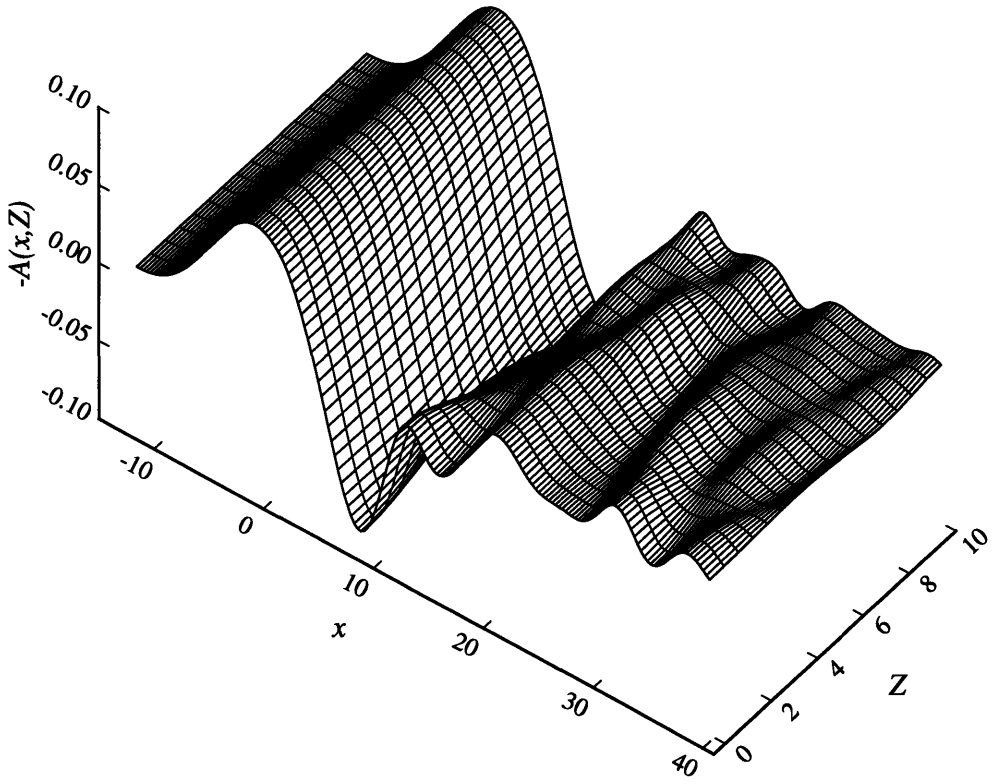


FIGURE 4-6. The solution of the nonlinear evolution equation at $T = 108$, with $\lambda_1 = \lambda_2 = 0$. The upstream wave is clearly two-dimensional.

is due, of course, to the quadratic nonlinearity. It is of interest to enquire what effect the absence of this nonlinearity would have. Figure 4-6 illustrates the wave pattern that is generated at $T = 108$ when $\lambda_1 = \lambda_2 = 0$, for the same value of $\eta$ as in figure 4-3. As anticipated, the upstream wave remains attached to the topography and no solitary waves are formed. Surprisingly enough, this upstream wave is also straight-crested although the downstream flow field exhibits spanwise modulations. This case is particularly important since it corresponds to a fluid with a perfectly uniform, Boussinesq stratification for which the equivalent KP problem would fail owing to the lack of balance between nonlinearity and dispersion.

We now turn our attention to the breaking time. This parameter assumes some impor-

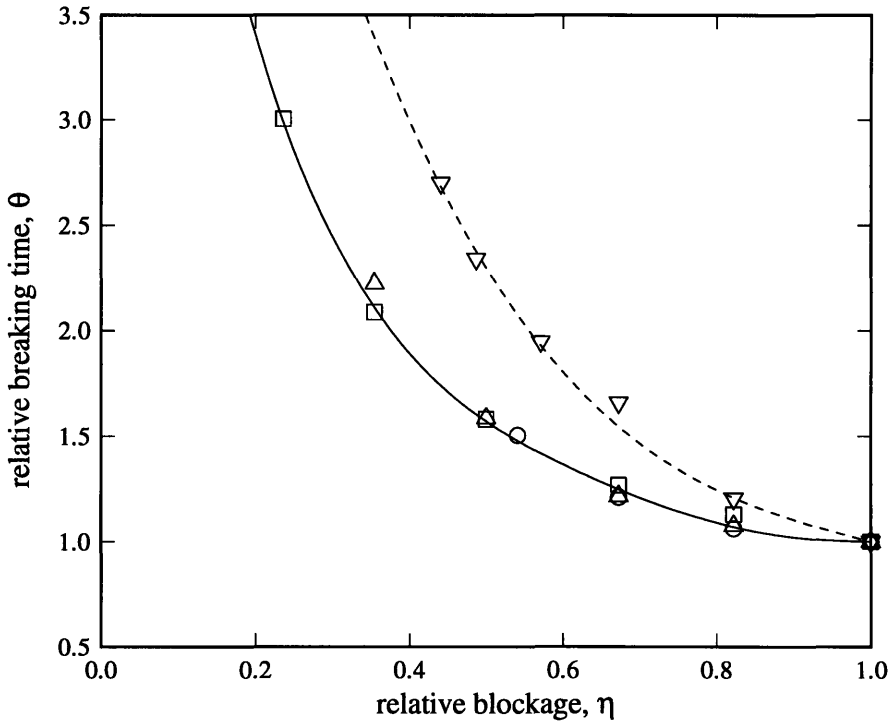


FIGURE 4-7. The dependence of the relative breaking time, $\theta$ on the detuning parameter, $\lambda_1$, nonlinearity parameter, $\lambda_2$, and relative blockage, $\eta$. The solid line represents $\lambda_2 = -3.0$ with $\lambda_1 = 0$ ($\square$), $\lambda_1 = -0.5$ ($\triangle$), $\lambda_1 = 0.1$ ($\bigcirc$). The symbols $\triangledown$ and the broken line represent $\lambda_1 = \lambda_2 = 0$.

tance in the context of geophysical flows. For example, in the case of tidal flow through straits, the relative magnitudes of the breaking time and the the timescale of the basic flow will determine whether or not overturning plays a significant role. It is found that with $\eta$ and $\lambda_2$ fixed, positive (negative) values of the detuning parameter, $\lambda_1$ cause the breaking time, $\mathcal{T}$ to increase (decrease). However, these variations in $\mathcal{T}$ are such that the *relative* breaking time, $\theta$ is independent of $\lambda_1$. This is illustrated in figure 4-7, where $\mathcal{T}$ is plotted as a function of $\eta$ as $\lambda_1$ and $\lambda_2$ are varied. With $\lambda_2$ held fixed at $-3.0$, it is seen that the values of $\theta$ for $\lambda_1 = -0.5, 0, 0.1$ fall on a single curve, represented by the solid line, implying that $\theta = \theta(\eta; \lambda_2)$. This is borne out by the broken line in figure 4-7, which shows the effect of setting $\lambda_2 = 0$.

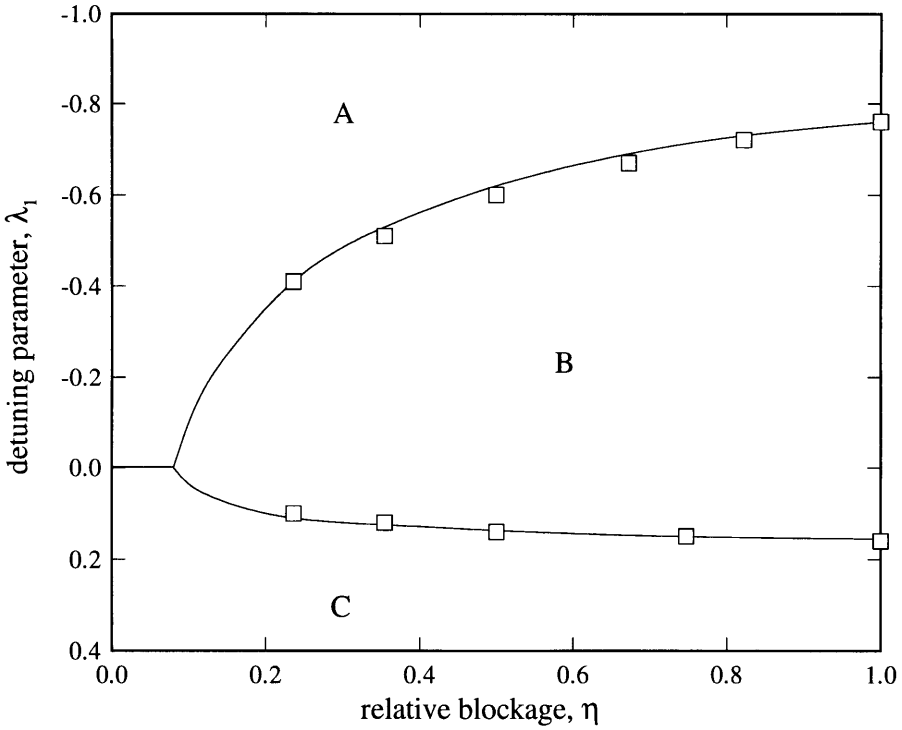


FIGURE 4-8. The breaking envelope in the $\lambda_1$–$\eta$ plane, with $\lambda_2 = -3.0$. The envelope divides the parameter space into three regions: A, corresponding to unsteady flow without wave breaking, B, in which the flow is unsteady and breaking occurs and C, where there is no breaking and the flow over the obstacle is stationary.

With $\lambda_1$ and $\lambda_2$ held constant, it is clear that breaking will not take place if $\eta$ is sufficiently small. This is also evident in figure 4-7, where it is observed that the relative breaking time, $\theta$ grows very rapidly as the spanwise length scale of the obstacle becomes smaller. Furthermore, there is a finite 'breaking range' of $\lambda_1$, when the other parameters are fixed. For when $|\lambda_1|$ is increased, the departure from exact resonance increases so that overturning is inhibited. In the case of a weakly nonlinear two-dimensional flow, Grimshaw & Smyth (1986) employed hydraulic theory to calculate a 'resonant band' of the detuning parameter. While their analysis does not apply to the fully nonlinear problem, the results of GY indicate that for constant $\lambda_2$, a similar band of $\lambda_1$ exists, within which breaking occurs. Here, because of the additional parameter, $\eta$, the 'breaking band' is transformed

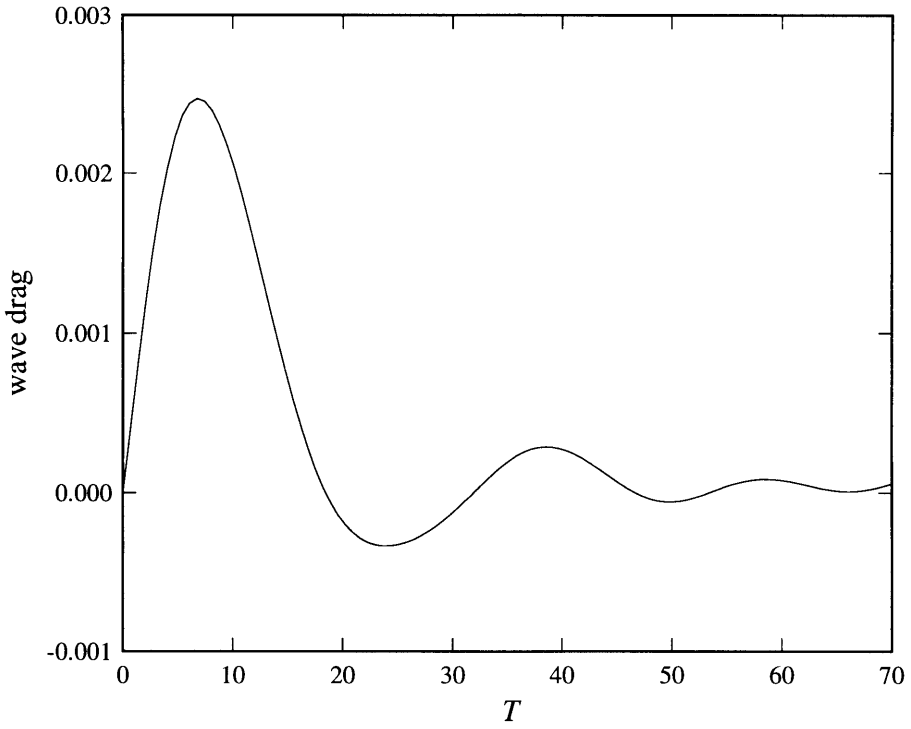


FIGURE 4-9. The temporal evolution of the wave drag for $\lambda_1 = -0.75$, $\lambda_2 = -3.0$.

to a 'breaking envelope', shown in figure 4-8 for $\lambda_2 = -3.0$. The lower and upper critical values of $\lambda_1$ (between which breaking takes place) are observed to asymptote to their two-dimensional values of $-0.76$ and 0.15 as $\eta \to 1$. As $\eta$ decreases, the breaking envelope shrinks rapidly. It is seen from figure 4-8 that the upper critical value of $\lambda_1$ is relatively insensitive to changes in $\eta$, in contrast to the behaviour of the lower critical value. Determination of the breaking envelope for $\eta \lesssim 0.25$ is difficult owing to the exceedingly heavy computational demands caused by the necessity of finer grids. Nevertheless, extrapolating the lines of best fit through the upper and lower critical values of $\lambda_1$, it is seen that the limiting value of $\eta$, below which there is no breaking is approximately 0.08.

The breaking envelope divides the $\lambda_1$–$\eta$ plane into three regions. In region B, the flow is unsteady (as indicated by the drag force in figure 4-5) and its evolution culminates in

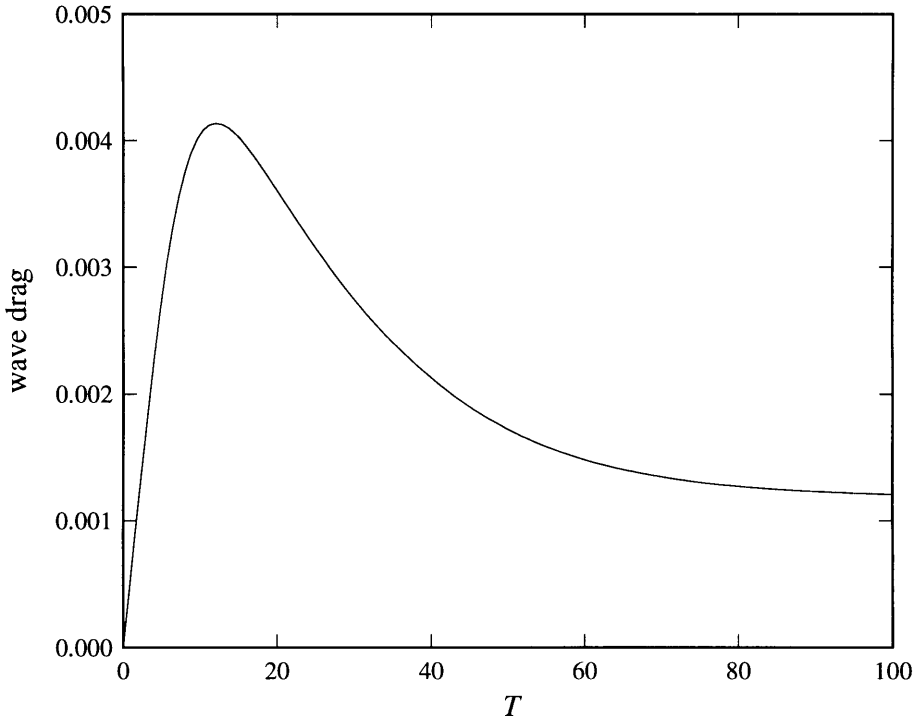


FIGURE 4-10. The temporal evolution of the wave drag for $\lambda_1 = 0.2$, $\lambda_2 = -3.0$.

breaking. While breaking does not occur in region A, the flow remains unsteady. The wave drag for the choice of parameters $\lambda_1 = -0.75$, $\eta = 0.498$ exhibits decaying oscillations, as shown in figure 4-9. In region C, the drag force rapidly achieves its maximum value and then asymptotically approaches a constant value as seen in figure 4-10 for $\lambda_1 = 0.2$, $\eta = 0.498$. In addition, the disturbance over the obstacle approaches a stationary value. As the breaking envelope is approached, the rate of decay becomes extremely slow, making the task of estimating the upper critical value of $\lambda_1$ a difficult one.

## 4.8 Summary and discussion

We have developed an asymptotic theory to describe the fully nonlinear, weakly three-dimensional waves that are generated by the resonant flow of a uniformly stratified, Boussinesq fluid past an obstacle. The evolution equation is shown to be of the integro-differential type in which three-dimensional effects are manifested as a nonlinear term. The equation reduces, in the small-amplitude limit to the fKP equation.

The theory is, however, not uniformly valid and breaks down for $x \gg 1$, owing to the formation of an infinite downstream shelf. In addition, it is found that neither mass nor energy is conserved as a result of a continuous flux of both quantities away from the resonant wave. By appropriately rescaling the far field, we showed that it consists of linear, propagating fronts of large, but finite streamwise extent. These fronts carry both mass and energy and it was shown, by explicit calculation that the total rate of change of mass within them is exactly the same as the mass flux out of the resonant wave. The amplitude of the shelf (and therefore of the fronts) was shown to be asymptotically small, $O(\mu)$, to be precise. Despite this, the shelf can actually have an appreciable magnitude in realistic geophysical flows. We also note that the shelf amplitude is an order of magnitude larger than it is in the corresponding two-dimensional problem, where it is $O(\mu^2)$.

While the far-field in this problem bears some qualitative similarities to the two-dimensional case, there is one significant difference. As emphasized in Chapter 3, shelf formation in two-dimensional flows occurs only as long as the flow is transient. However, we observe from (4.73$a$,$b$) that a shelf can exist even when the flow is steady, owing to the three-dimensional contributions. This implies that a steady state, such as that described by Yih's equations (Yih 1967) will feature a downstream flow field of infinite extent; the

amplitude in the far-field is nevertheless, asymptotically small.

We have also examined numerical solutions of the nonlinear evolution equation for a flow configuration consisting of a ridge-like obstacle in a channel. The wave pattern was found to differ significantly from that predicted by the fKP equation. The scaling of the breaking time for a specific choice of parameters was studied and the breaking envelope was determined. Experimental data for three-dimensional flows are limited. The most comprehensive study is perhaps that of Castro & Snyder (1993). However, a direct comparison with their results is not possible owing to the fact that the long-wave parmeter, $\mu$ is large. This difference between the two investigations notwithstanding, there are some points of qualitative agreement. It was observed, for example that although the flow was steady (even close to a resonance) in most of the runs, unsteadiness, accompanied by oscillations in the wave drag occurred when the spanwise length scale of the obstacle was increased. This is to be expected since the KP scaling then begins to be applicable. Furthermore, in their figure 7, Castro & Snyder indicate qualitatively the flow regimes that may exist. Specifically, in the neighborhood of a low mode-number resonance, it is seen that the regime map bears a striking resemblance to figure 4-7. We note however that the present model cannot reproduce features such as separation and vortex shedding (also observed by Castro & Snyder), which are inherently viscous phenomena.

# CHAPTER 5

# CONCLUDING REMARKS

We now summarize the salient findings of the present thesis and suggest possibilities for future research, where appropriate. Three problems concerned with the physics of finite-amplitude internal waves in a uniformly stratified Boussinesq fluid were investigated. This type of stratification is typical of that used in laboratory experiments and is also relevant to geophysical flows. However, the present results have broader implications, for the configurations considered here may be regarded as being representative of large-amplitude internal waves in arbitrarily stratified flows.

In the first problem, we examined large-depth flow past finite-amplitude topography of large streamwise extent. Under the assumption that there is no upstream influence, the steady state for this configuration is given by Long's model, which predicts a critical value of the non-dimensional mountain amplitude, $\epsilon$, above which overturning occurs. The stability of this steady state to vertical modulations was studied using the asymptotic theory of Kantzios & Akylas (1993). A linear analysis was employed to demonstrate that Long's steady flow is unstable to such modulations at mountain amplitudes significantly smaller than the critical overturning value. In contrast to the conjectures of past investigations, the mechanism of the instability was shown to be of the shear flow type, wherein a small disturbance grows by extracting energy from the mean flow. Moreover, using an eigenvalue analysis, we showed that a necessary condition for instability is the existence of a discrete spectrum of modes that are trapped close to the topography in the streamwise direction.

The effect of nonlinearity on the linear perturbation was studied by numerically solving the transient problem, mimicking the near-impulsive startup conditions used in typical laboratory experiments. Not surprisingly, Long's steady state was achieved for linearly stable flows. However, in the eventuality that the flow is linearly unstable, it was found to undergo oscillations about Long's steady state over a long timescale. Further study revealed that transient wave breaking does not take place even when the amplitude of the topography is 90% of the critical value for overturning. These results are in qualitative agreement with experimental observations. In this study, attention was restricted to hydrostatic flow, where streamwise dispersion is entirely negligible. It is anticipated that the primary effect of restoring dispersion would be to stabilize the flow. Nevertheless, it would be of interest to examine the effect of dispersion on the the stability margin as well as the possibility of permanent-wave solutions.

In the second problem, we addressed the phenomenon of shelf formation, primarily in the context of fully nonlinear internal waves in a uniformly stratified Boussinesq fluid of finite depth. These waves are described by the theory of Grimshaw & Yi (1991). It was shown that this theory breaks down in the far-field owing to the formation of an infinite downstream shelf of asymptotically small amplitude. Although it does not affect the results of Grimshaw & Yi, which pertain to the near field of the nonlinear wave, the shelf is of fundamental importance because its presence causes mass conservation to be violated. We showed moreover, that the appearance of the shelf is a consequence of the fact that the scales inherent in the nonlinear theory cease to hold in the far-field. This necessitates the use of matched asymptotic expansions, with the nonlinear theory being valid in an 'inner region', while the outer region consists of propagating, linear, long-wave modes. It was

demonstrated by explicit calculation that the total rate of change of mass within the outer region is exactly equal to the mass flux out of the inner region. The mechanism by which the shelf is generated was found to be a self-interaction of the nonlinear wave, where flow transience is an essential ingredient. In addition, recent numerical simulations were shown to contain evidence for shelf formation. We also examined weakly nonlinear, long waves in an arbitrarily stratified fluid layer, which are described to leading order by the Korteweg-de Vries equation and demonstrated that a shelf is formed in this case as well. However, the shelf is rather different in that it extends both upstream and downstream of the main wave, in general. When the nonlinear wave is generated by resonant forcing, this shelf would represent a new type of upstream influence that has not been observed before. This is a logical extension of the present results but is worth verifying by means of direct simulation. An added advantage of performing such a simulation is that it would permit shorter waves to be examined, where the amplitude of the shelf can be expected to be significant. Finally, we note that the prediction of shelves needs to be experimentally verified. It is plausible that shelves were indeed formed in past laboratory studies but escaped attention because attention was focused on the resonant response.

In the third problem, we investigated the resonant generation of fully nonlinear, weakly three-dimensional waves in a channel of finite depth. An asymptotic theory was developed and the governing equation was found to be of the integro-differential type, wherein both unsteady and three-dimensional effects are represented by highly nonlinear terms. This evolution equation was shown to be valid until the occurrence of incipient breaking. As in the analogous two-dimensional problem of Grimshaw & Yi (1991), the theory is not uniformly valid owing to the formation of a downstream shelf. However, the amplitude

of the shelf has a larger amplitude and the region of validity of the nonlinear theory is smaller, leading to severe theoretical and numerical difficulties. Specifically, it was found that in addition to a net flux of mass, there is also a net flux of energy from the resonant wave. The methods developed for the two-dimensional problem were brought to bear here and a procedure for constructing the outer solution was outlined. Numerical solutions of the evolution equation for a ridge-like obstacle placed in a channel were examined and the flow was found to differ significantly from the Kadomtsev–Petviashvili solution for the equivalent surface-wave problem. By holding certain parameters fixed, the parameter space was considerably reduced and consisted of the relative blockage, the relative breaking time, a detuning from exact resonance and a parameter representing non-Boussinesq effects. The scaling of the relative breaking time was examined in some detail and it was found that overturning occurs only within a finite 'breaking envelope'. As we have noted earlier, the study of the parameter space in this problem is far from complete and requires futrther detailed investigation. In addition, there is no comprehensive study of this flow using numerical simulations and, while this would entail a considerable computational effort, it would serve to complement the present investigation.

# APPENDIX A

# CALCULATION OF EIGENVALUES AND TRAPPED MODES

The procedure employed to determine the eigenvalues and mode shapes of the linear stability problem is described here. The generalized matrix eigenvalue problem,

$$[C]\{z\} = \lambda[E]\{z\} \tag{A 1}$$

is first solved on a coarse grid to obtain a rough approximation of the spectrum. This was accomplished using EISPACK routines implemented on MATLAB. The grid was then refined and a more exact estimate to the previously determined eigenvalue was generated using a procedure similar to that outlined by Gourlay & Watson (1973, p. 56).

Introducing the eigenvalue shift $q$, (A 1) is transformed to

$$([C] - q[E])\,\{z\} = (\lambda - q)[E]\{z\}. \tag{A 2}$$

We now use inverse Rayleigh iteration to solve for the eigenvalue $(\lambda - q)$ of the problem specified by (A 2). Denoting the iteration count by $p$, we define

$$\{z\}^{(p)} = \frac{\{y\}^{(p)}}{||\{y\}^{(p)}||_\infty},$$

where the norm used is defined by

$$\left|\left|\{y\}^{(p)}\right|\right|_\infty = \max\{|y|\}^{(p)}.$$

The next iteration for the eigenvector is determined by solving

$$([C] - q[E])\,\{y\}^{(p+1)} = [E]\{z\}^{(p)}. \tag{A 3}$$

Since $([C] - q[E])$ does not change with the iteration count, $p$, it proves convenient to use LU decomposition to solve (A 3): it is therefore necessary to determine the lower and upper triangular matrices only once. The eigenvalue is then calculated by making use of the relation

$$\lim_{p\to\infty} y_{imax}^{(p)} = \frac{1}{(\lambda - q)},$$

where $imax$ is the index corresponding to the location of the norm $||\{y\}^{(p)}||_\infty$. Using $\left(||\{y\}^{(p)}||_\infty\right)^{-1}$ as the convergence criterion, it was found that this criterion achieved a value of $10^{-6}$ within five iterations. Furthermore, the eigenvalue was found to converge rapidly as the grid spacing was decreased so that a minimum spacing of 0.01 was found to be more than adequate.

# APPENDIX B

## NUMERICAL IMPLEMENTATION OF BOUNDARY CONDITION

This Appendix illustrates the procedure used to implement the boundary condition (2.12) for the nonlinear transient problem. An identical procedure is used in the case of the linear stability problem, with the difference that the boundary condition is then given by (2.22). In both cases, equation (2.15*b*) (or (2.21*b*)) is first used to solve for $b(x,0)$ (or $\widetilde{b}(x,0)$) and the appropriate boundary condition is then used to obtain $a(x,0)$ (or $\widetilde{a}(x,0)$).

The $x$ and $Y$ grid indices are denoted by $i$ and $j$ respectively, while the time step is denoted by $n$. The source of numerical instability in other schemes that were attempted was found to be the 'cross-coupling' term $K_{21}^c a_T$ in (2.15*b*). The instability was found to be eliminated by evaluating this term implicitly (at time step $(n+1)$) on $j=1$. The kernels and the intergal term were also evaluated in a similar manner using the trapezoidal rule. Making the definitions

$$\Delta x_i = x_i - x_{i-1}, \qquad \Omega = \frac{\Delta T}{(\Delta x_i + \Delta x_{i+1})\Delta Y_1},$$

and

$$\begin{aligned} T_1 &= \Omega \frac{\Delta x_i}{\Delta x_{i+1}}, \\ T_2 &= \Omega \left( \frac{\Delta x_{i+1}}{\Delta x_i} - \frac{\Delta x_i}{\Delta x_{i+1}} \right), \\ T_3 &= \Omega \frac{\Delta x_{i+1}}{\Delta x_i}, \end{aligned}$$

it is found that equation (2.15*b*) yields

$$T_1 a_{i+1,0}^{(n+1)} + T_2 a_{i,0}^{(n+1)} - T_3 a_{i-1,0}^{(n+1)} + K_{22}^c b_{i-1,0}^{(n+1)} =$$

$$K_{21}^c \left[ a_{i,1}^{(n)} - a_{i,1}^{(n+1)} \right] + K_{22}^c b_{i,0}^{(n)} + a_{xY} \Delta T - \int_{-\infty}^{x} \mathrm{d}x' [K_{21x} a_T' + K_{22x} b_T'], \qquad \text{(B 1)}$$

where $a_{xY}$ is evaluated implicitly using second order forward differences in $Y$ and centered differences in $x$. Similarly, the discretised form of the boundary condition (2.12) gives

$$a_{i,0}^{(n+1)} = b_{i,0}^{(n+1)} \tan \epsilon f_i^{(n+1)} - \frac{1}{2} \epsilon f_i^{(n+1)} \sec \epsilon f_i^{(n+1)}. \qquad \text{(B 2)}$$

Using (B 2), we now eliminate $a^{(n+1)}\Big|_{j=0}$ from the left-hand side of (B 1) to obtain

$$\left[ -T_3 \tan \epsilon f_{i-1}^{(n+1)} \right] b_{i-1,0}^{(n+1)} + \left[ T_2 \tan \epsilon f_i^{(n+1)} + K_{22}^c \right] b_{i,0}^{(n+1)} + \left[ T_1 \tan \epsilon f_{i+1}^{(n+1)} \right] b_{i+1,0}^{(n+1)} =$$

$$K_{21}^c \left[ a_{i,1}^{(n)} - a_{i,1}^{(n+1)} \right] + K_{22}^c b_{i,0}^{(n)} + a_{xY} \Delta T - \int_{-\infty}^{x} \mathrm{d}x' [K_{21x} a_T' + K_{22x} b_T'] + G, \qquad \text{(B 3)}$$

where

$$G = \frac{1}{2} \epsilon \left[ T_1 f_{i+1}^{(n+1)} \sec \epsilon f_{i+1}^{(n+1)} + T_2 f_i^{(n+1)} \sec \epsilon f_i^{(n+1)} + T_3 f_{i-1}^{(n+1)} \sec \epsilon f_{i-1}^{(n+1)} \right].$$

The tridiagonal system represented by (B 3) is solved using Thomas' algorithm to obtain $b^{(n+1)}\Big|_{j=0}$. Finally, $a^{(n+1)}\Big|_{j=0}$ is calculated using (B 2).

# APPENDIX C

# ENERGETICS OF A SMALL LOCALIZED DISTURBANCE

Here we demonstrate how the energy-balance equation (2.34) for the evolution of a small localized disturbance to Long's steady state is expressed in terms of the scaled variables used in the asymptotic theory of KA.

We begin with the rate of change of kinetic energy

$$\frac{\mathrm{d}}{\mathrm{d}t}\mathrm{KE} = \frac{1}{2}\frac{\mathrm{d}}{\mathrm{d}t}\int_{-\infty}^{\infty}\mathrm{d}x\int_{\epsilon f}^{\infty}\mathrm{d}y\,\widetilde{u}^2.$$

Since $\widetilde{u} = \widetilde{\psi}_y$ and

$$\widetilde{\psi} = 2(\widetilde{a}\cos y - \widetilde{b}\sin y), \tag{C 1}$$

one has to leading order in $\mu$

$$\int_{\epsilon f}^{\infty}\mathrm{d}y\,\widetilde{\psi}_y^2 \sim \frac{2}{\mu^2}\int_0^{\infty}\mathrm{d}Y(\widetilde{a}^2 + \widetilde{b}^2).$$

Hence,

$$\frac{\mathrm{d}}{\mathrm{d}t}\mathrm{KE} = \frac{\mathrm{d}}{\mathrm{d}T}\left\langle \widetilde{a}^2 + \widetilde{b}^2 \right\rangle,$$

in agreement with (2.35$a$).

We next consider the rate of change of potential energy

$$\frac{\mathrm{d}}{\mathrm{d}t}\mathrm{PE} = \frac{1}{\beta}\int_{-\infty}^{\infty}\mathrm{d}x\int_{\epsilon f}^{\infty}\mathrm{d}y\,\widetilde{\rho}\widetilde{v},$$

where $\widetilde{v} = -\widetilde{\psi}_x$ and, from (2.9),

$$\widetilde{\rho} = -\beta\widetilde{\psi} + \mu^2\beta\int_{-\infty}^{x}\left.\frac{\widetilde{\psi}_T}{\overline{\psi}_y}\right|_{\overline{\psi}}\mathrm{d}x'.$$

Therefore,

$$\frac{\mathrm{d}}{\mathrm{d}t}\mathrm{PE} = \tfrac{1}{2}\int_{-\infty}^{\infty}\mathrm{d}x\int_{\epsilon f}^{\infty}\mathrm{d}y\left(\widetilde{\psi}^2\right)_x - \mu^2\int_{-\infty}^{\infty}\mathrm{d}x\int_{\epsilon f}^{\infty}\mathrm{d}y\,\widetilde{\psi}_x\int_{-\infty}^{x}\left.\frac{\widetilde{\psi}_T}{\overline{\psi}_y}\right|_{\overline{\psi}}\mathrm{d}x'. \tag{C 2}$$

By integration by parts, invoking the boundary conditions (2.4) and (2.22), the first term above can be readily shown to vanish. Using then (C 1) and

$$\overline{\psi} = y + 2\left(\overline{a}\cos y - \overline{b}\sin y\right), \tag{C 3}$$

the integrand of the second term in (C 2) gives

$$\int_{\epsilon f}^{\infty}\mathrm{d}y\,\widetilde{\psi}_x\int_{-\infty}^{x}\left.\frac{\widetilde{\psi}_T}{\overline{\psi}_y}\right|_{\overline{\psi}}\mathrm{d}x' \sim \frac{2}{\pi}\frac{1}{\mu^2}\int_0^{\infty}\mathrm{d}Y\int_{-\infty}^{x}\mathrm{d}x'\int_0^{2\pi}\mathrm{d}\overline{\psi}\,\frac{1}{\overline{\psi}_y\overline{\psi}'_y}\left(\widetilde{a}_x\cos y - \widetilde{b}_x\sin y\right)\left(\widetilde{a}'_T\cos y' - \widetilde{b}'_T\sin y'\right). \tag{C 4}$$

However, from (C 3),

$$\sin y = \tfrac{1}{2}\,y_{\overline{b}}\,\overline{\psi}_y, \qquad \cos y = -\tfrac{1}{2}\,y_{\overline{a}}\,\overline{\psi}_y, \tag{C 5}$$

and combining (C 2) with (C 4) and (C 5) yields (2.35*b*).

Finally, using (2.11), (C 1) and (C 3), the power-input term takes the form

$$\mathcal{R} = -\tfrac{1}{2}\epsilon\int_{-\infty}^{\infty}\mathrm{d}x f_x\,\widetilde{\psi}_y^2\Big|_{y=\epsilon f} - \mu^2\left\{\int_{-\infty}^{\infty}\mathrm{d}x\int_{\epsilon f}^{\infty}\mathrm{d}y\overline{H}\left(\mathrm{i}\widetilde{\psi}_x\overline{A} - \widetilde{\psi}_y\overline{A}_x\right)\mathrm{e}^{\mathrm{i}y} + \text{c.c.}\right\}, \tag{C 6}$$

where

$$\overline{H} = -\frac{\partial}{\partial\overline{\psi}}\int_{-\infty}^{x}\left.\widetilde{\psi}_{yT}\right|_{\overline{\psi}}\mathrm{d}x' + \frac{\partial}{\partial\overline{\psi}}\int_{-\infty}^{x}y\left.\frac{\widetilde{\psi}_T}{\overline{\psi}_y}\right|_{\overline{\psi}}\mathrm{d}x' - y\frac{\partial}{\partial\overline{\psi}}\int_{-\infty}^{x}\left.\frac{\widetilde{\psi}_T}{\overline{\psi}_y}\right|_{\overline{\psi}}\mathrm{d}x'.$$

Now, using (C 1) and (C 3), it follows that

$$\int_{\epsilon f}^{\infty}\mathrm{d}y\overline{H}\left(\mathrm{i}\widetilde{\psi}_x\overline{A} - \widetilde{\psi}_y\overline{A}_x\right)\mathrm{e}^{\mathrm{i}y} + \text{c.c.} \sim -\frac{1}{\mu^2}\int_0^{\infty}\mathrm{d}Y\,P(x,Y,T), \tag{C 7}$$

where

$$P = \frac{1}{2\pi}\int_0^{2\pi} \mathrm{d}\overline{\psi}\,\overline{\psi}_y\,\overline{H}\left\{\left(\widetilde{a}_x\overline{b}-\widetilde{b}\overline{a}_x\right)y_{\overline{a}}^2+\left(\widetilde{a}\overline{b}_x-\widetilde{b}_x\overline{a}\right)y_{\overline{b}}^2 - \left(\widetilde{a}_x\overline{a}-\widetilde{b}_x\overline{b}-\widetilde{a}\overline{a}_x+\widetilde{b}\overline{b}_x\right)y_{\overline{a}}y_{\overline{b}}\right.$$

and

$$\overline{H} = -\frac{\partial}{\partial\overline{\psi}}\int_{-\infty}^{x}\mathrm{d}x'y'\left(\widetilde{a}'_T y'_{\overline{a}}+\widetilde{b}'_T y'_{\overline{b}}\right)-\int_{-\infty}^{x}\mathrm{d}x'\left(\widetilde{a}'_T y'_{\overline{a}}+\widetilde{b'}_T y'_{\overline{b}}\right) + y\frac{\partial}{\partial\overline{\psi}}\int_{-\infty}^{x}\mathrm{d}x'\left(\widetilde{a}'_T y'_{\overline{a}}+\widetilde{b}'_T y'_{\overline{b}}\right).$$

Combining then (C 6) with (C 7) yields (2.35*c*).

# APPENDIX D

## ENERGETICS OF TRANSIENT RESPONSE

Here we give details of the manipulation involved in expressing the energy-balance equation (2.40) for the transient response in terms of the scaled variables used in the asymptotic theory of KA.

The rate of change of kinetic energy is

$$\frac{\mathrm{d}}{\mathrm{d}t}\mathrm{KE} = \frac{1}{2}\frac{\mathrm{d}}{\mathrm{d}t}\int_{-\infty}^{\infty}\mathrm{d}x\int_{\epsilon f}^{\infty}\mathrm{d}y\,\widehat{u}^2,$$

where $\widehat{u} = \widehat{\psi}_y$ and

$$\widehat{\psi} = 2(a\cos y - b\sin y).$$

Therefore,

$$\int_{\epsilon f}^{\infty}\mathrm{d}y\,\widehat{\psi}_y^2 \sim \frac{2}{\mu^2}\int_0^{\infty}\mathrm{d}Y(a^2+b^2),$$

and

$$\frac{\mathrm{d}}{\mathrm{d}t}\mathrm{KE} = \frac{\mathrm{d}}{\mathrm{d}T}\langle a^2+b^2\rangle$$

as in (2.41$a$).

We next consider the rate of change of potential energy

$$\frac{\mathrm{d}}{\mathrm{d}t}\mathrm{PE} = \frac{1}{\beta}\int_{-\infty}^{\infty}\mathrm{d}x\int_{\epsilon f}^{\infty}\mathrm{d}y\,\widehat{\rho}\widehat{v},$$

where $\widehat{v} = -\widehat{\psi}_x$ and, from (2.9),

$$\widehat{\rho} = -\beta\widehat{\psi} + \mu^2\beta\int_{-\infty}^{x}\left.\frac{\widehat{\psi}_T}{\psi_y^{(0)}}\right|_{\psi^{(0)}}\mathrm{d}x'. \tag{D 1}$$

Therefore,

$$\frac{\mathrm{d}}{\mathrm{d}t}\mathrm{PE} = \tfrac{1}{2}\int_{-\infty}^{\infty}\mathrm{d}x\int_{\epsilon f}^{\infty}\mathrm{d}y\left(\widehat{\psi}^2\right)_x - \mu^2\int_{-\infty}^{\infty}\mathrm{d}x\int_{\epsilon f}^{\infty}\mathrm{d}y\,\widehat{\psi}_x\int_{-\infty}^{x}\left.\frac{\widehat{\psi}_T}{\psi_y^{(0)}}\right|_{\psi^{(0)}}\mathrm{d}x'. \tag{D 2}$$

Upon integration by parts, the first term above becomes

$$\tfrac{1}{2}\int_{-\infty}^{\infty}\mathrm{d}x\int_{\epsilon f}^{\infty}\mathrm{d}y\left(\widehat{\psi}^2\right)_x = \tfrac{1}{2}\epsilon\int_{-\infty}^{\infty}\mathrm{d}x\,f_x\,\widehat{\psi}^2\Big|_{y=\epsilon f},$$

and, invoking the boundary condition (2.12), this term vanishes. Furthermore,

$$\int_{\epsilon f}^{\infty}\mathrm{d}y\,\widehat{\psi}_x\int_{-\infty}^{x}\left.\frac{\widehat{\psi}_T}{\psi_y^{(0)}}\right|_{\psi^{(0)}}\mathrm{d}x' \sim \frac{2}{\pi}\,\frac{1}{\mu^2}\int_0^{\infty}\mathrm{d}Y\int_{-\infty}^{x}\mathrm{d}x'\int_0^{2\pi}\mathrm{d}\psi^{(0)}\frac{1}{\psi_y^{(0)}\psi_y^{(0)\prime}}\left(a_x\cos y - b_x\sin y\right)\left(a_T'\cos y' - b_T'\sin y'\right). \tag{D 3}$$

Combining then (D 2) with (D 3), using

$$\sin y = \tfrac{1}{2}y_b\psi_y^{(0)}, \qquad \cos y = -\tfrac{1}{2}y_a\psi_y^{(0)}, \tag{D 4}$$

yields (2.41*b*).

Finally, from (2.39*b*),

$$\widehat{p}|_{y=\epsilon f} = \int_{\epsilon f}^{\infty}\widehat{\rho}\,\mathrm{d}y,$$

where $\widehat{\rho}$ is given by (D 1), and the rate of energy imparted to the flow takes the form

$$\mathcal{R} = -\epsilon\int_{-\infty}^{\infty}\mathrm{d}x\,f_x\int_{\epsilon f}^{\infty}\mathrm{d}y\,\widehat{\psi} + \mu^2\epsilon\int_{-\infty}^{\infty}\mathrm{d}x\,f_x\int_{\epsilon f}^{\infty}\mathrm{d}y\int_{-\infty}^{x}\left.\frac{\widehat{\psi}_T}{\psi_y^{(0)}}\right|_{\psi^{(0)}}\mathrm{d}x'. \tag{D 5}$$

In view of (2.11) and (D 4), one has

$$\int_{\epsilon f}^{\infty}\mathrm{d}y\,\widehat{\psi} \sim -2(a\sin\epsilon f + b\cos\epsilon f)_{Y=0} + \frac{1}{2\pi}\int_0^{\infty}\mathrm{d}Y\int_0^{2\pi}\mathrm{d}\psi^{(0)}\frac{1}{\psi_y^{(0)}}H^{(0)}, \tag{D 6}$$

where

$$H^{(0)} = -\frac{\partial}{\partial\psi}\int_{-\infty}^{x} \mathrm{d}x'y'\,(a'_T y'_a + b'_T y'_b) - \int_{-\infty}^{x} \mathrm{d}x'\,(a'_T y'_a + b'_T y'_b) + y\frac{\partial}{\partial\psi^{(0)}}\int_{-\infty}^{x} \mathrm{d}x'\,(a'_T y'_a + b'_T y'_b).$$

Also,

$$\mu^2\int_{\epsilon f}^{\infty}\mathrm{d}y\int_{-\infty}^{x}\frac{\widehat{\psi}_T}{\psi_y^{(0)}}\bigg|_{\psi^{(0)}}\mathrm{d}x' \sim \frac{1}{2\pi}\int_0^{\infty}\mathrm{d}Y\int_{-\infty}^{x}\mathrm{d}x'\int_0^{2\pi}\mathrm{d}\psi^{(0)}\frac{1}{\psi_y^{(0)}}\frac{\widehat{\psi}'_T}{\psi_y^{(0)\prime}}. \qquad \text{(D 7)}$$

Combining then (D 5) with (D 6) and (D 7), and making further use of (D 4), yields (2.41$c$).

# APPENDIX E

## FUNCTIONS APPEARING IN BOUNDARY VALUE PROBLEMS

Here, we list the terms that appear in the sequence of boundary value problems that appear in §3.5.

$O(\epsilon)$:

$$E_1 = \frac{1}{2\beta c_n^3}\overline{\rho}_{yy}\phi^{(0,0)^2} - \frac{2r}{\beta c_n^3}\overline{\rho}_y\phi^{(0,0)} - \frac{1}{2c_n}\left(\overline{\rho}_y\phi^{(0,0)}\phi_y^{(0,0)}\right)_y - \frac{1}{2c_n}\left[\overline{\rho}\left(\phi_y^{(0,0)^2} - \phi_{yy}^{(0,0)}\phi^{(0,0)}\right)\right]_y \tag{E 1}$$

$$E_2 = -\frac{2s}{\beta c_n^3}\overline{\rho}_y\phi^{(0,0)} - \overline{\rho}\phi^{(0,0)} \tag{E 2}$$

$O(\epsilon^2)$:

$$c_nP_1 = 2\rho_y^{(0,0)}\phi^{(1,0)} + \rho_y^{(1,0)}\phi^{(0,0)} - 2\phi_y^{(0,0)}\rho^{(1,0)} - \rho^{(0,0)}\phi_y^{(1,0)} - 4r\rho^{(1,0)} - 3\lambda_1\rho^{(0,0)} \tag{E 3}$$

$$c_nP_2 = \rho_y^{(0,0)}\phi^{(0,1)} - \rho^{(0,1)}\phi_y^{(0,0)} - 2s\rho^{(1,0)} - 2r\rho^{(0,1)} - \lambda_2\rho^{(0,0)} \tag{E 4}$$

$$c_nP_3 = \phi^{(0,0)}\rho_y^{(0,1)} - \rho^{(0,0)}\phi_y^{(0,1)} - 6r\rho^{(0,1)} - \lambda_3\rho^{(0,0)} \tag{E 5}$$

$$S_1 = \frac{P_1}{\beta} - 4r\left(\overline{\rho}\phi_y^{(1,0)}\right)_y - c_n\left(\rho^{(1,0)}\phi_y^{(0,0)}\right)_y - 3\overline{\rho}\phi_y^{(0,0)}\phi_y^{(1,0)} - 3\lambda_1\phi_{yy}^{(0,0)} + \overline{\rho}\left(2\phi_{yy}^{(0,0)}\phi^{(1,0)} + \phi^{(0,0)}\phi_{yy}^{(1,0)}\right) + \left[\rho^{(0,0)}\left(\phi_{yy}^{(0,0)}\phi^{(0,0)} - \phi_y^{(0,0)^2}\right)\right]_y \tag{E 6}$$

$$S_2 = \frac{P_2}{\beta} - 2c_n\overline{\rho}\phi^{(1,0)} - \left[2\overline{\rho}\left(s\phi_y^{(1,0)} + r\phi_y^{(0,1)}\right)\right]_y - \overline{\rho}\phi_y^{(0,0)}\phi_y^{(0,1)} - \lambda_2\overline{\rho}\phi_{yy}^{(0,0)} + \overline{\rho}\phi^{(0,1)}\phi_{yy}^{(0,0)} - \overline{\rho}\phi^{(0,0)}\phi_y^{(0,0)} - c_n\rho^{(0,0)}\phi^{(0,0)} - s\left(\rho^{(0,0)}\phi_y^{(0,0)}\right)_y \tag{E 7}$$

$$S_3 = \frac{P_3}{\beta} - 6c_n\overline{\rho}\phi^{(1,0)} - 6r\left(\overline{\rho}\phi_y^{(0,1)}\right)_y - c_n\left(\rho^{(0,1)}\phi_y^{(0,0)}\right)_y - \overline{\rho}\phi_y^{(0,0)}\phi_y^{(0,1)}$$
$$+ \overline{\rho}\phi^{(0,0)}\phi_{yy}^{(0,1)} + \overline{\rho}\phi^{(0,0)}\phi_y^{(0,0)} - c_n\rho^{(0,0)}\phi^{(0,0)} - \lambda_3\overline{\rho}\phi_{yy}^{(0,0)} \tag{E 8}$$

$O(\epsilon^3)$:

$$c_nR_2 = \rho_y^{(0,0)}\phi_1^{(1,1)} - \rho_1^{(1,1)}\phi_y^{(0,0)} + \rho_y^{(1,0)}\phi^{(0,1)} - \rho^{(0,1)}\phi_y^{(1,0)}$$
$$- 3s\rho^{(2,0)} - 2r\rho_1^{(1,1)} - 2\lambda_2\rho^{(1,0)} - \gamma_2\rho^{(0,0)} \tag{E 9}$$

$$c_nR_3 = \rho_y^{(0,0)}\phi_1^{(1,1)} + 2\rho_y^{(0,0)}\phi_2^{(1,1)} + \phi^{(0,0)}\rho_{1y}^{(1,1)} - \rho^{(0,0)}\phi_{1y}^{(1,1)}$$
$$- 2\phi_y^{(0,0)}\rho_2^{(1,1)} - \phi_y^{(0,0)}\rho_1^{(1,1)} + 2\rho_y^{(0,1)}\phi^{(1,0)} - 2\rho^{(1,0)}\phi_y^{(0,1)}$$
$$-8r\rho_1^{(1,1)} - 4r\rho_2^{(1,1)} - 2\lambda_3\rho^{(1,0)} - \gamma_3\rho^{(0,0)} \tag{E 10}$$

$$c_nR_4 = \phi^{(0,0)}\rho_{2y}^{(1,1)} - \rho^{(0,0)}\phi_{2y}^{(1,1)} - 4r\rho_2^{(1,1)} - \gamma_4\rho^{(0,0)} \tag{E 11}$$

$$Q_2 = \frac{R_2}{\beta} - 3c_n\overline{\rho}\phi^{(2,0)} - \left[\overline{\rho}\left(3s\phi_y^{(2,0)} + 2r\phi_{1y}^{(1,1)}\right)\right]_y$$
$$- c_n\left(\rho^{(0,0)}\phi_{1y}^{(1,1)} + \rho^{(1,0)}\phi_y^{(0,1)}\right)_y - 2\lambda_2\left(\overline{\rho}\phi_y^{(1,0)}\right)_y$$
$$- \left[\overline{\rho}\left(\phi_y^{(0,0)}\phi_{1y}^{(1,1)} + \phi_y^{(1,0)}\phi_y^{(0,1)} + \phi_1^{(1,1)}\phi_{yy}^{(0,0)}\phi^{(0,1)}\phi_{yy}^{(1,0)}\right)\right]_y - \gamma_2\left(\overline{\rho}\phi_y^{(0,0)}\right)_y$$
$$- \left[\rho^{(0,0)}\left(\phi_y^{(0,0)}\phi_y^{(0,1)} - \phi^{(0,1)}\phi_{yy}^{(0,0)}\right)\right]_y - \overline{\rho}\left(\phi^{(0,0)}\phi_y^{(1,0)} + 2\phi_y^{(0,0)}\phi^{(1,0)}\right)$$
$$-c_n\rho^{(1,0)}\phi^{(0,0)} - 2\rho^{(0,0)}\phi^{(1,0)} - 2\left[\rho^{(0,0)}\left(r\phi_y^{(0,1)} + s\phi_y^{(1,0)}\right)\right]_y$$
$$-\lambda_2\left(\rho^{(0,0)}\phi_y^{(0,0)}\right)_y - \rho^{(0,0)}\phi^{(0,0)}\phi_y^{(0,0)} \tag{E 12}$$

$$Q_3 = \frac{R_3}{\beta} - 18c_n\overline{\rho}\phi^{(2,0)} - 4r\left[\overline{\rho}\left(2\phi_{1y}^{(1,1)} + \phi_{2y}^{(1,1)}\right)\right]_y$$
$$- c_n\left[\rho^{(0,0)}\left(\phi_{1y}^{(1,1)} + 2\phi_{2y}^{(1,1)}\right) + \rho_1^{(1,1)}\phi_y^{(0,0)} + 2\rho^{(0,1)}\phi_y^{(1,0)}\right]_y$$

$$
\begin{aligned}
&- 2\left[\overline{\rho}\left(\phi_y^{(0,0)}\phi_{1y}^{(1,1)} + \phi_y^{(0,0)}\phi_{2y}^{(1,1)} + \phi_y^{(1,0)}\phi_y^{(0,1)}\right)\right]_y \\
&+ \left[\overline{\rho}\left(\phi_1^{(1,1)}\phi_{yy}^{(0,0)} + 2\phi^{(1,1)}\phi_{yy}^{(0,0)} + \phi^{(0,0)}\phi_{yy}^{(1,1)} + 2\phi^{(1,0)}\phi_{yy}^{(0,1)}\right)\right]_y \\
&- \gamma_3\left(\overline{\rho}\phi_y^{(0,0)}\right)_y - \left[\rho^{(0,0)}\left(\phi_y^{(0,0)}\phi_y^{(0,1)} - \phi^{(0,0)}\phi_{yy}^{(0,1)}\right)\right]_y \\
&+ \left[\rho^{(0,1)}\left(\phi^{(0,0)}\phi_{yy}^{(0,0)} - {\phi_y^{(0,0)}}^2\right)\right]_y + 2\overline{\rho}\left(\phi^{(0,0)}\phi_y^{(1,0)} - 2\phi_y^{(0,0)}\phi^{(1,0)}\right) \\
&- 2c_n\rho^{(1,0)}\phi^{(0,0)} - 8\rho^{(0,0)}\phi^{(1,0)} - 2r\left(3\rho^{(0,0)}\phi_y^{(0,1)} + \rho^{(0,1)}\phi_y^{(0,0)}\right)_y \\
&- \lambda_3\left(\rho^{(0,0)}\phi_y^{(0,0)} + 2\overline{\rho}\phi_y^{(0,1)}\right)_y
\end{aligned}
\tag{E 13}
$$

$$
\begin{aligned}
Q_4 = \frac{R_4}{\beta} &- 6c_n\overline{\rho}\phi^{(2,0)} - 4r\left(\overline{\rho}\phi_{2y}^{(1,1)}\right)_y - c_n\left(\rho_2^{1,1)}\phi_y^{(0,0)}\right)_y \\
&+ \left(\overline{\rho}\phi^{(0,0)}\phi_{2yy}^{(1,1)}\right)_y - \gamma_4\left(\overline{\rho}\phi_y^{(0,0)}\right)_y + 2\overline{\rho}\phi^{(0,0)}\phi_y^{(1,0)} \\
&- 2\rho^{(0,0)}\phi^{(1,0)} + \rho^{(0,0)}\phi^{(0,0)}\phi_y^{(0,0)}
\end{aligned}
\tag{E 14}
$$

# APPENDIX F

# ALTERNATE DERIVATION OF GOVERNING EQUATIONS

Here we show how the governing equations (4.27),(4.31) may be derived using a vorticity approach. For simplicity, we consider the case of a uniform stratification with a background flow speed $V = c_n$, implying an exact mode-$n$ resonance. Defining the vorticity $\boldsymbol{\omega}$ in the usual way and non-dimensionalizing it with $N$, we have

$$\boldsymbol{\omega} = \mu(w_y - v_z)\boldsymbol{i} + (u_z - w_x)\boldsymbol{j} + \mu(v_x - u_y)\boldsymbol{k},$$

where all variables are dimensionless and $\boldsymbol{i}, \boldsymbol{j}, \boldsymbol{k}$ are the unit vectors along $x, y, z$. The momentum equations can be expressed as

$$\beta\rho\frac{\partial}{\partial t}\left(u, \mu^2 v, w\right) - \beta\rho\boldsymbol{u} \times \boldsymbol{\omega} = \\ - \boldsymbol{\nabla} H + y\boldsymbol{\nabla}\rho + \frac{1}{2}\beta\left(u^2 + \mu^2 v^2 + w^2\right)\boldsymbol{\nabla}\rho, \tag{F 1}$$

where $H$ is the Bernoulli function and is defined by

$$H = p + \frac{1}{2}\beta\rho\left(u^2 + \mu^2 v^2 + w^2\right) + \rho y. \tag{F 2}$$

Simplifying using (4.20) and implementing the stretched timescale $T = \mu^2 t$, () is transformed to

$$\mu^2\beta\rho\frac{\partial}{\partial T}\left(u, \mu^2 v, w\right) - \beta\rho\boldsymbol{u} \times \boldsymbol{\omega} = -\boldsymbol{\nabla} H + y\boldsymbol{\nabla}\rho. \tag{F 3}$$

Next, we make use of the property that the vorticity vector must lie along planes of constant density for an inviscid flow that is started from rest (Yih 1980); this implies that

$$\boldsymbol{\omega} \cdot \boldsymbol{\nabla}\rho = 0. \tag{F 4}$$

Inserting the expression for $\rho$ from (4.20) into (F 4), it is found that

$$\boldsymbol{\omega}\cdot\boldsymbol{\nabla}\Psi=\mu^3\left[\mathcal{W}_y\frac{\Psi_T}{\Psi_y}-\Psi_{yy}\int_{-\infty}^{\infty}\mathrm{d}x'\frac{\partial}{\partial Z}\left(\frac{\Psi_T}{\Psi_y}\right)\bigg|_{\Psi}\right]+O(\mu^4). \tag{F 5}$$

Consequently, we may express $\boldsymbol{\omega}$ as

$$\boldsymbol{\omega}=\boldsymbol{\gamma}\times\boldsymbol{\nabla}\Psi+\mu^3\boldsymbol{\alpha},$$

where $\boldsymbol{\gamma}$ is arbitrary and

$$\boldsymbol{\alpha}\cdot\boldsymbol{\nabla}\Psi=\mathcal{W}_y\frac{\Psi_T}{\Psi_y}-\Psi_{yy}\int_{-\infty}^{\infty}\mathrm{d}x'\frac{\partial}{\partial Z}\left(\frac{\Psi_T}{\Psi_y}\right)\bigg|_{\Psi}. \tag{F 6}$$

Defining $\Phi\equiv z+\mu\phi$ and using (F 5), it may be shown that

$$\boldsymbol{u}\times\boldsymbol{\omega}=-(\boldsymbol{\omega}\cdot\boldsymbol{\nabla}\Phi)\boldsymbol{\nabla}\Psi+\mu^3(\boldsymbol{\alpha}\cdot\boldsymbol{\nabla}\Psi)\boldsymbol{\nabla}\phi. \tag{F 7}$$

From (F 3) and (F 6), we obtain

$$\beta\rho(\boldsymbol{\omega}\cdot\boldsymbol{\nabla}\Phi)\Psi_x=-H_x+y\rho_x-\mu^2\beta\rho\Psi_{yT}+O(\mu^4), \tag{F 8$a$}$$

$$\beta\rho(\boldsymbol{\omega}\cdot\boldsymbol{\nabla}\Phi)\Psi_y=-H_y+y\rho_y+O(\mu^4), \tag{F 8$b$}$$

$$\beta\rho(\boldsymbol{\omega}\cdot\boldsymbol{\nabla}\Phi)\Psi_z=-H_z+y\rho_z+O(\mu^3). \tag{F 8$c$}$$

Eliminating $\Psi$ from (F 8$a,b$), it is found that

$$J(H,\Psi)=yJ(\rho,\Psi)-\mu^2\beta\rho\Psi_{yT}\Psi_y; \tag{F 9}$$

this process of elimination may also be interpreted as an integration along a streamline. We may then integrate (F 9) to yield

$$H=\overline{H}(\Psi)-\mu^2\overline{\rho}_{\Psi}\int_{-\infty}^{x}\mathrm{d}x'\,\frac{y\Psi_T}{\Psi_y}\bigg|_{\Psi}-\mu^2\beta\overline{\rho}\int_{-\infty}^{x}\mathrm{d}x'\,\Psi_{yT}|_{\Psi}\,, \tag{F 10}$$

where $\overline{H}$ is the value of the Bernoulli function far upstream. Inserting the expression for $H$ from (F 10) into (F 8$b$) and using (F 2) to evaluate $\overline{H}$, it is found that

$$\beta\rho\,(\boldsymbol{\omega}\cdot\boldsymbol{\nabla}\Phi) = \beta\overline{\rho}\frac{\Psi}{c_n^2} + y\overline{\rho}_\Psi + \mu^2\beta\overline{\rho}R + O(\beta^2), \tag{F 11}$$

where $R$ is defined by (4.28). Next, substituting for $\boldsymbol{\omega}$ in (F 11) and replacing the independent variable, $y$ with $\Psi$, we obtain

$$\Psi_{yy} + \frac{\Psi - c_n y}{c_n^2} = -\mu^2\left[\Psi_{xx} + R + \left(\mathcal{U}\Psi_y + \frac{1}{2}\mathcal{W}^2\right)_\Psi\right]. \tag{F 12}$$

We rewrite the last term in (F 12) as

$$\left(\mathcal{U}\Psi_y + \frac{1}{2}\mathcal{W}^2\right)_\Psi = \frac{\partial}{\partial\Psi}\int_{-\infty}^{x} \mathrm{d}x'\,\{\mathcal{U}_x\Psi_y + \mathcal{U}(\Psi_y)_x + \mathcal{W}\mathcal{W}_x\}|_\Psi\,. \tag{F 13}$$

Making use of (4.32) and (4.16), the integral on right-hand side of (F 13) may be simplified, resulting in

$$\begin{aligned}\mathcal{U}\Psi_y + \frac{1}{2}\mathcal{W}^2 = &\int_{-\infty}^{x} \mathrm{d}x'\,\mathcal{U}\Psi_y|_\Psi + \int_{-\infty}^{x} \mathrm{d}x'\,\phi_Z\,(\Psi_{yx}\Psi_y - \Psi_{yy}\Psi_x)|_\Psi \\ &- \int_{-\infty}^{x} \mathrm{d}x'\,\phi_x\,(\Psi_{yZ}\Psi_y - \Psi_{yy}\Psi_Z)|_\Psi\,.\end{aligned} \tag{F 14}$$

Combining (F 12),(F 13) and (F 14), we recover (4.27), with $q = \sigma = 0$. Finally, returning to (F 5) and substituting for $\boldsymbol{\omega}$, we obtain (4.31).

# APPENDIX G

## REDUCTION PROPERTY OF THREE-DIMENSIONAL TERM

We demonstrate here how the property (4.51) satisfied by the three-dimensional term of (4.47) is derived. Assuming solutions of the from $A = A(x + pZ, T)$, the quantities $\mathcal{W}^{(0)}$ and $\phi^{(0)}$ are given by

$$\mathcal{W}^{(0)} = p \int_{-\infty}^{x} \mathrm{d}x'\, G'|_{\Psi}\,, \tag{G 1$a$}$$

$$\phi^{(0)} = -p \int_{-\infty}^{x} \mathrm{d}x' \int_{-\infty}^{x'} \mathrm{d}x^{+}\, y'_{\Psi} G^{+}|_{\Psi}\,,$$

where

$$G = pA_x \left(\cos n\pi y + \frac{A}{c_n^2}\right). \tag{G 1$b$}$$

It is then readily shown using (4.14) that

$$\mathcal{U}^{(0)} = -p^2 \int_{-\infty}^{x} \mathrm{d}x'\, G'|_{\Psi}\,, \tag{G 2}$$

and that

$$\phi_Z^{(0)}\Big|_{\Psi} \Psi_{yy}^{(0)} = \frac{p^2}{c_n^2} A \sin n\pi y\; y_{\Psi} \int_{-\infty}^{x} \mathrm{d}x'\, G'|_{\Psi}\,. \tag{G 3}$$

Making use of (G 1$a$), (G 2) and (G 3), we find that

$$\begin{aligned}\mathcal{H}^{(0)} = {} & -p^2 \frac{\partial}{\partial y} \int_{-\infty}^{x} \mathrm{d}x'\, G'|_{\Psi} \\ & + p^2 \frac{\partial}{\partial \Psi} \left\{ \int_{-\infty}^{x} \mathrm{d}x'\, G'|_{\Psi} - \frac{A}{c_n} \cos n\pi y \right\} \int_{-\infty}^{x} \mathrm{d}x'\, G'|_{\Psi}\,.\end{aligned}$$

Differentiating and integrating the second term inside the braces with respect to $x$ at constant $\Psi$ and using (G 1$b$), it follows that

$$\mathcal{H}^{(0)} = -p^2 \frac{\partial}{\partial y} \int_{-\infty}^{x} \mathrm{d}x'\, G'|_{\Psi}$$
$$+ p^2 \frac{\partial}{\partial \Psi} \int_{-\infty}^{x} \mathrm{d}x'\, A'_x \cos n\pi y' \,(y'_{\Psi} - n\pi)|_{\Psi} \int_{-\infty}^{x} \mathrm{d}x'\, G'|_{\Psi}$$
$$+ \frac{p^2}{c_n^2} \frac{\partial}{\partial \Psi} \int_{-\infty}^{x} \mathrm{d}x'\, A' A'_x \cos^2 n\pi y' y'_{\Psi}\Big|_{\Psi} \int_{-\infty}^{x} \mathrm{d}x'\, G'|_{\Psi}\,. \qquad \text{(G 4)}$$

It is readily shown that the the last two terms in (G 4) cancel each other so that we have

$$c_n^3 \int_0^{c_n} \mathrm{d}\Psi \mathcal{H}^{(0)} y_A = -c_n^3 p^2 \int_0^1 \mathrm{d}y \sin n\pi y \frac{\partial}{\partial y} \int_{-\infty}^{x} \mathrm{d}x'\, G'|_{\Psi}\,,$$

which, upon integrating by parts and using (G 1*b*) yields (4.51).

# REFERENCES


ABLOWITZ, M.J. & WANG, X.-P. 1995 Initial time layers and Kadomtsev–Petviashvili type equations. Unpublished manuscript.

BAINES, P.G. 1987 Upstream blocking and airflow over mountains. *Ann. Rev. Fluid Mech.* **19**, 75.

BAINES, P.G. & HOINKA, K.P. 1985 Stratified flow over two-dimensional topography in fluid of infinite depth: a laboratory simulation. *J. Atmos. Sci.* **42**, 1614.

BENNEY, D.J. 1966 Long nonlinear waves in fluid flows. *J. Math. Phys.* **45**, 52.

CASTRO, I.P. & SNYDER, W.H. 1993 Experiments on wave breaking in stratified flow over obstacles. *J. Fluid. Mech.* **255**, 195.

CLARKE S.R. & GRIMSHAW R.H.J. 1994 Resonantly generated internal waves ina contraction. *J. Fluid Mech.* **274**, 139.

CLARK, T.L. & PELTIER, W.R. 1977 On the evolution and stability of finite-amplitude mountain waves. *J. Atmos. Sci.* **34**, 1715.

DRAZIN, P.G. & REID, W.H. 1981 *Hydrodynamic Stability.* Cambridge University Press.

ERTEKIN, R.C., WEBSTER, W.C. & WEHAUSEN, J.V. 1984 Ship-generated solitons. In *Proc. 15$^{\text{th}}$ Symp. Naval Hydrodyn., Hamburg*, National Academy of Sciences, Washington.

GOURLAY, A.R. & WATSON, G.A. 1973 *Computational Methods for Matrix Eigenproblems.* Wiley, New York.

GRIMSHAW, R. 1985 Evolution equations for weakly nonlinear long internal waves in a rotating fluid. *Stud. Appl. Maths* **73**, 1

GRIMSHAW, R. & MELVILLE, W.K. 1989 On the derivation of the modified Kadomtsev–Petviashvili equation. *Stud. Appl. Maths* **80**, 183

GRIMSHAW, R.H.J. & SMYTH, N. 1986 Resonant flow of a stratified fluid over topography. *J. Fluid Mech.* **169**, 429.

GRIMSHAW, R. & YI, Z. 1991 Resonant generation of finite-amplitude waves by the flow of a uniformly stratified fluid over topography. *J. Fluid Mech.* **229**, 603.

HANAZAKI, H. 1994 On the three-dimensional internal waves excited by topography in the flow of a stratified fluid. *J. Fluid Mech.* **263**, 293.

HOWARD, L.N. & MASLOWE, S.A. 1973 Stability of stratified shear flows. *Boundary-Layer Meteor.* **4**, 511.

KANTZIOS, Y.D. & AKYLAS, T.R. 1993 An asymptotic theory of nonlinear stratified flow of large depth over topography. *Proc. R. Soc. Lond.* A **440**, 639.

KATSIS, C. & AKYLAS, T.R. 1987*a* On the excitation of long nonlinear water waves by a moving pressure distribution. Part 2. Three-dimensional effects. *J. Fluid Mech.* **177**, 49.

KATSIS, C. & AKYLAS, T.R. 1987*b* Solitary internal wave in a rotating channel: a numerical study. *Phys. Fluids* **30**, 297.

KAUP, D.J. & NEWELL, A.C. 1978 Solitons as particles and oscillators in slowly varying media: a singular perturbation theory. *Proc. R. Soc. Lond.* A **361**, 413.

KNICKERBOCKER, C.J. & NEWELL, A.C. 1980 Shelves and the Korteweg-de Vries equation. *J. Fluid Mech.* **98**, 803.

KO, K. & KUEHL, H.H. 1978 Korteweg-de Vries soliton in a slowly varying medium. *Phys. Rev. Lett.* **4**, 233.

KODAMA, Y. & ABLOWITZ, M.J. 1981 Perturbations of solitons and solitary waves. *Stud. Appl. Maths* **64**, 225.

LAMB, K.G. 1994 Numerical simulations of stratified inviscid flow over a smooth obstacle. *J. Fluid Mech.* **260**, 1.

LAPRISE, R. & PELTIER, W.R. 1989*a* The linear stability of nonlinear mountain waves: Implications for the understanding of severe downslope windstorms. *J. Atmos. Sci.* **46**, 545.

LAPRISE, R. & PELTIER, W.R. 1989*b* The structure and energetics of transient eddies in a numerical simulation of breaking mountain waves. *J. Atmos. Sci.* **46**, 565.

LEIBOVICH, S. & RANDALL, J.D. 1973 Amplification and decay of long nonlinear waves. **58**, 481.

LILLY, D.K. & KLEMP, J.B. 1979 The effects of terrain shape on nonlinear hydrostatic mountain waves. *J. Fluid Mech.* **95**, 241.

LONG, R.R. 1953 Some apects of the flow of stratifed fluids. I. A theoretical investigation. *Tellus* **5**, 42.

MELVILLE, W.K. & HELFRICH, K.R. 1987 Transcritical two-layer flow over topography. *J. Fluid Mech.* **178**, 31.

MCINTYRE, M.E. 1972 On Long's hypothesis of no upstream influence in uniformly stratified or rotating flow. *J. Fluid Mech.* **52**, 209.

MILES, J.W. 1969 Waves and wave drag in stratified flows. *Proc. 12$^{\text{th}}$ Intl. Congress of Applied Mechanics*, Springer, Berlin.

MILES, J.W. & HUPPERT, H.E. 1969 Lee waves in stratified flow. Part 4. Perturbation

approximations. *J. Fluid Mech.* **35**, 497.

PEDERSEN, G. 1988 Three-dimensional wave patterns generated by moving disturbances at transcritical speeds. *J. Fluid Mech.* **196**, 39.

PIERREHUMBERT, R.T. & BACMEISTER, J.T. 1987 On the realizability of Long's model solutions for nonlinear stratified flow over an obstacle. In *Proc. 3rd Intl. Symposium on Stratified Flows* (ed. E. J. List & G. Jirka). ASCE.

PIERREHUMBERT, R.T. & WYMAN, B. 1985 Upstream effects of mesoscale mountains. *J. Atmos. Sci.* **42**, 977.

PRASAD D. & AKYLAS, T.R. 1996*a* On the generation of shelves by long nonlinear waves in stratified flows. *J. Fluid Mech., sub judice*

PRASAD, D. & AKYLAS, T.R. 1996*b* Dynamics of three-dimensional fully nonlinear internal waves in uniformly stratified flow over topography. *J. Fluid Mech., sub judice.*

PRASAD, D., RAMIREZ J. & AKYLAS, T.R. 1996 Stability of stratified flow of large depth over finite-amplitude topography. *J. Fluid Mech.* **320**, 369.

RAMIREZ, J. 1993 Stability of nonlinear stratified flow over topography. SM Thesis, Department of Mechanical Engineering, MIT.

ROTTMAN, J.W., BROUTMAN, D. & GRIMSHAW, R. 1996 Numerical simulations of uniformly stratified fluid flow over topography. *J. Fluid Mech.* **306**, 1.

SHAPIRO, R. 1975 Linear filtering. *Math. Comput.* **29**, 1094.

TOMASSON, G.G. & MELVILLE, W.K. 1991 Flow past a constriction in a channel: a modal description. *J. Fluid Mech.* **232**, 21.

WARN, T. 1983 The evolution of finite amplitude Rossby waves on a weak shear. *Stud.*

*Appl. Maths* **69**, 127.

YI, Z. & WARN, T. 1987 A numerical method for solving the evolution equation of solitary Rossby waves on a weak shear. *Adv. Atmos. Sci.* **4**, 43.

YIH, C.-S. 1967 Equations governing steady two-dimensional large-amplitude motion of a stratified fluid. *J. Fluid Mech.* **29**, 539.

YIH, C.-S. 1980 *Stratified flows.* Academic, New York.